Insights from Observations and Modelling into the Evolution of Supraglacial Lakes on the Greenland Ice Sheet

Amber Alexandra Leeson

Submitted in accordance with the requirements for the degree of
Doctor of Philosophy

The University of Leeds

School of Earth and Environment

Monday, 10 June 2013

Declaration of Authorship

The candidate confirms that the work submitted is her own, except where work that has formed part of jointly authored publications, has been included. The contribution of the candidate and the other authors to this work has been explicitly indicated below. The candidate confirms that appropriate credit has been given within the thesis where reference has been made to the work of others.

Publications

Chapters 2 and 3 are based on work from: Leeson, A. A., Shepherd, A., Palmer, S., Sundal, A. & Fettweis, X. 2012. Simulating the growth of supraglacial lakes at the western margin of the Greenland ice sheet. *Cryosphere,* 6**,** 1077-1086.

The candidate designed and developed the model described in this publication, performed the entirety of the analysis and wrote the manuscript. Professsor Shepherd supervised the work and provided scientific and editorial comments on the manuscript. The remaining co-authors provided data and editorial comments on the manuscript.

Chapter 4 is based on work from: Leeson, A. A., Shepherd, A., Sundal, A. V., Johansson, A. M., Selmes, N., Briggs, K., Hogg, A., Fettweis, X. 2013. A comparison of supraglacial lake observations at the western margin of the Greenland ice sheet. *Journal of Glaciology.*

The candidate performed the entirety of the analysis detailed in this publication and wrote the manuscript. Professor Shepherd supervised the work and provided scientific and editorial comments. The remaining co-authors provided data and editorial comments on the manuscript.

Acknowledgements

Abstract

Supraglacial lakes (SGLs) form when runoff (meltwater + rain) pools in depressions on the Greenland ice sheet (GrIS). SGLs can collectively affect seasonal ice sheet flow rates when they drain episodically; although the net impact on flow speed is uncertain. In this thesis: 1) a new model of SGL Initiation and Growth (the SLInG model) is presented, 2) existing SGL observations are evaluated and combined to form a single optimised dataset, 3) these data are used to evaluate the model and 4) this model is used to investigate past trends in SGL evolution in south west Greenland.

SLInG is a 2-dimensional transient hydrology model which routes runoff, which has been simulated using a regional climate model, over a digital elevation model (DEM) of the ice sheet surface. Water is routed using Darcy's law for flow through a porous medium and Manning's equation for open channel flow, and is allowed to collect in depressions in the DEM, thus forming SGLs. Observations of SGLs can be temporally sparse and variation in reported lake frequency can be significant between datasets. Three observational datasets of SGLs, automatically derived from satellite data, were found to omit a sizeable (29 to 48%) fraction of lakes identified manually. These datasets were combined using a hierarchical scheme, leading to a 67% increase in the number of lakes reported.

By comparison with satellite observations, SLInG is found to be 19 times more likely to correctly predict the location, or absence, of a lake, than not. In addition, simulated and observed lake onset dates are highly correlated (r= ~0.8) and model estimates of the rate of growth of lake covered area are, on average, just 14% greater than observed values. SLInG was forced with 40 years of reanalysis data in order to investigate historical variation in the temporal evolution of SGLs. SLInG shows that SGLs have responded to recent dramatic changes in local climate by migrating inland by 150 m a.s.l. (3.75 m a.s.l. per year) during 1971-2010. This modelled trend is in good agreement with recent satellite observations and suggests that SGLs, by forming and draining at higher elevations, where pre-existing surface-bed conduits such as moulins and crevasses are rare, may contribute more significantly to ice sheet dynamics in the future.

Table of Contents

List of Tables

List of Figures

Abbreviations

AMO	Atlantic Multidecadal Oscillation
AR4	Fourth Assessment Report
ASTER	Advanced Spaceborne Thermal Emission and Reflectance Radiometer
AVHRR	Advanced Very High Resolution Radiometer
AWS	Automatic Weather Station
CEN	Centre d'Etudes de la Neige
DEM	Digital Elevation Model
ECHAM5	Ecmwf Hamburg 5
ECMWF	European Centre for Medium-Range Weather Forecasts
ETM+	Enhanced Thematic Mapper Plus
GBI	Greenland Blocking Index
GCM	General Circulation Model
GDEM	Global Digital Elevation Model
GIMP	Greenland Mapping Project
GrIS	Greenland ice sheet
HIRLAM	High Resolution Limited Area Model
HSS	Heidke Skill Score
InSAR	Interferometric Synthetic Aperture Radar
IPCC	Intergovernmental Panel on Climate Change
ISM	Ice Sheet Model
MAR	Modèle Atmosphérique Régional
MODIS	Moderate-resolution Imaging Spectroradiometer
MPI	Max Planck Institute
NAO	North Atlantic Oscillation
NASA	National Aeronautics and Space Administration
PCC	Pearson Correlation Coefficient
PDD	Positive Degree Day
PMM5	Polar Mesoscale Model (fifth generation)
RACMO	Regional Atmospheric Climate Model
RCM	Regional Climate Model
RCP	Representative Concentration Pathway
RK4	Fourth-order Runge Kutta
RMSD	Root-Mean-Squared Deviation
SAR	Synthetic Aperture Radar

SGL	Supraglacial Lake
SICOPOLIS	Simulation Code for Polythermal Ice Sheets
SLInG	Supraglacial Lake Initiation and Growth (model)
SMB	Surface Mass Balance
UTM	Universal Transverse Mercator

Chapter 1

Introduction and background

1.1 Introduction

The Greenland ice sheet (GrIS) is the second largest ice mass in the world, after the Antarctic ice sheets, and contains 2.9×10^6 km^3 of ice (Bamber et al., 2001). If the GrIS were to melt completely, enough water would be released to raise global sea level by 7.2 m (Gregory et al., 2004). With Arctic temperatures set to rise by 4-8 ^{o}C by 2100 (Meehl, 2007), processes by which this temperature change may influence ice sheet mass balance are becoming increasingly important. Rising temperatures have a direct effect on mass balance by promoting additional melting, which, in turn, may also contribute to mass loss through changes in ice dynamics. In the fourth assessment report (AR4) of the Intergovernmental Panel on Climate Change (IPCC), a lack of understanding concerning the processes which contribute to changes in ice dynamics was highlighted as a concern (Lemke, 2007).

Supraglacial lakes (SGLs), formed when runoff (meltwater + rain) pools in depressions on the ice sheet, may impact the mass balance of the GrIS in three ways. First, they reduce the area-averaged albedo of the ice and promote increased melting accordingly (Perovich et al., 2002, Tedesco et al., 2012). Second, they have been observed to drain rapidly through hydrofracture (Das et al., 2008, Doyle et al., 2013, Selmes et al., 2011). This mode of SGL drainage has been correlated with seasonal and shorter-term velocity fluctuations in ice sheet flow (Shepherd et al., 2009). The third potential impact of SGLs on surface mass balance may arise as a result of this velocity perturbation. If a net speed-up of the ice sheet were to occur, fluctuations in ice sheet hypsometry would render a larger surface area available for melting (Parizek and Alley, 2004).

As SGLs may potentially have a large impact on ice sheet dynamics when they drain, they have been the subject of numerous observational and modelling studies (e.g. Echelmeyer et al., 1991, Clason et al., 2012). Typically, observations of SGLs are made either in-situ (e.g. Box et al., 2006, Boon and Sharp, 2003) or remotely using satellite sensors (e.g. Georgiou et al., 2009, Liang et al., 2012). In-situ observations are generally limited to short time periods, for example, a single melt season, because of logistical and economic concerns.

Satellite data offers the advantage of a longer time series of observations. However, temporal sampling is typically sparse within individual years. Although a clearer picture of SGL evolution is slowly coming together from the many, short/sparse datasets available, there is still a great degree of uncertainty surrounding the behaviour of SGLs and scientific understanding of the processes that drive their evolution is lacking. Modelling studies have been conducted in an attempt to address this uncertainty (Luthje et al., 2006b, Clason et al., 2012, Banwell et al., 2012). However, these models of SGL evolution are limited by heavy parameterisation of water routing and ponding and a somewhat empirical approach to snowpack/firn processes such as retention and refreezing. In addition, these models depend on in-situ measurements for forcing purposes, limiting their application to where and/or when these data are available.

This thesis describes the development of a new, and the first, physically based model of SGL evolution. This model is forced by regional climate model (RCM) data and is hence optimised as a prognostic tool. In Section 1.2 of this chapter, SGLs are introduced. In Section 1.3 the potential impact of SGLs on the mass balance of the GrIS is discussed. In Section 1.4 observational studies of SGL evolution are reviewed. Section 1.5 describes potential SGL modelling strategies, with reference to previously published work. Section 1.6 presents the aim and objectives of research described in this thesis and in Section 1.7 the structure of the thesis is outlined.

1.2 Characteristics and behaviour of supraglacial lakes.

Supraglacial lakes form during the spring/summer melt season across much of the ablation zone of the GrIS (e.g. McMillan et al., 2007, Sneed and Hamilton, 2007b, Sundal et al., 2009). They are a key component of the supraglacial hydrological network, which transports runoff over the ice and through firn, under gradients in hydraulic potential, en-route to its final destination off the ice sheet. Runoff is defined as the portion of surface melt plus rainwater, which is free flowing, as opposed to being retained or refrozen. The supraglacial hydrological network also includes water-filled streams/channels, crevasses and moulins (Figure 1.1). Laterally flowing streams form from the accumulation of runoff from overland flow. These streams incise channels into the ice (Jarosch and Gudmundsson, 2012). Crevasses and moulins provide a conduit by which runoff is routed to the englacial and subglacial environments (e.g. Catania et al., 2008, Clason et al., 2012, Phillips et al., 2011). Both the englacial and subglacial hydrological networks mirror that of the surface; water may flow laterally in channels, be stored temporarily in lakes/pockets, and from the

englacial environment, water may be routed vertically to base of the ice sheet (e.g. Gulley et al., 2009, Jansson et al., 2003, Irvine-Fynn et al., 2011).
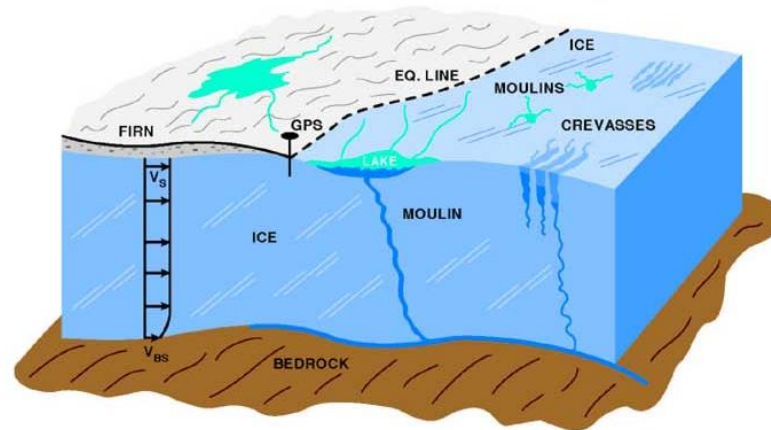
Figure 1.1: Glaciological features in the equilibrium and ablation zones, including surface lakes, inflow channels, crevasses, and moulins. Reproduced from Zwally et al. (2002).

SGLs form when runoff pools in topographic depressions in the ice sheet surface. These depressions are intransient features, formed by the transmission of the basal bedrock profile through the ice. This transmission depends upon the shape of the bedrock itself and basal conditions such as 'sticky spots' (Lampkin and VanderBerg, 2011, Gudmundsson, 2003). Thus, SGLs are found to form in the same locations year-on-year (Echelmeyer et al., 1991, Selmes et al., 2011). SGL initiation begins shortly after the start of the melt season (e.g. Georgiou et al., 2009, Colgan et al., 2011), when a threshold quantity of runoff has been produced (Johansson and Brown, 2013). They begin to appear first at low elevations, close to the margin, and form progressively further inland as the melt season progresses (Sundal et al., 2009). In south west Greenland, SGLs form up to about 2000 m a.s.l. (Howat et al., 2013). The depressions in the ice sheet in which SGLs form are limited in size by the ice sheet topography (Luthje et al., 2006b). This provides a potential constraint on the maximum size of SGLs. However, SGLs may also grow through enhanced melting at the lake bed (Tedesco et al., 2012, Luthje et al., 2006b). The area of individual lakes has been observed to grow up to 8.9 km^2 in west Greenland (Box and Ski, 2007).

When SGLs become brim-full, they overflow and provide a temporary water storage site for runoff on its way downstream (Banwell et al., 2012). However, ultimately, they are transient features and their cessation occurs in three discrete ways. Firstly, SGLs have been observed to empty rapidly through drainage (e.g. Figure 1.2). This rapid drainage can occur on timescales of the order of hours (Das et al., 2008, Doyle et al., 2013). Presumably, this rapid drainage occurs through hydrofracture; the propagation of existing cracks and

crevasses in the lake bed to the base of the ice sheet, by a sufficient volume of meltwater (Boon and Sharp, 2003, Krawczynski et al., 2009, van der Veen, 2007). SGLs are often intersected by channels that continuously supply water to, and drain water from the lake, as part of the surficial hydrological network (Figure 1.3). Lake drainage, by the propagation of lateral channels has been observed on glaciers in Svalbard and Alaska (Liestøl, 1980, Raymond and Nolan, 2000). It has recently been proposed that this also occurs on the GrIS (Selmes et al., 2013, Tedesco et al., 2011b). Overflow, from the lowest part of the lake rim, or discharge from the lake via a meltwater stream, incises a channel deeper than the level of water in the lake. An increase in discharge from the lake through the channel propagates the vertical evolution of the channel bed (e.g. Knighton, 1981, Gulley et al., 2009, Jarosch and Gudmundsson, 2012). This process allows water to drain laterally until the lake is empty. If a lake does not drain completely by either of these two mechanisms, it may refreeze when runoff is no longer being produced and there is a negative energy exchange between the lake and the atmosphere (Selmes et al., 2011, Johansson et al., 2013). At the west GrIS margin, 98% of runoff volume is stored in SGLs which are large enough to hydrofracture (Krawczynski et al., 2009). However, it is unclear at present what proportion of lakes drain in this way every year. Observational studies performed to date suggest that as few as 13% (Selmes et al., 2011), or as many as 84% (Johansson et al., 2013) of lakes drain through hydrofracture. The remaining 83% or 16% either drain laterally or refreeze.
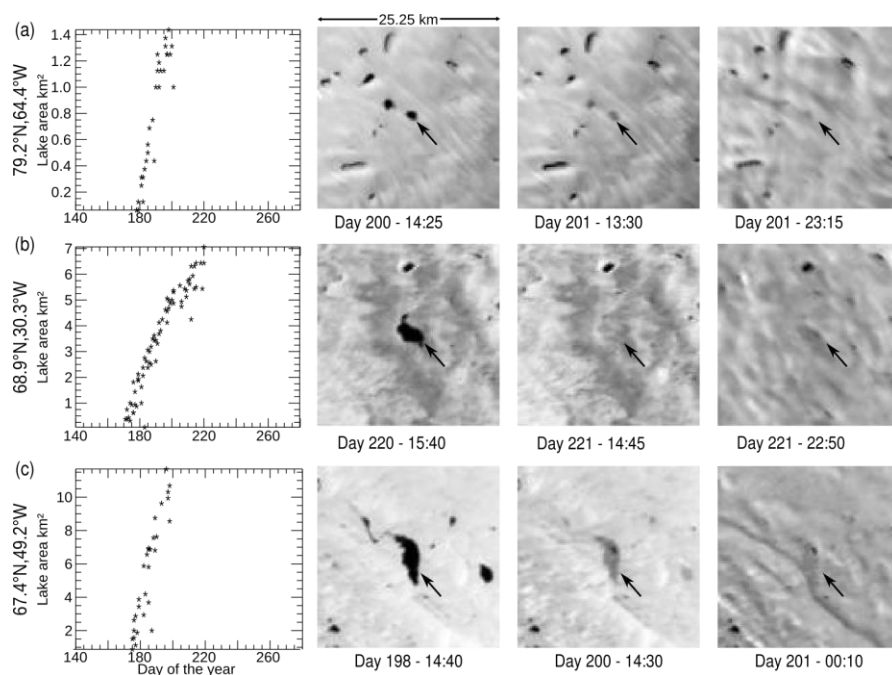
Figure 1.2: Examples of supraglacial lakes that drain rapidly. Three lakes (rows a, b and c) in MODIS band 1 images, at the same scale, before and after drainage. Area/time plots correspond to lakes indicated by arrows. Reproduced from Selmes et al. (2013).

Figure 1.3: A large SGL intersected by meltwater channels on the GrIS. Photo: Ian Willis.

1.3 The mass balance of the Greenland ice sheet and feedback between melting and ice dynamics

The mass balance of the GrIS, ΔM, can be calculated as a linear sum of precipitation, P, runoff, R, sublimation, S, and discharge, D (Equation 1.1).

$$\Delta M = P - R - S - D \qquad\qquad 1.1$$

Precipitation falls in solid form (i.e. as snow) across most of the ice sheet, however at lower elevations during the summer, precipitation may fall as rain (Fettweis, 2007). Sublimation is mass lost through the phase change of water from solid (ice and snow) to gaseous (water vapour) form, without passing through the intermediate liquid stage. Discharge is mass lost through large bodies of ice becoming detached from the ice sheet, for example through calving into the sea or marginal lakes at the terminus of outflow glaciers.

The first three terms in the right hand side of Equation 1.1 are collectively known as the surface mass balance (SMB). Surface mass balance exhibits seasonal, inter-annual and longer-term variability, following the distribution of accumulation and ablation. Although ablation rates are correlated with air temperature (e.g. Reeh, 1991, Braithwaite and Olesen, 1984), surface air temperatures greater than the melting point of ice (0° C) do not necessarily mean melting will take place. Likewise, it is also possible for melting to occur when surface air temperatures are less than this value. Ablation depends on the net energy balance at the ice sheet surface, i.e. ΔE in Equation 1.2 must be positive.

$$\Delta E = SW_{in} + SW_{out} + LW_{in} + LW_{out} + SHF + LHF + G_s \qquad\qquad 1.2$$

Here, SW_{in} and SW_{out} are the incoming and outgoing short wave radiation, LW_{in} and LW_{out} are the incoming and outgoing long wave radiation, SHF and LHF are the sensible and latent heat fluxes and G_s is the sub-surface heat flux. Higher values of ΔE are observed in the summer, during which period ablation (melting and sublimation) dominates the surface mass balance equation. Conversely, lower or negative values of ΔE are observed in the winter, and because accumulation rates are also at a maximum during the winter months, a positive change in surface mass occurs.

1.3.1 *Past changes in the Greenland ice sheet mass balance*

In the recent past, changes to the GrIS mass balance can be characterised by inland thickening due to increased precipitation in the interior (e.g. Thomas et al., 2006, Johannessen et al., 2005), and thinning around the 6000 km ice sheet perimeter primarily through discharge and particularly in the proximity of the fast moving outlet glaciers (e.g. Abdalati and Steffen, 2001, Rignot and Kanagaratnam, 2006). As recently as the 1990's, the trend in Greenland SMB has been positive (Hanna et al., 2005). However, there is a consensus that the total GrIS mass balance has been negative since at least 1995 (e.g. Velicogna and Wahr, 2006, Thomas et al., 2006, Ramillien et al., 2006, Box et al., 2006, Rignot and Kanagaratnam, 2006). Mass loss since the year 2000 has been attributed equally to a decrease in surface mass balance and an increase in dynamic discharge (van den Broeke et al., 2009, Joughin et al., 2008, Krabill et al., 2004). The most recent, reconciled mass balance estimates for Greenland, made using a variety of techniques, are summarised in Figure 1.4.

Global sea level has been rising slowly throughout the twentieth century, at a rate of 1.0-2.0 mm yr^{-1}. Of this, Greenland and Antarctica are thought to have contributed around 1% (Rignot and Thomas, 2002, Church, 2001). Various techniques have been used to attempt to quantify the contribution of Greenland to global sea level rise. Rignot and Thomas (2002) and Krabill et al. (2004) used altimetry to estimate this number to be 0.13 mm yr^{-1} for the 1990s, and 0.22 (+/- 0.03) mm yr^{-1} for 1997-2003. Velicogna and Wahr (2006) used satellite gravimetry, to estimate that the rate of mass change during the period 2002-2004 led to a sea-level contribution of 0.22 (+/-0.06) mm yr^{-1}. Most recently, a reconciled estimate of the

GrIS mass balance has been assembled from data acquired using an input-output method, as well as laser altimetry and gravimetry (Shepherd et al., 2012). This study concluded that the GrIS has contributed 8 (+/- 1.2) mm to global sea level rise since 1992.
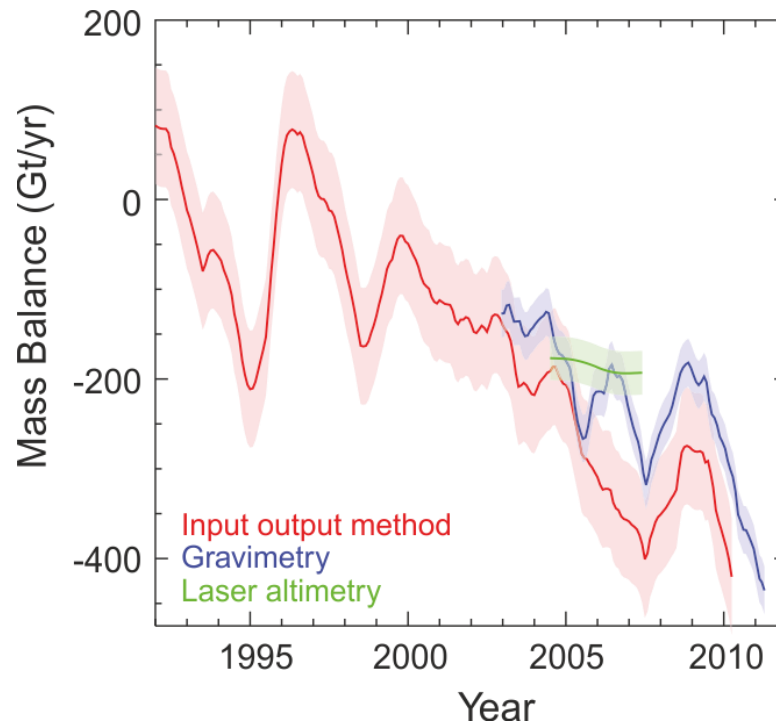
Figure 1.4: Rate of mass change of the GrIS, as derived from the input-output method (red), satellite laser altimetry (green), and satellite gravimetry (blue), with uncertainty ranges (light shading). The rate of mass balance derived from laser altimetry data was computed as a time-varying trend. The gravimetry mass trend was computed after applying a 13-month moving average to a relative mass time series. Modified from Shepherd et al. (2012).

1.3.2   *Correlations between fluctuations in ice sheet flow and ice sheet surface melting*

Evidence suggests that over the past decade, mass loss through discharge has increased (Rignot and Kanagaratnam, 2006) indicating a change in ice sheet dynamics. Glaciers and ice sheets are able to flow, through either internal deformation or sliding at the ice-bed interface. Internal deformation exhibits a very slow response to changes in climate, because changes in the surface mass balance impose low magnitude thinning rates (Zwally et al., 2002). However, it has been proposed that ice motion through basal sliding may respond rapidly to changes in climate through a melt-dynamics feedback. Ice motion shows a seasonal variability of up to 200% (Zwally et al., 2002, Palmer et al., 2011, Joughin et al., 2008, Bartholomew et al., 2010). This speed-up has been shown to be coincident with the melt season (e.g. Figure 1.5) at both the main body of the GrIS and its faster flowing outlet

glaciers (e.g. Shepherd et al., 2009, Palmer et al., 2011, Sole, 2011). This has been shown to be more significant for the main body of the ice sheet, with a 48% summer increase over winter background flow rates, than the faster flowing outlet glaciers which exhibit a summer velocity increase of just 8.6% (Joughin et al., 2008). It has been suggested that the routing of runoff to the bed of the ice sheet provides the means for this to occur by lubricating flow (Zwally et al., 2002, Shepherd et al., 2009). This suggests that in a warmer year, faster than average ice sheet flow may occur. However, observations have also shown that in warm years, where melting is greater than average, no net speed-up of either marine-terminating or land-terminating outlet glaciers is observed when velocity changes are integrated over the whole year (Figure 1.6).

The rate of basal sliding is controlled by adhesion (of the ice to the bed), bed roughness, base roughness (from rock debris held in the ice) and the quantity and distribution of basal water. Basal water either results from melting at the base of the ice or is surface runoff which has been routed to the base from the supraglacial and englacial hydrological networks. Basal water mediates sliding principally by allowing de-coupling of the ice and bed. The extent to which this occurs is dependent on the effective pressure; the sum of the vertically downwards acting ice overburden pressure and the vertically upwards acting basal water pressure. An increase in water pressure, perhaps by a sudden influx of a large volume of runoff from a draining lake, counters the ice overburden pressure resulting in a reduction in effective pressure. This results in a weakening of the ice-bed contact and faster sliding is enabled. Logic suggests that this means that effective pressure is controlled by the quantity of basal water; a greater abundance of water would increase the water pressure, decrease the effective pressure and provide for a subsequent increase in glacier flow velocity. However, in actuality, the mode of sub-glacial drainage provides a major control on effective pressure which can overcome this relationship (Schoof, 2010). Sub-glacial drainage may occur through 1.) an efficient, channelised drainage system (Röthlisberger, 1972) or 2.) an inefficient inter-connected cavity based drainage system (Walder, 1986). At steady state, an efficient, channelised regime enables high basal water flux when effective (water) pressure is high (low) and under a system of linked cavities, basal water flux is high when effective (water) pressure is low (high). As a corollary, under a channelised regime, one would expect a reduction in flow speed over that under a linked-cavity regime. However, the response time of this system to changes in water influx is slow. Temporary spikes in water pressure can therefore lead to transient acceleration of the ice sheet even once an efficient channelised system has been established (Schoof, 2010, Bartholomew et al., 2012, Das et al., 2008, Sole, 2011). SGL drainage may contribute to observed seasonal speed-up by enabling

these periods of transient acceleration (Palmer et al., 2011, Joughin et al., 2004).
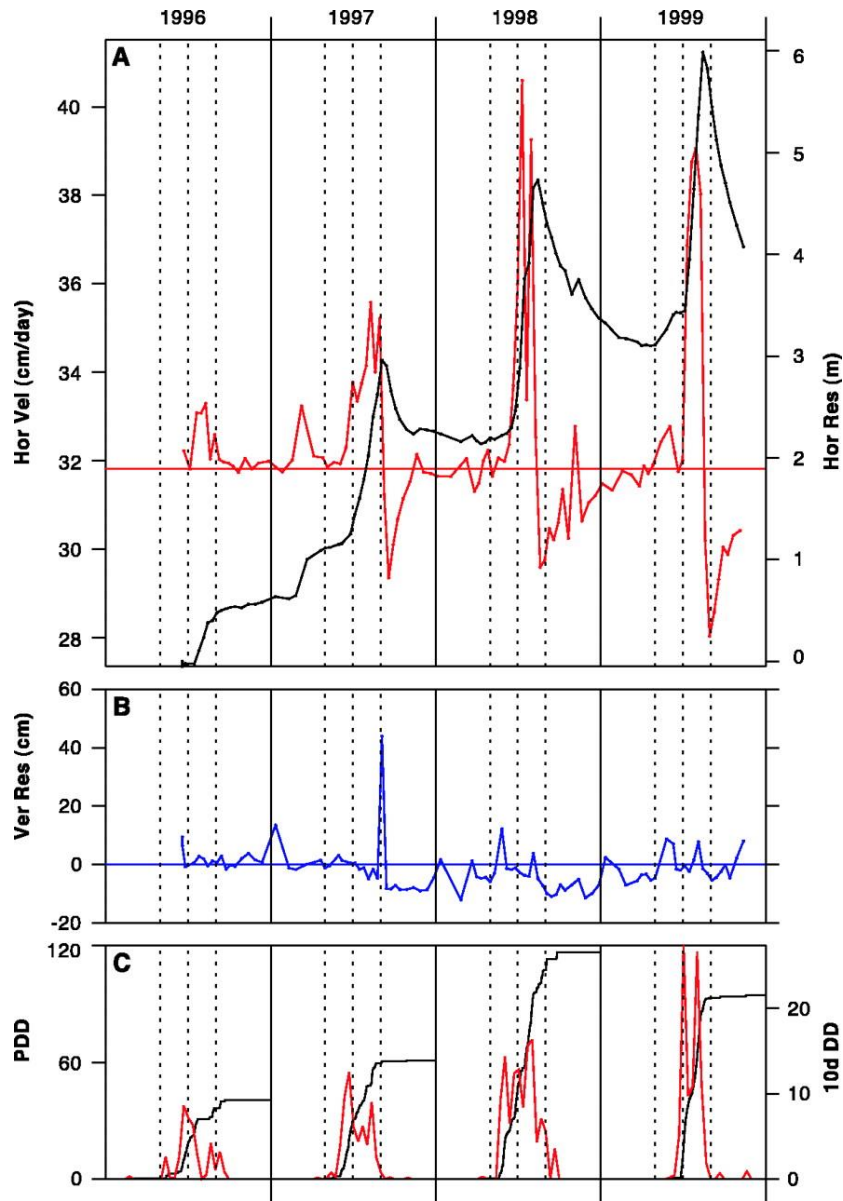
Figure 1.5: Seasonal speed-up correlated with meltwater availability. (A) Horizontal ice velocity (red curve) along a smoothed line of motion showing ice accelerations during the summer melt seasons and the abrupt transitions to deceleration around the times of melt cessation. The cumulative additional motion (horizontal residual, black) relative to a wintertime-average velocity of 31.33 cm/day is 6.0 m by the time of the maximum velocity in 1999. (B) The vertical residual (blue) indicates a 50-cm uplift at the time of the 1997 transition from accelerating flow to decelerating flow. (C) Cumulative positive degree days (PDDs) and PDDs for 10-day intervals (10d DD, red) from temperatures measured at the Swiss Camp, showing correlations of the melting with the intensity and timing of the ice accelerations and decelerations. Vertical dotted lines mark May 1, July 1, and September 1 for each year. Reproduced from Zwally et al. (2002).

Although it is uncertain whether the supraglacial forcing of basal sliding has a significant net impact in the present day, there have been few studies that investigate how this could change in a warming world. This is because current generation ice sheet models do not typically address fast-flowing ice dynamics because of the complex physics involved and high spatial resolution required of such a model. This was identified as a key uncertainty in the IPCC AR4 (Lemke, 2007).
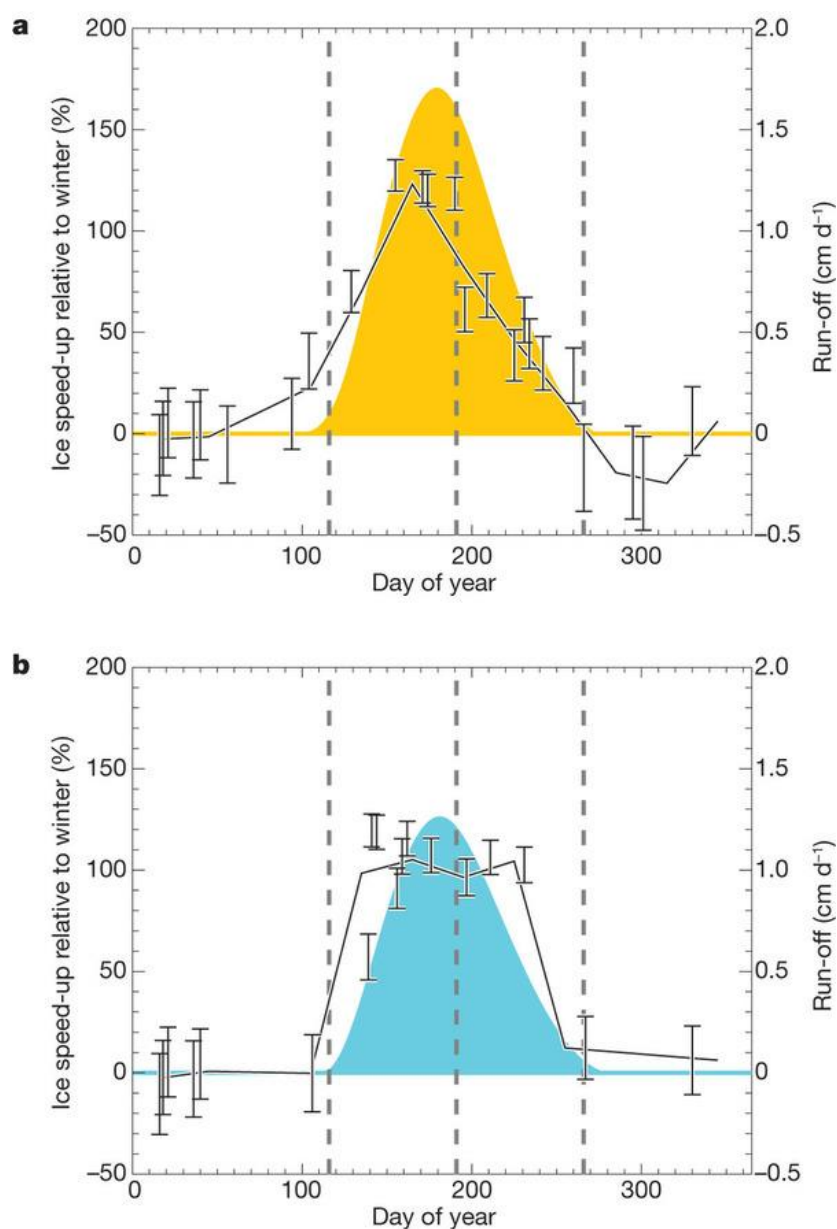
Figure 1.6: (a) Speed-up in years of high melting (1995 and 1998). (b) Speed-up in years of low melting (1993, 1996 and 1997). Point data are 35-day ice-velocity averages relative to the winter mean. Error bars show the 1 σ uncertainty in speed-up measurements. Solid lines: monthly averaged data. Coloured regions: model estimates of daily surface runoff averaged during years of high (orange) and low (blue) melting. Vertical dashed lines indicate the shoulders and midway-point of the runoff period. Modified from Sundal et al. (2011).

1.3.3 *The impact of supraglacial lakes on ice sheet mass balance*

Supraglacial lakes may affect the ice sheet mass balance in three ways. Firstly, they enhance melt-rates at the lake bed with respect to the melt rates of the surrounding ice (Tedesco et al., 2012), thus reducing the area-averaged albedo of the ablation (melt) zone (Perovich et al., 2002). Secondly, by providing a surface-bed conduit for large volumes of runoff when they drain, SGLs may affect ice dynamics through enhanced basal lubrication (Joughin et al., 2004, Shepherd et al., 2009, Palmer et al., 2011).

Enhanced melting has been shown to occur beneath sea ice melt ponds (hereafter 'melt ponds') and SGLs, since the optical properties of water are such that their albedo is significantly smaller than that of bare ice (Taylor and Feltham, 2004, Perovich et al., 2002, Greuell et al., 2002, Fetterer and Untersteiner, 1998). In fact, SGLs have been found to have an albedo 71% lower than bare ice and 82% lower than snow in the Kangerlussuaq region of Greenland (Greuell et al., 2002). SGLs grow in size throughout the melt season through the accumulation of runoff and enhanced melting beneath the lake. Observations have been made on sea ice suggesting that melt ponds can enhance the area-averaged albedo of the ice by up to 56% (Perovich et al., 2002). However, since sea ice is very flat, melt ponds can grow more or less indefinitely and have been found to cover as much as 36% of the available surface. For the GrIS case however, where the potential maximum area of lakes is constrained by topography (Luthje et al., 2006b), the area covered by lakes is significantly lower. Studies of the Swiss Camp, Russell Glacier, Ryder Glacier and Nioghalfjerdsbrae/Zachariae Isstrom regions of the GrIS between 2001 and 2007 suggest that maximum SGL coverage never exceeds 1% of the total area (McMillan et al., 2007, Sundal et al., 2009). Despite this, SGLs may act as a climate feedback, in a small way, in that lakes enable enhanced melting, which leads to lake growth, which leads to a greater area over which enhanced melting takes place.

At higher elevations on the ice sheet, SGLs have the potential to enable surface-to-bed connections when they drain, where conduits such as moulins and crevasses are rare (Howat et al., 2013, Phillips et al., 2011). This may have serious consequences for ice sheet dynamics, despite the relative rarity of drainage events at high elevations compared to low elevations (Selmes et al., 2013). In this region, surface water delivery to the base is too small to enable the establishment of efficient, channelized systems. Because of this, an increase in basal water pressure due to the draining of SGLs may enable faster sliding (Bartholomew et al., 2011b). In addition, if an SGL, through drainage, were to create a new

surface-bed connection in a region of frozen bed, this could enable a local decoupling of the ice sheet and bedrock, potentially allowing a greater area of the ice sheet to slide (Howat et al., 2013). It has also been proposed that draining lakes provide a means of cryo-hydrologic warming, i.e. that the passage of (warm) water through the (colder) ice causes an increase in ice temperature, reducing the effective viscosity of the ice and increasing flow through internal deformation (Phillips et al., 2010). If SGL drainage were found to contribute to a net increase in ice sheet flow speed, this may lead to a third mechanism through which ice sheet mass balance may be altered. This is in addition to increased ablation and discharge due to changing climate. Changes in the flow of ice can lead to additional changes in ablation, through modified hypsometry; this may serve to thin and flatten the ice sheet, effectively moving the equilibrium line further inland.

1.4 Observations of supraglacial lakes

In-situ surveys of SGL characteristics in west Greenland focus on a particular lake or lake drainage event and produce detailed data for a single melt season (Doyle et al., 2013, Das et al., 2008). The evolution of a single lake may also be reviewed using satellite imagery (e.g. Georgiou et al., 2009, Sneed and Hamilton, 2007a). However, it has been more common to review multiple lakes (e.g. Selmes et al., 2011), or a lake covered region, using remote sensing data (e.g. Liang et al., 2012, McMillan et al., 2007). This enables the exploitation of the full potential of the data available. Remote sensing products which have been used to observe lakes include aerial photography (e.g. Thomsen, 1989, Russell, 1993) and satellite-mounted sensors such as the Advanced Spaceborne Thermal Emission and Reflectance Radiometer (ASTER) (e.g. Georgiou et al., 2009), the Landsat Enhanced Thematic Mapper Plus (ETM+) (e.g. Lampkin, 2011) and the Moderate Resolution Imaging Spectroradiometer (MODIS) (e.g. Sundal, 2009). The western GrIS margin has undergone particular scrutiny due to an abundance of lakes, lakes which regularly drain rapidly, and well-documented seasonal and shorter term changes in ice dynamics (e.g. Joughin et al., 2008, Bartholomew et al., 2012). Typically, observational studies have focused on the Swiss Camp, Jakobshavn (contiguous with Swiss Camp) and Russell Glacier regions. The Russell Glacier region is, on balance, the most studied.

SGLs may be identified in images obtained using remote sensing instruments by manual interpretation, where each lake is digitised by hand (e.g. Georgiou et al., 2009, McMillan et al., 2007), or by a semi-automated or fully-automated method (e.g. Sundal et al., 2009, Liang et al., 2012). Both ASTER and Landsat ETM+ images have a high spatial resolution

(of the order ~10 m), conducive to accurate lake area delineation. By comparison, the spatial resolution of the MODIS instrument is significantly coarser (250 m). Temporally, ASTER and Landsat ETM+ have a sampling frequency of the order of several days, whereas MODIS images are available twice daily. Typically, studies of seasonal and inter-annual variability in modes of SGL evolution are investigated using MODIS (e.g. Johansson and Brown, 2013, Selmes et al., 2011), as a result of this relatively dense temporal sampling. A number of automated methods of reporting SGL distribution from MODIS images on the GrIS have been developed, although specific methods vary between datasets. Automated mapping of lakes enables a number of images, containing numerous lakes, to be processed efficiently. For example, Figure 1.7 shows an ASTER image of SGLs near Russell Glacier.
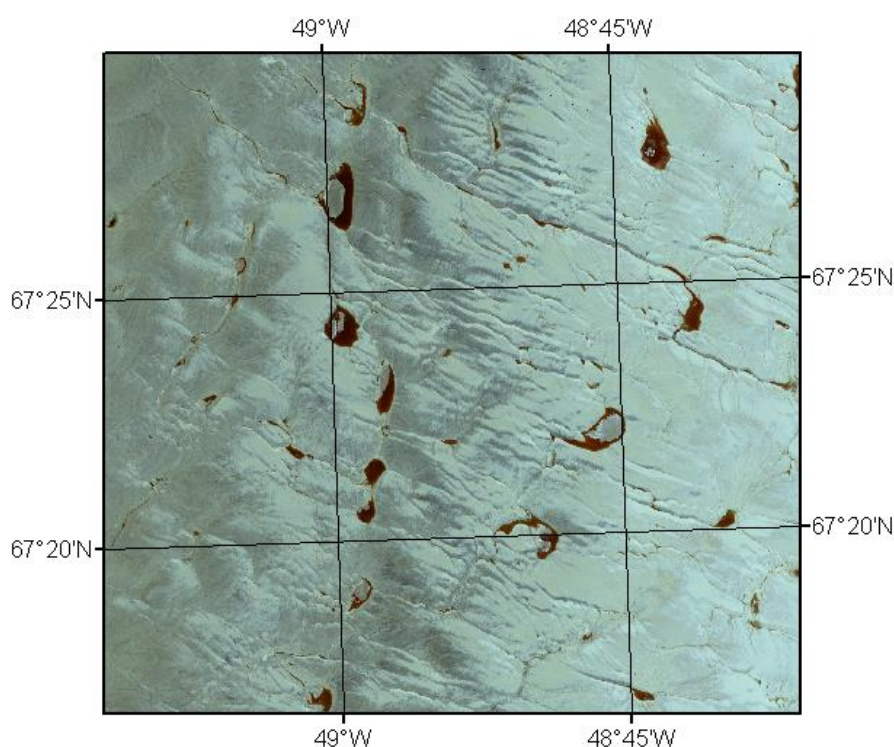
Figure 1.7: Supraglacial lakes observed using the ASTER instrument, in the Russell Glacier catchment on the Greenland ice Sheet, on 1st August 2001.

The five most extensive satellite surveys of SGL evolution are summarised here. Each of these studies uses a semi- or fully-automated lake classification system. Semi-automated methods are so-called because they require the user to pre-select images on which a lake tracking algorithm is applied. With the exception of Howat et al. (2013), these surveys were derived from MODIS imagery. The MODIS instrument has been in operation on board the National Aeronautics and Space Administration (NASA) Terra satellite since 1999 and on board the NASA Aqua satellite since 2002. The spatial resolution of each dataset is

imposed by the resolution of the MODIS instrument (250 m). Typically, the temporal sampling of each dataset is different, depending on the selection of MODIS images for inclusion in the record. The chief limitation in temporal sampling is cloud cover; if cloud is present in the image, some/all lakes may not be resolved. This also means that the date of lake appearance (or demise) and maximum lake covered area may also be incorrectly recorded, if cloud cover was present on the actual date of onset/demise/maximum lake covered area. In years of abundant cloud cover, there may be as few as 12 completely cloud free images per melt season (Sundal et al., 2009).

Sundal et al. (2009) use 268 band 1 (red, 0.620-0.670 μm) MODIS images for 2003 and 2005-2007 to chart the seasonal evolution of SGLs in three climatologically distinct regions of the GrIS, including the Russell Glacier region. These data consist of 28 (cloud-free) observation days in 2003 and 12 (cloud-free) days per year for 2005-2007. Lake distribution was automatically derived using a semi-automated object-oriented segmentation and classification method (e.g. Figure 1.8). The classification of 'lake' or 'not-lake' objects was achieved using fuzzy logic membership functions. This method assigns lake or not-lake status based on the degree of membership to the lake or not-lake class, in terms of reflectance, rather than using a fixed threshold. Sundal et al. (2009) evaluate their method by comparing automatically delineated lakes from a MODIS image to manually delineated lakes from 15 m ASTER scenes. Both images were acquired on 1st August 2001. They estimate that 12% of all possible lakes are omitted from the automatically delineated record, as they are too small to be resolved by MODIS.

Johansson and Brown (2013) employ a similar (semi-automated) method to Sundal et al. (2009) in their survey of the Russell Glacier region on the GrIS. However, they extend their method of classification to include parameters such as lake length and shape, in addition to reflectance. They also allow the threshold values of each parameter to evolve with season. Data available from this study include up to 586 individual lakes identified in ~10 band 2 (near infra-red, 0.841-0.876 μm) and band 4 (green, 0.545-0.565 μm) MODIS images in each year for the period 2001-2010. Johansson and Brown (2013) evaluate their method using seven Landsat (ETM+) images acquired between two to six days prior to/after the acquisition of four MODIS images, over two years. Typically, < 10% of lakes reported using this method are found to be 'false positives' when compared to Landsat imagery. In addition, Johansson and Brown (2013) suggest that the uncertainty associated with the absence of sub-resolution lakes in the dataset is around 11%; in agreement with the similar assessment performed by Sundal et al. (2009).
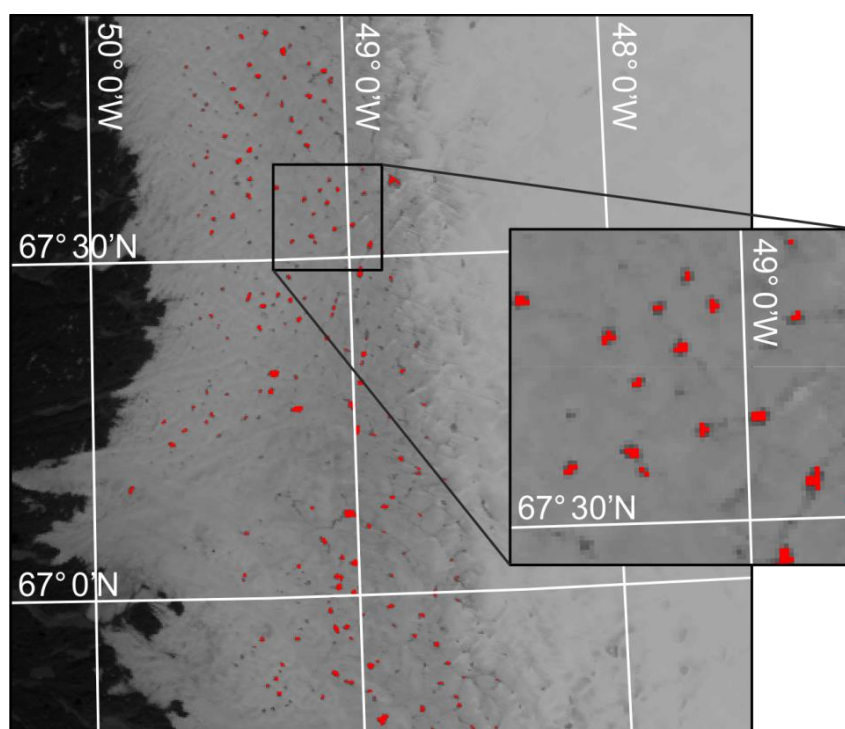
Figure 1.8: An example of automatically delineated lakes on the 10th June 2003. Observed lakes from Sundal et al. (2009) are superimposed on the original MODIS image from which these lakes were delineated.

Selmes et al. (2011) describe the distribution of fast draining lakes on the GrIS between 2005 and 2009 using band 1 images from MODIS covering the whole of the ice sheet area. They employ a semi-automated method of lake delineation, which does not use object-oriented segmentation. Instead, they operate from an a-priori assumed lake distribution, considering each known lake location in turn. At each location, pixels are assigned lake or not-lake status based on a threshold reflectance value of 65% of a standard reference window. This a-priori lake distribution was determined from a supervised classification of a subset of images, and includes those lakes that exhibit a maximum area greater than 0.125 km^2. By tracking individual lakes, rather than considering a wide area, this approach enables greater exploitation of the MODIS image library; cloud cover is not considered a limitation, provided at least one lake is visible in each image (e.g. Figure 1.9). Selmes et al. (2011) evaluated their method using 15 m ASTER scenes over a three-year period, across two regions of the ice sheet. One hundred lake images were used in total and it was concluded that this method under-predicts individual lake area by around 1.77%.

Liang et al. (2012) use a fully automated lake tracking algorithm to report inter-annual variability in SGL evolution during the period 2001-2010 in their 16,500 km^2 study area which encompasses both the Swiss Camp region and Jakobshavn glacier. Liang et al. (2012)

also exploited cloudy as well as part-cloudy images to assemble their dataset by delineating all lakes present in the cloud-free portion of 893 images, covering the ten year period. They adopt a novel classification approach whereby a moving window of 25 x 25 pixels (6.25 km x 6.25 km) is used to assess, based on the presence or absence of a positive tail in a histogram of reflectance values, whether a lake is present in that window. If a lake is present, those pixels with reflectance values greater than a threshold determined from the histogram are categorised as lake pixels. This algorithm is evaluated by comparison with high-resolution ASTER imagery with favourable results. It was concluded that, using this method, 99% of lakes manually identified in ASTER imagery are reported and up to 6% of identified lakes are false positives.

The observational dataset with the longest time series is that of Howat et al. (2013). In their study, 402 scenes are used over 40 years and 12 different regions on the GrIS are considered. This includes both the Russell Glacier and Swiss Camp regions. Howat et al. (2013) semi-automatically derive SGL distribution using a method based on Liang et al. (2012), in images from July and/or August each year, acquired by several Landsat instruments and the ASTER instrument on board the Terra satellite. They also use 5 m SPOT-5 imagery for 2007 and 2008. Although Howat et al. (2013) has the longest time series, gaps of up to 25 years exist in their record, due to data scarcity.
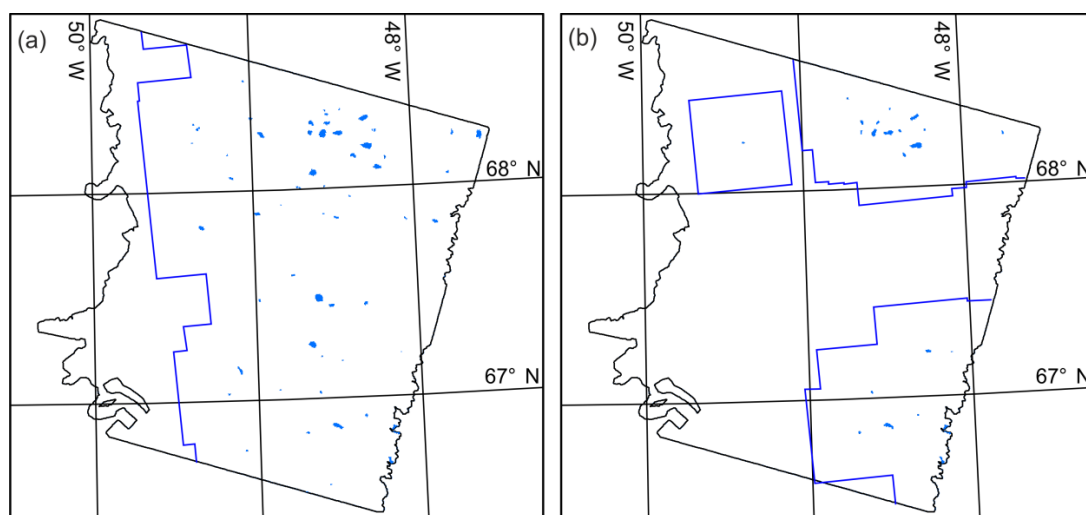
Figure 1.9: Automatically delineated lakes on (a) a cloud free, and (b) a cloudy day in the vicinity of the Russell Glacier on the GrIS. Lake distribution is mosaicked from multiple tiles, each featuring a single lake from the Selmes et al. (2011) dataset. Solid blue lines delimit the extent of this mosaic on each day. The two days reported here are (a) day 220, the 8th of August 2005 and (b) day 219, the 7th of August 2005.

Although the SGL datasets described here are the most extensive observational studies to date in space and time, they still provide a limited record. The studies of Sundal et al.

(2009), Johansson and Brown (2013) and Liang et al. (2012) provide data for small areas. Sundal et al. (2009), Johansson and Brown (2013) and Howat et al. (2013) exhibit generally sparse temporal sampling. Also, because they include cloudy days in their record, Selmes et al. (2011) and Liang et al. (2012) do not exhibit consistent temporal sampling; some lakes may be sampled 30 times and other lakes may be sampled 3 times within a given year. In addition, Sundal et al. (2009) and Selmes et al. (2011) have short time series (4 and 5 years of data respectively), and Howat et al. (2013) has an incomplete time series. Some of these data are known to report false positives and not all possible lakes are reported by each dataset. Because of the interference of cloud, and the fact that the MODIS instrument began operation in 1999, it is not possible to derive a temporally dense, uniformly sampled, long-term record of SGL evolution using satellite imagery.

1.5 Modelling supraglacial lakes

Models describing the evolution of melt ponds have been widely used because melt ponds have a significant impact on the area-averaged albedo of sea ice (Ebert and Curry, 1993, Taylor and Feltham, 2004, Flocco and Feltham, 2007, Skyllingstad et al., 2009, Luthje et al., 2006a). Although melt ponds have been modelled extensively, there are only three models of SGL evolution independent of the work described in this thesis. These are described in Luthje et al. (2006b), Clason et al. (2012) and Banwell et al. (2012). Models of SGL evolution can potentially provide a temporally continuous, full ice sheet, record of SGL evolution as long as sufficient forcing data are available. Thus, models of SGL evolution add value to observational studies of SGLs and can help to constrain the impact SGLs may have on ice albedo and ice dynamics. In addition, a prognostic model has the potential to be useful in quantifying any contribution SGLs may make to future changes in these areas.

There are four distinct stages of lake evolution which describe the full seasonal cycle (Figure 1.10); runoff production, lake growth, lake drainage and lake re-freezing. Together, these form a relatively complex system. In Section 1.5.1 to Section 1.5.4, a range of different approaches to modelling these four stages are described with reference to previous modelling work. In Section 1.5.5, recommendations for a new, improved, SGL modelling strategy are presented. Models of sea ice melt ponds (which are conceptually similar) are also considered, given the scarcity of specific SGL models. The physical principles governing the evolution of melt ponds are similar to those of SGLs with the key difference being the presence of salt in the sea ice, which affects its optical and thermodynamic properties. In addition, the presence of brine pockets means that sea ice is porous.
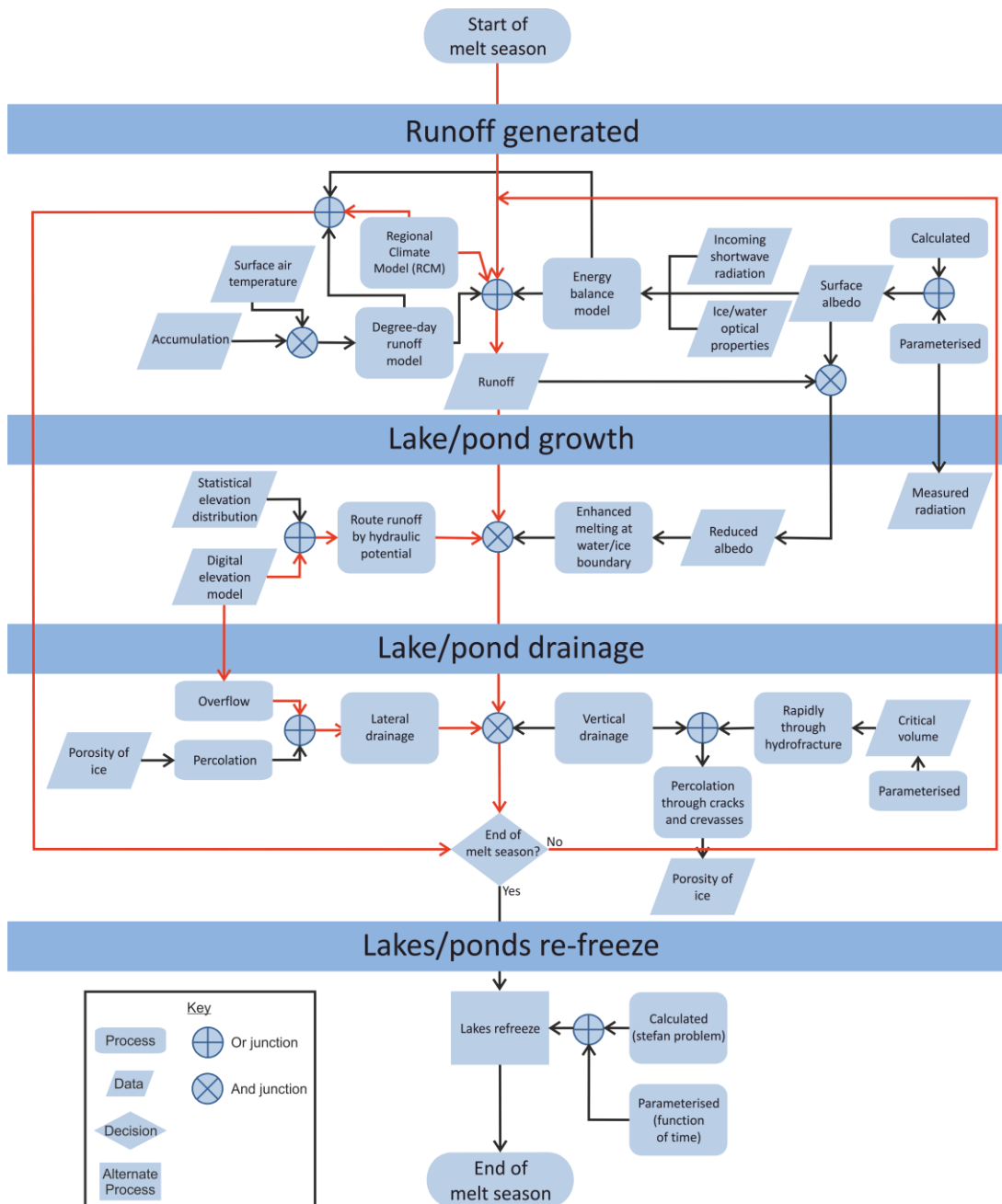
Figure 1.10: Modelling strategies for the four distinct stages of SGL evolution. The proposed methodology for the model described in this thesis is indicated in red.

1.5.1   *Runoff simulation*

The first stage in the evolution of melt ponds and SGLs is runoff production. Typically, in lake modelling studies, runoff is approximated by melting (Luthje et al., 2006b, Clason et al., 2012), which can be calculated explicitly using a physically based energy balance model (Taylor and Feltham, 2004, Skyllingstad et al., 2009, Luthje et al., 2006b, Banwell et al.,

2012) or parameterised using a degree day model (e.g. Clason et al., 2012). Some lake models also include parameterisations for retention and refreezing of this meltwater (Banwell et al., 2012). Advances in regional climate modelling have meant that there is also a third option; the use of runoff calculated by a high resolution regional climate model (RCM) which has been optimised for use over ice, such as the MAR (Modèle Atmosphérique Régional) (Lefebre et al., 2005) or RACMO (Regional Atmospheric Climate Model) (van Meijgaard, 2008) models.

The energy balance approach calculates the surface energy surplus/deficit using Equation 1.2, accounting for the diffusion of energy between snow, ice and water. In their study of melt ponds, Taylor and Feltham (2004) consider meltwater production as a Stefan problem, and consequently use this net surface energy calculation to track the phase boundary of sea ice between solid and liquid states. This is a 1-dimensional solution where if net surface energy is positive, the phase boundary shifts in favour of the liquid state, i.e. the ice melts. Others use the net surface energy calculation to quantify ablation, based on known values of accumulation and snow and ice density (Luthje et al., 2006b, Banwell et al., 2012). Energy balance models are advantageous in that they provide physical justification for calculated ablation rates. However, they require measurements of incoming/outgoing shortwave/longwave radiation, air temperature and atmospheric pressure. Heavy data dependence is a limitation of this method since high-resolution data is not available for large areas of the GrIS; all of these parameters may be expected to be spatially variable. This also limits this type of model in terms of predictive capacity.

An alternative approach to modelling melt is using a parameterisation which is a function of a small number of variables, for which there is ample data, such as the use of a degree day model (Clason et al., 2012). A degree day model is an empirical parameterisation, shown to produce accurate results, of ablation as a function of surface temperature (Braithwaite and Olesen, 1984, Reeh, 1991). The degree day figure, Y, can be calculated using Equation 1.3 below (Braithwaite, 1984).

$$Y = \frac{1}{M} \sum_{m=1}^{m=M} \sum_{n=1}^{n=N} \alpha_{nm} T_{nm} \qquad\qquad 1.3$$

Here, α is defined as 1, if T_{nm} is greater than or equal to 0, and 0 if T_{nm} is less than zero (no melting). T_{nm} is the temperature at the mth observation on the nth day and M is the number of observations in the day (Braithwaite and Olesen, 1989). This number can then be used to

approximate ablation by applying a degree day factor (melt rate per degree day) (Braithwaite, 1984). Degree day factors are typically developed through observations (Braithwaite, 1984, Reeh, 1991). This limits the effective use of degree day modelling to locations where degree day factors have been measured.

RCMs may calculate runoff using a degree day modelling approach to simulate ablation, then parameterise retention and refreezing (for example the ECMWF-downscale model, Hanna et al., 2002) or, more commonly, using a full energy balance method with a snow and ice model (for example the Polar Fifth-Generation Mesoscale Model (Polar MM5), Box et al., 2009). Detailed snow and ice schemes simulate ablation (using a full energy balance method), incorporate simulated values of rainfall from the climate component of the model, and also take into account snow thermodynamic and metamorphic properties. This allows water which is retained in the snow/firn (retention) and refrozen at the surface or at depth (refreezing) to be accounted for. Studies have shown that in order to accurately simulate runoff and SMB using an RCM, a detailed snow physics scheme is essential (Rae et al., 2012). A limitation of this method is that RCM resolution may be rather coarse; MAR typically operates at 25 km resolution (Figure 1.11), and RACMO operates at 11 km resolution. A resolution of 25 km has been shown to be effective in reproducing SMB, in all regions of the GrIS except for that immediately adjacent to the ice sheet margin (Franco et al., 2012).
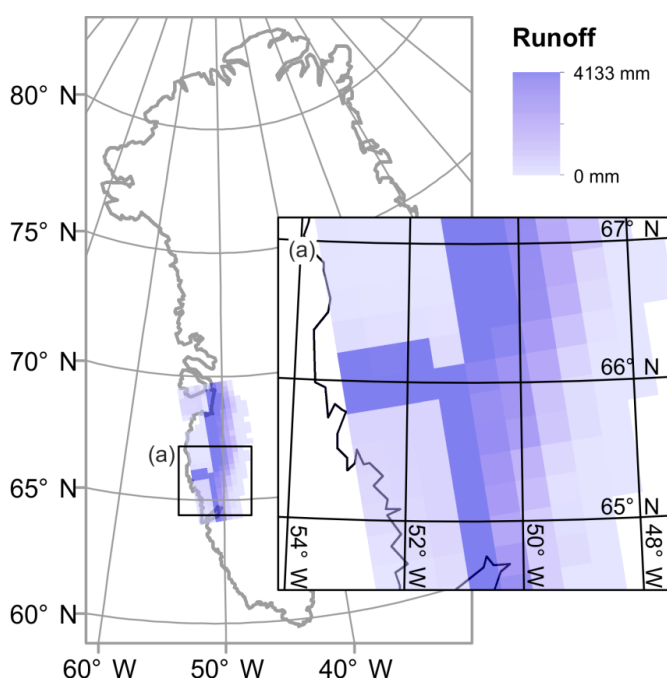
Figure 1.11: Typical resolution of RCM simulated runoff over the GrIS. Shown, is the total annual runoff in 2003, simulated at 25 km resolution using the MAR model (Fettweis, 2007).

1.5.2 *Supraglacial lake growth*

The principal mode of SGL growth is through the accumulation of runoff, laterally transported due to elevation (hydraulic potential) gradients either by overland flow or in meltwater channels. The principal mode of melt pond growth is through enhanced melting at the lake bed and sides (Scott and Feltham, 2010). Melt ponds also grow through laterally transported runoff, however since sea ice is porous, the mechanism by which this occurs is lateral percolation, which is not a significant mechanism in SGL growth (e.g. Scott and Feltham, 2010, Luthje et al., 2006a). Likewise, SGLs also grow through enhanced melting, but the contribution of enhanced melting to lake growth is much smaller than that of runoff accumulation (Tedesco et al., 2012).

Lake growth from overland flow can be simulated by routing runoff over measurements of surface elevation. This can be achieved using a digital elevation model (DEM) where topography may be derived from a range of sources, including visual images (Skyllingstad et al., 2009), ice-penetrating radar data (Clason et al., 2012) or synthetic aperture radar (SAR) data (Luthje et al., 2006b). In order to redistribute runoff with respect to elevation/hydraulic gradients, a routing algorithm is required in conjunction with the DEM. This combination may be described as a hydrology model which may be simple or complex as appropriate. For runoff routing experiments where physical justification is not necessarily required, a simple parameterisation of flow rate, such as the prescription of a horizontal meltwater flux vector which is proportional to the surface gradient may be applied (Luthje et al., 2006b). The depth/volume of water in each grid cell is predicted at each time step by integrating this parameterised flux. Another possibility is the use of weighted flow accumulation based on the amount of meltwater generated and a single flow-direction routine (Clason et al., 2012). Both of these approaches benefit from being simple, however each method is somewhat empirical.

The model described in Banwell et al. (2012), which was developed at the same time as the work described in this thesis, routes meltwater by linking a lake and catchment identification algorithm with a flow delay algorithm. The lake and catchment identification algorithm calculates the path of flow from each cell by following the direction of steepest descent, until descent is no longer possible. The flow delay algorithm calculates the 'travel time' for water to follow this path of flow using Manning's equation for open channel flow and Darcy's law for flow through a porous medium and allocates water into lake cells on an hourly basis accordingly. This method improves on those described in Clason et al. (2012)

and Luthje et al. (2006b) by being more physically based. However, by not simulating the rate of change of water in each cell at each time-step, this method does not represent a full time-varying solution of water routing. In addition, physical parameters used in the flow delay equations are tuned to one specific lake filling event, which may be considered a weakness of the model when applied to a larger area.

Meltwater channels form from the accumulation of overland flow, in a network which follows the distribution of hydraulic potential on the ice sheet surface (Lewis and Smith, 2009, Paterson, 1994). These channels are typically of the order of metres in width and are consequently sub-grid scale features with respect to SGL evolution models (Clason et al., 2012, Banwell et al., 2012, Luthje et al., 2006b). Because of this, meltwater/runoff channels are not accounted for in the models of Luthje et al. (2006b) and Clason et al. (2012). Banwell et al. (2012) parameterise for channelised flow by switching between Darcy's law for flow through a porous medium when snow is present and Manning's equation for open channel flow where flow is over bare ice.

Enhanced melting is most properly calculated using a radiative transfer/energy balance type model which calculates the melt rate beneath, and at the sides of, the lake explicitly (e.g. Taylor and Feltham, 2004, Skyllingstad et al., 2009). A full, time-varying, physical solution is particularly important for sea ice melt ponds since the optical properties of sea ice vary dramatically as the season progresses. However, this is less important on ice sheets. This enables enhanced melting beneath SGLs to be more easily parameterised. One form which this parameterisation may take, is as a fraction of an enhanced melt rate, applied proportional to melt pond depth (e.g. Luthje et al., 2006a, Flocco and Feltham, 2007).

1.5.3 *Supraglacial lake drainage*

SGLs and sea ice melt ponds drain both laterally and vertically; albeit with different modes of behaviour. Drainage of sea ice melt ponds is well understood and may be modelled using Darcy's law for flow through a porous medium (Flocco and Feltham, 2007, Skyllingstad et al., 2009); where the rate of drainage is controlled by the hydraulic head of meltwater (height above sea level). The drainage of SGLs however, is less well understood. Two dominant modes of drainage have been proposed; rapid drainage through hydrofracture and less rapid drainage from channel incision (Krawczynski et al., 2009, Selmes et al., 2013). It is also reasonable to assume that some slow seepage occurs from lakes, particularly above the permanent snow line where firn is present. However this slow seepage may be ignored

since flow through a saturated snow/firn pack is much slower than open channel flow (Fountain, 1996), or drainage through hydrofracture (Das et al., 2008, Doyle et al., 2013).

Lake overspill is inherently represented in the DEM/flow routing approach; once a depression in which a lake may form is full, any additional water is passed downstream. Drainage via meltwater channels, a relatively recently proposed phenomenon, is more complicated. At present, this process is not included in SGL models since channels are typically a sub-grid scale feature. However, models which simulate the incision of meltwater channels specifically, e.g. Jarosch and Gudmundsson (2012), could be adapted for use in an SGL evolution model. Jarosch and Gudmundsson (2012) combine ice dynamics, open-channel hydraulics and heat transfer between runoff and ice to simulate channel evolution. Although their model is fairly complex, they identify channel slope, meltwater flux and meltwater temperature loss to the ice as the dominant factors which control channel evolution. This suggests that it is possible for a parameterisation to be developed based on these factors.

It has been theorised that rapid vertical drainage occurs when the volume of water held in a lake exceeds a critical value beyond which hydrofracture may occur (Krawczynski et al., 2009). However, this pre-supposes the existence of a crack/crevasse in the lake bed and (Selmes et al., 2011) observe that only 13% of lakes in south west Greenland, which contain enough water to propagate fractures, actually drain rapidly. It has been suggested that these cracks arise as a result of the tensile stress regime resulting from the flow of the ice sheet (Clason et al., 2012). However, lakes that by this metric should not have cracks, have nonetheless been observed to exhibit hydrofracture and subsequent rapid drainage (Doyle et al., 2013). Cracks and crevasses are difficult to capture with a numerical model (Clason et al., 2012). One approach to predicting the distribution of areas of surface crevassing is to use strain rates calculated from interferometric synthetic aperture radar (InSAR) velocity measurements (Clason et al., 2012). This method, however, is limited to locations in space and time for which InSAR velocity data are available. A simpler approach could be to prescribe a random distribution of cracks, based on the observed fraction of lakes that drain. A linear elastic fracture mechanics model may then be applied in order to calculate crack propagation (van der Veen, 2007). This simplistic approach could not be used for the study of individual lakes, although it may be of use in producing estimates of spatially averaged behaviour. Rapid vertical drainage is not included in the models of Luthje et al. (2006a) and Banwell et al. (2012).

1.5.4 *Supraglacial lake refreezing*

The proportion of SGLs which drain/refreeze is not well constrained (Johansson et al., 2013, Selmes et al., 2011), hence, refreezing has hitherto not been considered in models of SGL evolution (e.g. Luthje et al., 2006b, Banwell et al., 2012). Since the drainage of sea ice melt ponds is better understood, modelling strategies addressing their refreezing have been developed. Models of melt pond evolution, which treat melting as a two-phase (Stefan) problem, include refreezing naturally in the solution (Taylor and Feltham, 2004). Melt ponds freeze from the top downward after the initial formation of an ice 'lid'. Since melt ponds are large and shallow, it is assumed that they re-freeze completely and become part of the sea ice floe. Likewise, models which use a general energy balance method can initiate re-freezing when the energy balance becomes negative (Flocco and Feltham, 2007). The refrozen portion of meltwater is then applied to the top or bottom of the pond, as the model requires. This process could be adapted for SGLs, if it was known which and how many SGLs refreeze and which drain.

1.5.5 *Limitations of present supraglacial lake models and scope for improvement*

The primary knowledge gaps in current SGL modelling methods exist in the treatment of runoff production, flow routing methods, the potential for the model to be applied where in-situ meteorological observations are not available, and the absence of drainage and lake refreezing. Rae et al. (2012) determined that in order to accurately simulate runoff, a snowpack model is required which calculates retention and refreezing explicitly. None of the currently available SGL models include such processes. SGL evolution can occur over very short timescales (e.g. Das et al., 2008, Selmes et al., 2013) thus transient flow routing is also important. Two of the existing SGL models (Luthje et al., 2006b, Clason et al., 2012) parameterise flow routing, and although Banwell et al. (2012) do employ physically based flow routing, they do not explicitly model the full path of flow. In their model, water moves directly from its originating cell to its final destination (i.e. into a lake or off the ice). Each of the existing SGL models (Luthje et al., 2006b, Banwell et al., 2012, Clason et al., 2012) are forced by in-situ meteorological observations and consequently cannot be used to investigate SGL behaviour in the absence of such data, for example in regions of the ice sheet not served by automatic weather stations (AWSs) and under future climate scenarios.

The use of RCM simulated runoff as forcing data would address some of these concerns as RCMs provide good spatial coverage, at high temporal resolution, with full physical representation of snow and ice processes (e.g. Lefebre et al., 2005, van Meijgaard, 2008). In

addition, continuous data is available extending from pre-industrial times and projected up to 2100 for a range of climate change scenarios. Current methods of transient flow routing in SGL modelling may also be improved upon by the use of a physically based cellular flow routing model which 1.) uses hydrological laws (i.e. Darcy's law and Manning's equation) to calculate flow and 2.) also simulates water depth in each cell at each time-step, by integrating flux between cells and runoff produced within the cell (e.g. Bates and De Roo, 2000). A recommended method for a new model of SGL evolution was illustrated in Figure 1.10. It is not appropriate to include lake drainage and refreezing in SGL evolution models at present since processes which affect lake drainage are not well understood (e.g. Doyle et al., 2013, Clason et al., 2012), nor are they adequately constrained by observations for parameterisation to be possible (e.g. Selmes et al., 2011, Johansson et al., 2013).

1.6 Research aim and objectives

The overarching aim of this thesis is to improve scientific understanding as to the behaviour of SGLs with the aid of observations and model simulations of their temporal evolution. This thesis will focus on the Russell Glacier area of the GrIS since in this region, SGLs are abundant (e.g. Sundal et al., 2009), have been observed to exhibit rapid drainage behaviour (e.g. Doyle et al., 2013, Selmes et al., 2011), ice sheet flow exhibits seasonal and shorter-term variability (e.g. Palmer et al., 2011, Bartholomew et al., 2012) and a link between the drainage of SGLs and velocity changes has been observed in this region (Shepherd et al., 2009). In order to achieve the overarching aim of this thesis, the following four specific research objectives have been formulated:

1. **Create a new model of supraglacial lake initiation and growth.**
   Develop a novel algorithm to route runoff, taken from state-of-the-art RCM simulations, over high-resolution digital elevation data. The new model should physically represent both overland and open channel flow to route runoff, supraglacially into SGLs. This will enable the creation of maps of daily lake distribution for a continuous time period.

2. **Inter-compare satellite derived observations of SGL evolution and assemble a combined (optimised) dataset.** Systematically intercompare and evaluate available remotely sensed observations of SGLs in the Russell Glacier region of the GrIS. Assess variability in reported SGL characteristics (e.g. lake size and

reported lake frequency) between selected datasets. Combine several datasets to produce a single, robust and optimised SGL index spanning multiple years.

3. **Evaluate the lake evolution model with the aid of satellite-derived observations.** Evaluate the new model described in (1.) using satellite observations of high temporal resolution, including the combined SGL index described in (2.). Evaluate the model against one year of data in order to assess the model's ability to reproduce seasonal variability in SGL evolution. Evaluate the model against multiple years of data in order to assess the model's performance at the inter-annual timescale.

4. **Examine inter-annual and longer-term trends in supraglacial lake evolution.** Use the model described in (1.) to examine the relationship between SGLs and runoff over the 2001-2010 period. For example, SGL onset day in high/low runoff years. Use the model described in (1.) to investigate the response of SGLs to changes in climate over the 1971-2010 period. For example, the maximum elevation at which lakes are found.

1.7 Thesis structure

The remainder of this thesis seeks to fulfil the objectives presented in Section 1.6. In Chapter 2, a new 2-dimensional transient model of SGL evolution is described and evaluated scientifically. The model configuration is described and the recommended set-up is justified. In Chapter 3, this model is evaluated operationally, against one year of observations, densely sampled in time. This chapter also investigates the potential for this model to be applied inter-annually. In Chapter 4, an inter-comparison of SGL observations is performed using three separate, previously published, observational datasets derived from MODIS imagery. These data are combined to form a new, robust, three-year observational record of SGL evolution. In Chapter 5, this new observational record is used to extensively evaluate the model presented in Chapter 2 at the inter-annual timescale. Also in Chapter 5, the model and observations are used to investigate inter-annual and longer-term variability of SGL evolution, including an assessment of the response of SGLs to recent changes in climate. Finally, Chapter 6 summarises the contents of this thesis, draws conclusions from the work described therein and makes recommendations for further study.

Chapter 2

The Supraglacial lake Initiation and Growth (SLInG) model

2.1 Introduction

Supraglacial lakes (SGLs) are an annual feature on the Greenland ice sheet (GrIS) and provide temporary storage for runoff (meltwater + wet precipitation) before it leaves the ice sheet (e.g. Echelmeyer et al., 1991, Sundal et al., 2009, Liang et al., 2012). SGLs are of interest due to their role in the supraglacial hydrological network and because they affect the mass balance of the GrIS, by reducing area-averaged albedo and perturbing ice sheet velocity when they drain rapidly through hydrofracture (Das et al., 2008, Doyle et al., 2013). Current scientific understanding on the evolution of SGLs is based on a number of observational studies (e.g. Das et al., 2008, Sundal et al., 2009, Selmes et al., 2011). Modelling SGLs is desirable, in conjunction with observations, in order to produce a continuous time series of lake evolution. Furthermore, models can be used when/where observation is not possible, for example, to provide information on days when cloud cover inhibits the retrieval of satellite observations (a known limitation of the observational record). In particular, modelling in conjunction with observations allows insight into drainage behaviour, which may have implications for ice sheet dynamics. Finally, the development of an SGL modelling framework will allow for forward projections in time. For example, to study possible changes to SGL behaviour under future, warmer, climates.

Models of SGL evolution need to consider the life cycle of SGLs, from runoff production to drainage or re-freezing. Previously published models of SGL evolution disregard the rainfall element of runoff and have focused on simulating the production of meltwater. Meltwater production in these models is commonly calculated using in-situ point observations of incoming and outgoing radiation in an energy balance model (Banwell et al., 2012, Selmes et al., 2011, Luthje et al., 2006b). While this is physically based, it precludes the use of such a model for forward prediction. These models also typically use empirical methods to route the simulated meltwater into lakes (Luthje et al., 2006b, Clason et al., 2012). In reality, meltwater routing is a function of hydraulic gradient, water depth and surface type, all of which are transient properties. The primary aim of this thesis is to develop a novel 2-dimensional (2-D) fully transient hydrology model capable of

dynamically routing runoff estimated using a regional climate model (RCM), allowing water to pool in topographic depressions forming SGLs.

The remainder of this chapter describes this 2-D transient hydrology model, which simulates Supraglacial Lake Initiation and Growth (hereafter the SLInG model). The SLInG model uses Manning's equation for open channel flow (Manning, 1891) and Darcy's law for flow through a porous medium (Chow, 1988) to route RCM simulated runoff over a digital elevation model (DEM) of the ice sheet. If snow is present (or absent) in the cell, according to the RCM output, Darcy-type flow (or Manning-type flow) is assumed. As runoff collects in intransient depressions in the elevation model, SGLs are formed. In this thesis, the model is applied to a region of the GrIS in the region of Russell Glacier, which incorporates much of that glacier's catchment. However providing sufficient forcing data (i.e. RCM output and a high resolution DEM) is available, the model may be used to simulate water routing over any freshwater ice surface. In this thesis, the MAR (Modèle Atmosphérique Régional) RCM (Lefebre et al., 2005) is used to provide runoff, snow depth and snow density forcing, and the high resolution DEM of Palmer et al. (2011) is used to represent the ice sheet surface. Section 2.2 of this chapter details the model architecture and includes a full description of the mathematical equations used to calculate the flow of water between model grid cells. Section 2.3 describes the data used to force the model in simulations described in this thesis. Section 2.4 explores the model setup, both generally and in the context of this application to the Russell Glacier region and provides scientific evaluation of the model configuration (for example the value of Manning's 'n' used in the model). Section 2.5 discusses the limitations of the model and Section 2.6 provides a summary of the work featured in this chapter. The majority of the work contained in this chapter has been published in the journal The Cryosphere (Leeson et al., 2012).

2.2 Model processes

The SLInG model, further described in this chapter, is a 2-dimensional transient hydrology model that employs Universal Transverse Mercator (UTM) coordinates on a regular grid of 100 m spacing. SLInG is composed of three main algorithmic elements; flow direction, water displacement and lake accumulation. These are considered in turn and each execute in a cell-wise manner. Firstly, each cell is assigned a flow direction based on steepest slope downward. Secondly, the water displacement between each cell and its destination cell is calculated. Finally, the lake accumulation algorithm identifies hydrological sink cells and designates water contained in them as lake/not-lake water as appropriate. This is repeated at

90 second intervals until at the end of each model day, SGL distribution is retrieved. The remainder of this section describes these algorithms in more detail.

2.2.1 *Flow direction algorithm*

The first step the model takes is to assign a flow direction to each cell based on free surface (ice + lake + water) slope. It is assumed that water can flow east-west, north-south or diagonally (Figure 2.1). The algorithm works on a cell-wise basis; it assigns a flow direction to each cell, which is towards the neighbouring cell with the lowest-lying free surface, with respect to the cell under consideration (cell a). If the cell itself is the lowest lying, then it is a 'sink' cell and the water it contains does not leave the cell (cell b). If the cell under consideration is at the border of the study area, i.e. has at least one 'no data' cell surrounding it, water is assumed to have been moved out of the study area/off the ice sheet (cell c).
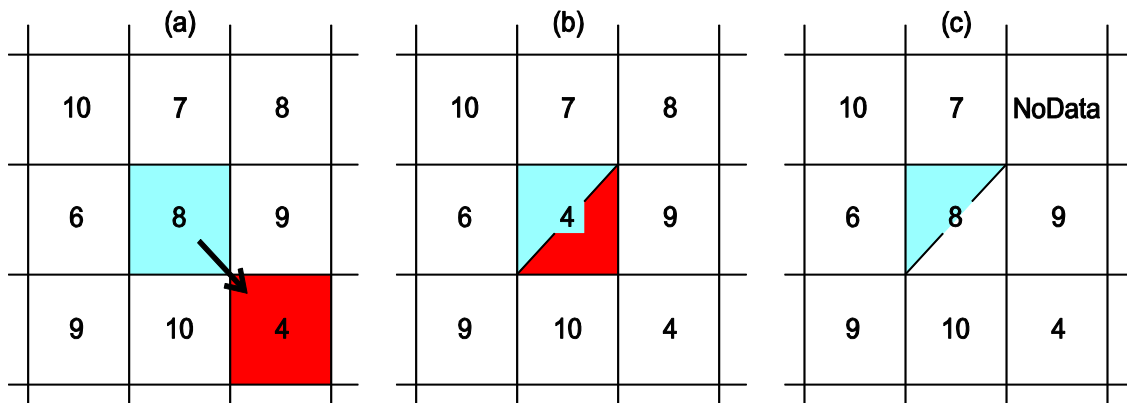
Figure 2.1: Schematic of possible flow options. Cells coloured blue are the originating cells, cells coloured red are the destination cells. Numbers indicate arbitrary surface heights. (a) Flow into lowest lying neighbour, (b) Sink cell, water stays in cell, (c) Border cell, water is assumed to leave the study area.

2.2.2 *Water displacement algorithm*

Water displacement is also calculated on a cell-wise basis. Typically, RCMs which have been developed to simulate the climate in the polar regions, such as MAR and RACMO (Regional Atmospheric Climate Model) (Ettema et al., 2010), feature a comprehensive snow model which includes retention and refreezing. This means that SLInG is able to use RCM estimates of runoff production directly. In order to estimate the change of water volume in any given cell, flux out of the cell is combined with the rate of runoff production within the cell, and the resulting equation is solved to estimate the change of volume within the cell for a given time-step. Volumetric flow rate, or flux, Q, can be calculated using Darcy's law for

flow through a porous medium (Chow, 1988) where snow is present in the cell. Where the cell is bare ice, Q can be calculated using Manning's equation for open channel flow (Manning, 1891) and the relationship $Q = Av$, where A is cross sectional area of the channel, and v is velocity of flow. In both cases flux is proportional to free surface slope, S, which is calculated by dividing the hydraulic head $z_a + d_a - z_b - d_b$ by the path length of flow, P (Figure 2.2).
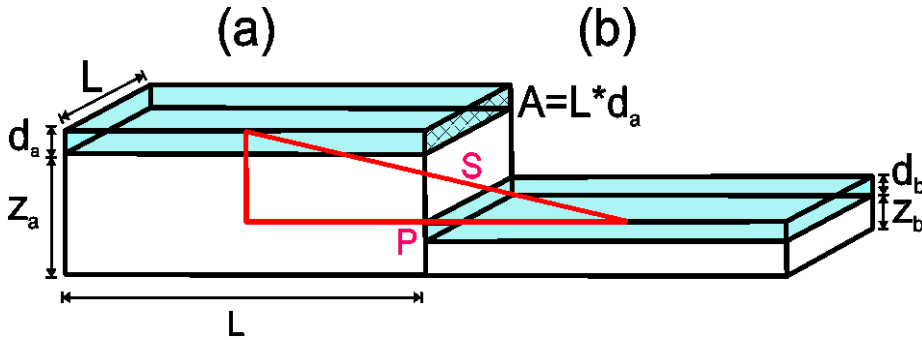
Figure 2.2: Two cell schematic illustrating parameters used to calculate flow rate. S is free surface slope between the two cells (a and b), A is cross sectional area of flow, L is the length of a side of the square cell and z and d are ice/lake surface height and depth of free water in the cell.

The path length is L for flow between cells which share a border and $\sqrt{2L^2}$ for cells with a diagonal path. The rate of change of depth ($\dot{d}$ -dot notation is used to denote the time derivative), due to flow out of the cell, can be calculated by stating that the volumetric flow rate is equal to the rate of change of depth multiplied by the surface area of the cell L^2 (Equation 2.1).

$$\dot{d}^{out} = \frac{Q}{L^2}$$
2.1

There is also likely to be a change in depth due to runoff production within the cell. Runoff produced within the cell through melting or precipitation is provided by an RCM in mm of depth per day. The contribution to depth change, in mm s^{-1}, from both of these mechanisms is therefore given in Equation 2.2.

$$\dot{d}_a = \frac{1}{L^2} \cdot Q + \frac{\dot{d}_a^{MAR}}{86400}$$
2.2

Because Q is proportional to surface slope, which is described as a function of two

independent variables, d_a and d_b, an additional equation is required in order to integrate

2.2 with respect to time. Equation 2.2 can be rewritten for d_b because $\dot{d}_b^{FLUX} = -\dot{d}_a^{FLUX}$,

the water that leaves cell (a) must arrive in cell (b).

$$d_b = -\frac{1}{L^2} \cdot Q + \frac{\dot{d}_b^{MAR}}{86400}$$ 2.3

This gives a system of coupled differential equations that are integrated with respect to a given time-step using a fourth order Runge-Kutta (RK4) approximation.

It is possible that one cell receives water from many contributing cells. The new depth of water in any given cell, n, at time, t, is calculated using Equation 2.4. Equation 2.4 adds the summation of water passed into the cell from its neighbours (if any) and the amount generated by the RCM within the cell, to the depth of water at time, $t = 0$, and then subtracts the displaced water due to flow. A condition is imposed where, if the calculated amount of displaced water is more than the sum of the depth of water in the origin cell at time, $t = 0$, and the water generated within the cell by the RCM, only the original cell content plus RCM generated runoff is displaced.

$$d_n^t = d_n^0 + \sum d_n^{in} + \int_0^t \dot{d}_n^{MAR} - \int_0^t \dot{d}_n^{out}$$ 2.4

The rest of this section describes the flux equation with respect to Darcy and Manning type flow.

2.2.2.1 Darcy's law for flow through a porous medium

As discussed, the model developed in this thesis is forced using runoff simulated by an RCM. Most RCM (e.g. MAR, RACMO) simulated runoff occurs over bare ice, however, runoff can occur over snow when the snow pack has a high liquid water content (6% or greater in MAR). The model assumes Manning-type flow if simulated snow depth is less that 20% of the runoff depth. If snow depth is greater than 20% of runoff depth, the model calculates flow velocity using Darcy's Law (Equation 2.5) (Chow, 1988). In Section 2.4.4, the sensitivity of the model to this 20% switch threshold is tested.

$$Q = \frac{kA}{\mu} S$$ 2.5

Here, A is the cross sectional area of flow (Figure 2.2), μ is the viscosity of water, taken here to be 1.763 x 10^{-3} Pa s, and k is the permeability of the snow. Permeability is determined using Shimizu et al (1969) who experimentally derived a relationship (Equation 2.6) between permeability and specific gravity of snow, ρ_s^*, and snow grain size, n. In this study, snow density is simulated by the RCM and a snow grain size of 1 mm is assumed. Section 2.4.6 tests the sensitivity of the model to this assumed snow grain size.

$$k = 0.077n \cdot e^{(-7.8\rho_s^*)} \qquad\qquad 2.6$$

Because,

$$A = d_a \cdot L, \qquad\qquad 2.7$$

and,

$$S = \frac{z_a + d_a - z_b - d_b}{P}, \qquad\qquad 2.8$$

where terms are as before, by substituting 2.6, 2.7 and 2.8 into 2.5 and 2.5 into 2.1, the rate of change of depth in cell (a) due to flow between cells (a) and (b) can be expressed as:

$$\dot{d}_a = \frac{k}{L\mu P} \cdot (d_a^2 - d_a d_b + d_a(z_a - z_b)) \qquad\qquad 2.9$$

2.2.2.2 Manning's equation for open channel flow

If according to the RCM, the snow depth in the cell is less that 20% of the runoff depth, the surface is assumed to be bare ice and Manning's equation for open channel flow is applied (Manning, 1891):

$$v = \frac{1}{n} R_h^{2/3} S^{1/2} \qquad\qquad 2.10$$

Where v is the cross sectional average flow velocity, n is 'Manning's n', an experimentally derived roughness co-efficient accounting for channel friction, S is as previously defined and R_h is the hydraulic radius of the 'channel' which can be approximated by depth of flow for wide, shallow channels. In this study, n takes the value 0.011; the midpoint of a range of n values (0.01-0.012) derived experimentally for ice by Lotter et al (1932). Section 2.4.5 discusses the sensitivity of the model to a range of n

values. The flux can be calculated by multiplying velocity by cross-sectional area of flow (Equation 2.11).

$$Q = Av$$

2.11

Here, $A = d_a \cdot L$. By substituting Equation 2.10 into 2.11 and 2.11 into 2.1, the rate of change of depth in cell (a) due to flow between cells (a) and (b) can be expressed as:

$$\dot{d} = \frac{1}{LnP^{1/2}} \cdot d^{5/3} \cdot (d_a - d_b + z_a - z_b)^{1/2}$$

2.12

2.2.3   *Lake accumulation algorithm*

Flux is modelled using a one-dimensional approximation; only the amount of outgoing water is explicitly calculated at each time-step. A result of this is that while water flowing *out of* a cell only has one destination, many cells may flow *into* the same cell. This also means that while the solution ensures that the cell under consideration is in hydraulic equilibrium with respect to its destination cell, it is not necessarily in hydraulic equilibrium with respect to the other cells that surround it. This results in no natural pooling occurring within the solution. Since the pooling of water is a desired outcome, a lake formation algorithm forms the final stage of the model. At the end of each time step, after the flow from each cell has been calculated, an iterative accumulation algorithm brings water together into lakes. In a similar manner to the flow direction algorithm, each cell is considered in turn and assigned sink/non-sink status based on the free surface height of its nearest neighbours. If a cell is found to be a sink, water sufficient to fill the cell to the height of its lowest lying nearest neighbour, is designated lake water and incorporated into the DEM of the fixed surface. The algorithm loops round the cells repeatedly until all sinks are filled, both original sinks and new sinks resulting from the filling of the old sinks. Once all possible lake water (runoff which 'fills' a depression) has been accumulated, the time-step is advanced and the program begins again.

2.2.4   *Drainage, refreezing and end of life processes*

At this time, the SLInG model simulates only lake growth, and does not incorporate end of life processes. This includes refreezing and processes leading to lake drainage, which is known to be an aspect of the seasonal cycle of some lakes (e.g. McMillan et al., 2007, Georgiou et al., 2009, Sundal et al., 2009, Selmes et al., 2011). In consequence, while the

SLInG model provides information about the location, onset, and cumulative area of SGLs, it cannot fully simulate the evolution of lakes. The conditions required to promote rapid drainage are not well understood (Clason et al., 2012), nor is the percentage of lakes which do drain well quantified (Selmes et al., 2011, Johansson et al., 2013). Therefore, at present, given this large uncertainty, it is inappropriate to include drainage in the SLInG model, either explicitly or as a parameterisation. Lakes refreeze from the top down; an ice lid forms on top of the lake and this grows downwards. Lid growth rate can be determined as a function of the lake surface temperature, which can be calculated from a surface heat budget using meteorological parameters from MAR. However, since it is not known which lakes refreeze and which lakes drain, it is also inappropriate to include refreezing in the SLInG model at this time.

2.3 Model domain and forcing data

In this thesis, the SLInG model is applied to a 6,753 km^2 region of western Greenland where SGLs are abundant (Sundal et al., 2009) and for which fine spatial resolution elevation data are available (Palmer et al., 2011). This incorporates much of the area of the Russell Glacier catchment (Figure 2.3). In this region, the ice sheet elevation ranges from 1100 to 1752 metres above sea level (m a.s.l.). This entire region experiences temperatures above freezing during the ablation season, leading to abundant melting and runoff. The model domain uses the UTM projection system and is represented on a grid of square cells of length 100 m; the finest resolution of the DEM. Prior to being input to the model, forcing data is re-projected, where necessary, into the UTM and re-sampled to the model grid. In the remainder of this section, these data are described and any potential sources of error, which may affect model performance, are discussed.

2.3.1 *InSAR digital elevation model*

The DEM used by SLInG is derived from interferometric synthetic aperture radar (InSAR) data acquired by the European Remote Sensing satellites in 1996 (Palmer et al., 2011). The DEM uses the UTM projection system and is posted at a grid resolution of 100 m. InSAR DEMs are derived using differential interferometry, a technique which is able to reproduce relative surface elevation using the difference between two pairs of radar images, which have been superimposed in order to be able to resolve phase information about the returned radar data (e.g. Mather, 2004, Kwok and Fahnestock, 1996). This information is then translated to the earth's surface using a number of ground control points (GCPs), where

independent estimates of surface elevation have been made by e.g. GPS or altimetry measurements. Potential sources of uncertainty in an InSAR DEM include the distance in space between each pair of images (baseline length), how well each image pair agrees on the returned radar signal (coherence), accuracy and number of GCPs, and penetration of the radar signal below the surface (e.g. Zebker et al., 1994, Massom and Lubin, 2006). Examples of these uncertainties with respect to the DEM in this study are given here.

Based on a comparison with airborne laser altimeter data, it has been estimated that DEMs formed from repeat pass InSAR data achieve a relative accuracy of between 2.5 m and 10.0 m, depending upon the length of the perpendicular baseline of the InSAR data (Joughin et al., 1996). In the present example, the DEM was formed with a perpendicular baseline of 120 m, and the associated relative accuracy is estimated to be 10.0 m. Radar elevation measurements correspond to horizons at depth relative to the ice sheet surface, due to penetration of the microwave signal into the snowpack. C-Band radar, such as that used to derive the DEM in this study, can penetrate as deep as 35 m in Greenland (Hoen and Zebker, 2000), but has a typical penetration depth of 0-3 m in the ablation zone and ~10 m in the accumulation zone. A study of InSAR derived topography has demonstrated that this horizon follows that of the ice sheet surface (Rignot et al., 2001). This is because topography is strongly correlated with basal conditions that are transmitted through the ice (Gudmundsson, 2003).

The DEM has been smoothed to reduce noise due to, for example, incoherent pixels in the interferogram, using boxcar averaging across a moving 5 pixel (500 m) window. While this process increases the signal-to-noise ratio, it may also result in a reduction in amplitude and an increase in bandwidth. As a result, depressions in the DEM in which lakes may form, may be artificially wide and shallow with respect to the actual ice sheet surface. However, given that the smoothing window (500 m) is on a much smaller spatial scale than the mean ice sheet gradient (~4 m per 1 km), the smoothing process is unlikely to affect large-scale topographic gradients, and as a corollary, water routing. Unrealistically large gradients exist in the DEM at the data coverage margin, which arise as an artefact of smoothing. The impact of these gradients on the model is minimised by removing all cells that exhibit gradients that differ by more than one standard deviation from the local mean. This removes a margin of 1-3 cells around the ice edge only.

The DEM was evaluated using 1689 points of known elevation from ICESat altimetry measurements (Palmer, pers. comm.). These data were also used to provide an overall uncertainty estimate. DEM heights were found to correlate very strongly with ICESat

elevation measurements (r=0.99), and a root mean square deviation (RMSD) of 19.6 m was calculated between DEM surface heights and observed values. SGLs form in depressions that are lower lying with respect to the surrounding surface; consequently, uncertainty in the DEM applies to the lake, as well as to the surrounding ice. In this thesis, it is assumed that topographic depressions in which lakes could potentially form are resolved with respect to the local topography of the ice sheet.
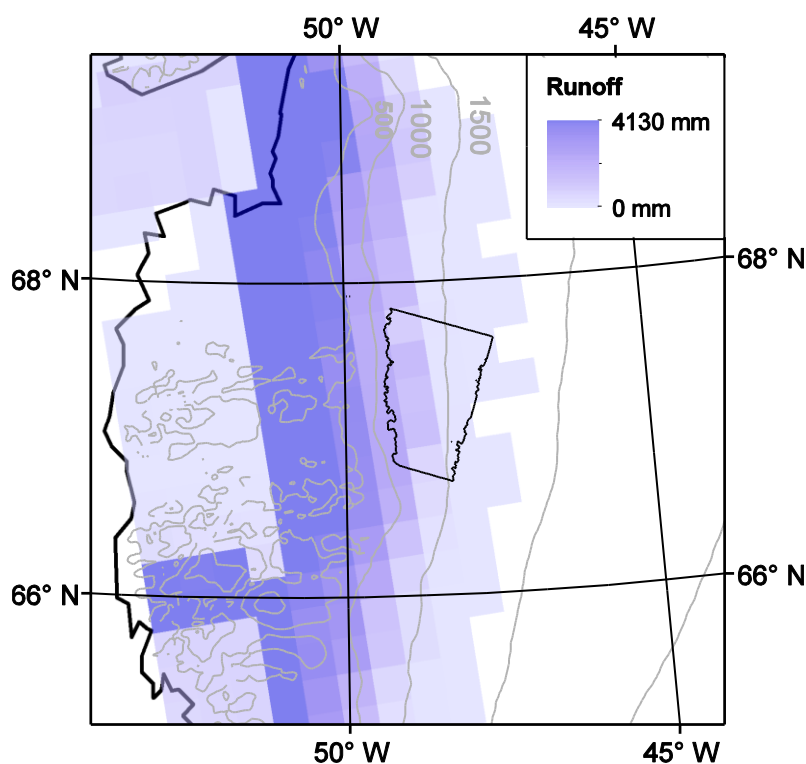
Figure 2.3: Map indicating study area considered in this chapter. Elevation contours at 500 m intervals from 500 m a.s.l. taken from Bamber et al. (2001), also shown is the MAR simulated total runoff for 2003 (blue -white areas represent zero runoff) and the DEM used in this study (bounded in black).

2.3.2   *MAR simulated daily runoff, snow depth and snow density*

SLInG uses estimates of surface runoff, snow depth and snow density derived from the MAR RCM, run at 25 km resolution over Greenland (Fettweis, 2007, Fettweis et al., 2011). MAR is a dynamic downscaling RCM, which takes a limited geographical area at fine spatial and temporal resolution, and embeds it in a global general circulation model (GCM) on a coarse grid/timescale. Atmospheric conditions such as temperature and pressure at the boundary of the RCM are prescribed every six model hours by the GCM, and additional physics is employed to downscale these data to a finer spatial and temporal resolution.

MAR is forced at the boundaries by the European Centre for Medium-Range Weather Forecast (ECMWF) ERA-Interim reanalysis. The runoff product provided by the MAR model has been calculated using a snow and ice model, which accounts for retention, percolation and refreezing of melt-water (Lefebre et al., 2003).

At the scale of the whole ice sheet, the uncertainty in surface mass balance (SMB; precipitation-runoff) values simulated by MAR has been estimated to be ~10% (Fettweis et al., 2013). Locally, this uncertainty could be higher, however MAR simulated SMB in this particular region of the GrIS is known to compare very well with observations (Vernon et al., 2013, Tedesco and Fettweis, 2012). In fact, when compared to field estimates taken along the K-transect (located in this region), MAR is found to reproduce annual mass growth to within 24% of observed values (Vernon et al., 2013). In the same study, the RACMO, Fifth-generation Polar Mesoscale Model (PMM5, Box et al., 2009) and ECMWF-downscale (Hanna et al., 2002) models were found to perform less well, reproducing annual SMB rates to within 38%, 29% and 95% respectively. In a similar study, MAR is also shown to out-perform two additional RCMs; the HadRM3P (a regional model based on the Hadley Centre Coupled Model version 3, HadCM3) and HIRHAM5 (a coupled version of the High Resolution Limited Area Model, HIRLAM and the ECHAM5 global model), in terms of reproducing observed SMB (Rae et al., 2012). Although runoff from MAR has not been explicitly validated due to a paucity of observations, it is known that runoff estimates contribute the greatest amount of uncertainty to MAR simulated SMB values, because of the use of a constant bare ice albedo in MAR (Fettweis et al., 2011). Therefore, it is reasonable to propose an upper limit to the uncertainty in MAR simulated runoff of 10%. Fettweis et al. (2011) have shown that the daily melt extent simulated by MAR compares well with that derived from satellite data over the period 1979-2009.

Although MAR, when run at 25 km resolution, has been shown to reproduce SMB successfully in general, it is less certain that MAR is able to resolve the steep SMB gradient close to the ice sheet margin. Franco et al (2012) perform simulations using MAR at a range of resolutions and find, by comparison with observations taken along the K-transect, that a 25 km resolution simulation is not fine enough to resolve SMB very close to the ice margin. Because of this, there is less confidence in runoff estimates for the region of the ice sheet situated below 1100 m a.s.l. (25 km and 1 grid cell away from the margin). Above this level, surface gradients are shallow; the mean west-east elevation gradient between 1100 and 1700 m a.s.l. in the study area is ~0.4%. Fausto et al (2009) calculated a lapse rate of -6.8°C (+/- 2.5) per 1 km in altitude over the GrIS. This suggests that along a 25 km transect of the

GrIS, between 1100 and 1700 m a.s.l., temperature range due to changing elevation is just 0.68°. And so, a 25 km grid box is able to adequately resolve temperature, which gives confidence in the resolution of other SMB components. A mean bias of -4% (-30 m) exists between the DEM and MAR topography, above 1100 m a.s.l.. However, DEM and MAR topography are very strongly correlated (r=0.93) and have similar mean west-east elevation gradients, 0.31% and 0.37% respectively. Applying the lapse rate of Fausto et al. (2009), over the longest east-west transect (77.7 km), the combined effect of the mean bias and elevation gradient would result in a temperature difference of 0.05°C, between MAR and DEM surfaces, at the most easterly end of the transect. Because this difference is small, and melting is correlated with temperature (Reeh, 1991), it is reasonable to use MAR data to represent runoff production over the DEM surface. The MAR data is re-projected and oversampled to the model domain before being supplied to the surface for routing.

2.4 Model configuration and source of parameters

The current model setup benefits from an extensive period of development and testing. This section justifies the choice of the current configuration, including the parameters used within the model. Details are provided specifically regarding the temporal resolution of the model, the sensitivity of the model to forcing (runoff and digital elevation) data, and the method by which flow is assigned to be Darcy/Manning type flow. Parameters which may take a range of values, such as snow density, snow grain size and Manning's n are used in the model equations. Therefore, here, the values used for these parameters are justified, and the sensitivity of the model output to chosen values is investigated. Observations of SGL evolution in 2003 are used to justify the model configuration where appropriate. These observations consist of a time series of daily SGL distributions, derived from Moderate-Resolution Imaging Spectroradiometer (MODIS) imagery and were described further in Chapter 1 (Sundal et al., 2009). All model simulations in the remainder of this chapter have been performed for 2003.

2.4.1   *Runoff (forcing) data*

Runoff is generated in each model cell at a constant rate, calculated using daily values supplied by MAR. In reality, runoff production exhibits a diurnal cycle (Figure 2.4). The model dependency on this constant rate of runoff was tested by running the model twice using a one-hour time-step. The first simulation was forced by hourly MAR runoff rates, and the second simulation was forced by a constant daily rate of runoff calculated from the

hourly MAR output integrated over a 1-day period. On average, the 24-hour sum of hourly output is 6% smaller than the daily output, this is likely due to missing time-steps (of 120 s each) in the hourly output and can be considered a programming error (Fettweis, pers. comm.). This is within the 10% uncertainty range in MAR generated runoff estimates proposed by Fettweis et al. (2013).
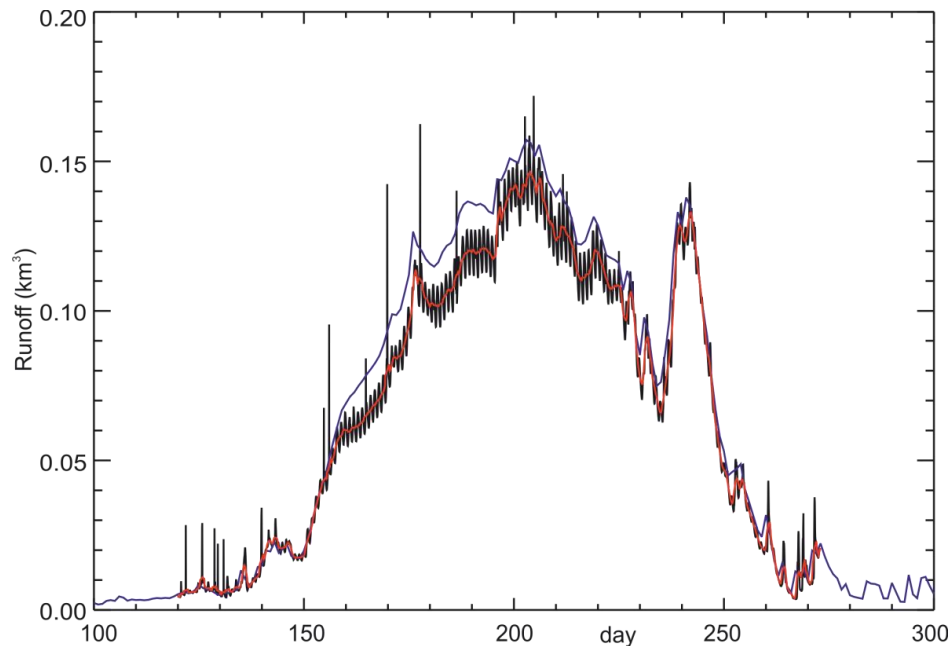
Figure 2.4: Hourly runoff integrated over the study area. Hourly runoff simulated by MAR (black), 24 hour low pass filter through these data (red), hourly runoff calculated from daily MAR output, assumed to be generated at a constant rate throughout the day (blue).

Less than 1% difference was found between simulations using hourly- and daily- data in all metrics applied. This suggests that in the experiments described in this thesis, the accumulation and routing of meltwater over the surface is not perturbed by small changes in runoff amount, and, that this process dampens out the diurnal signal of runoff production, with respect to the growth of supra-glacial lakes. Consequently, in the SLInG model, they exhibit no diurnal variability in their evolution. This is of course, limited to this model and may not be the case for lakes that drain.

Because MAR estimated runoff data have not been independently evaluated, simulations were performed with fixed fractions of runoff amount, including a doubling of runoff, and then compared to the observations of Sundal et al. (2009). The MAR model can, for example, overestimate the quantity of runoff by up to ~ 10 % (Fettweis et al., 2013) due to the use of a constant bare ice albedo (~0.45) for the entire bare ice area of the GrIS (Fettweis et al., 2011). Simulations were performed, in which the runoff predicted by MAR was

scaled by the following factors, 2.0, 1.5, 1.0, 0.75, 0.5 and 0.25. The location of SGLs shows little dependence on the amount of runoff supplied to the ice sheet surface, when that amount is between half and double that predicted by MAR; 64-66% of simulated lakes are co-located with observations for scaling factors of 0.5-2.0 the MAR simulated runoff. These sensitivity tests indicate that lakes would still form in the spatial patterns observed under a wide range of runoff scenarios, allowing for relative uncertainty in the forcing data.

Maximum simulated lake area is the metric upon which modifying the runoff amount has the most significant impact (Figure 2.5); in these simulations maximum lake area is directly correlated with runoff quantity ($r=0.96$). This suggests that in high runoff years, SGLs may be expected to grow larger. This is in agreement with the findings of Sundal et al. (2009) who find a positive correlation between runoff amount and maximum SGL area in their observational study of SGL evolution. In addition, lake onset is initiated sooner with an increase in runoff amount occurring approximately on days 153, 154, 155, 157, 159 and 160 when the runoff is scaled by 2.0, 1.5, 1.0, 0.75, 0.5 and 0.25, respectively. This is in agreement with the findings of Johansson et al. (2013) who find that lake growth is consistently initiated after 40 (+/-18.5) positive degree days. In high runoff years, this threshold would most likely be reached earlier.
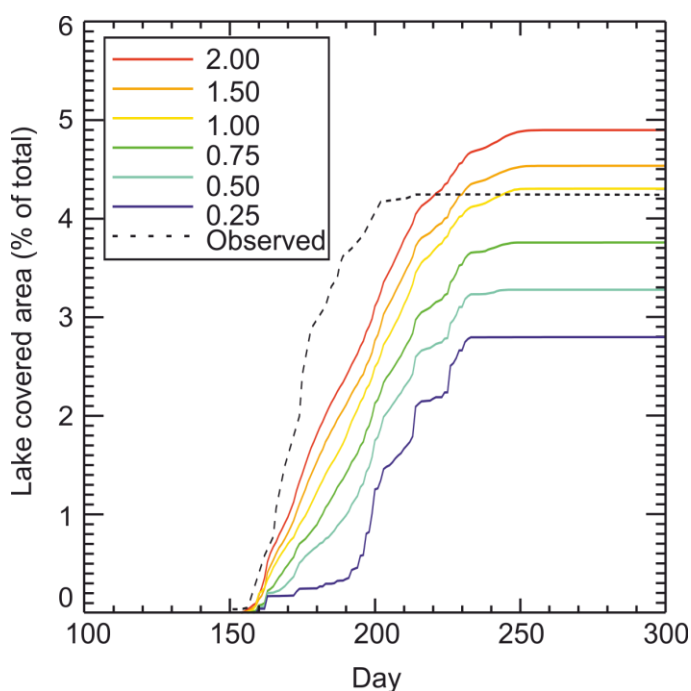
Figure 2.5: Sensitivity of modelled lake covered area with respect to runoff amount. Presented here are lake area profiles simulated by SLInG, when using the full runoff amount and runoff scaled by factors of 2, 1.5, 0.75, 0.5, and 0.2. Also shown is the cumulative lake area profile, derived from observations of Sundal et al. (2009) (black dashed).

2.4.2   *Spatial resolution of digital elevation model*

In order to test the sensitivity of the model to DEM resolution, simulations are performed using SLInG and four DEMs with a range of spatial resolution. This comparison study uses a grid of square cells of length 100 m (standard resolution), 300 m, 500 m and 1000 m. In these experiments, the resolution of the DEM is reduced by neighbourhood averaging.
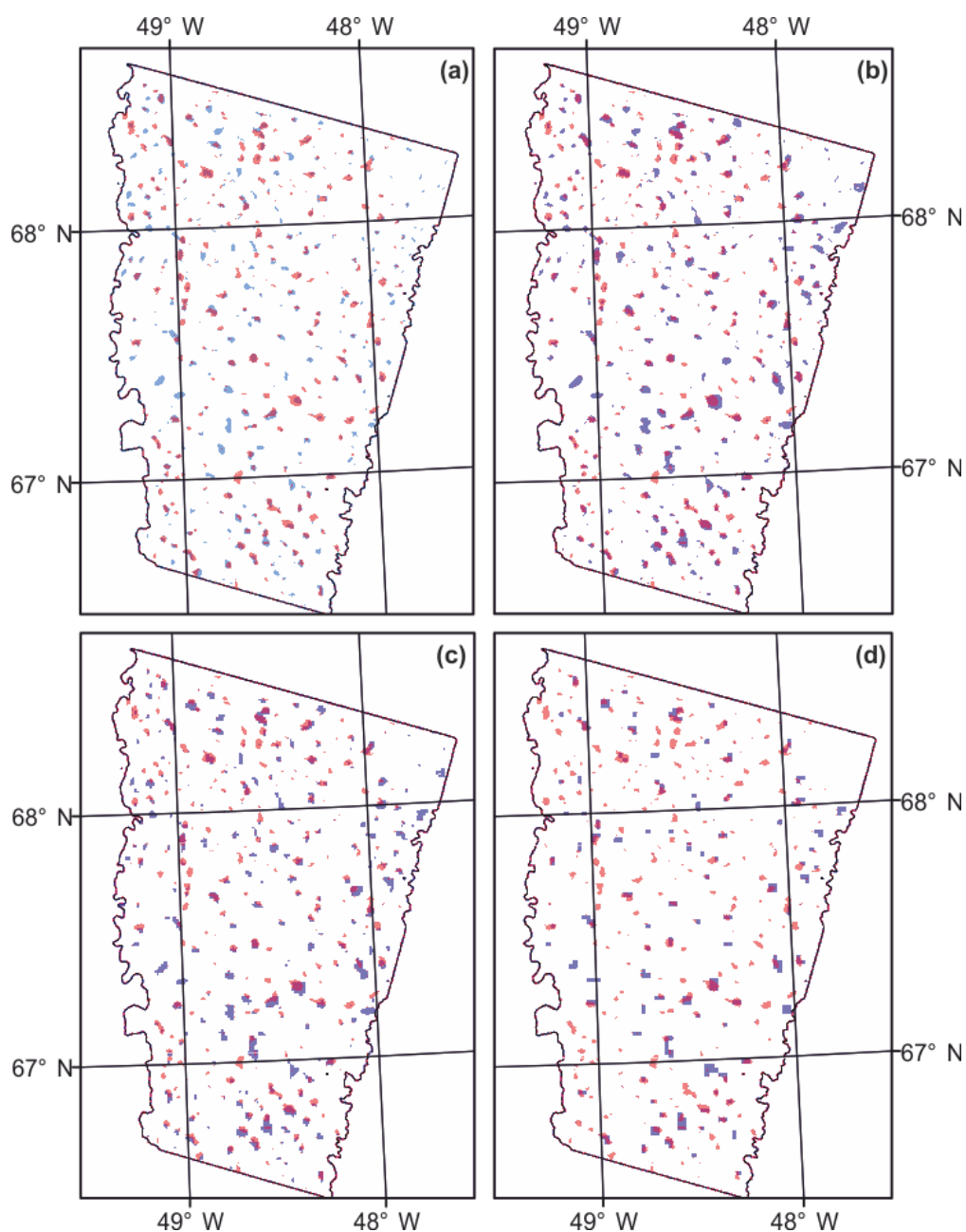
Figure 2.6: Distribution of SLInG simulated lakes (blue) for the year 2003 modelled at a resolution of (a) 100 m, (b) 300 m, (c) 500 m and (d) 1000 m. Also shown are lakes observed in Sundal et al. (2009) (red), and the area coincident in both modelled and observed lake distribution (purple).

SLInG, when using a DEM posted at 300 m, performs reasonably well when compared to observations (Figure 2.6). SLInG co-locates 54% of observed lakes, just 28 less lakes than are resolved using a posting of 100 m (Table 2.1). Simulated maximum lake covered area is 0.4 km^2 greater than that using the DEM posted at 100 m, despite these 'missing' lakes. This suggests that the neighbourhood averaging method smooths out some of the smaller depressions in the DEM and that the depressions that remain are artificially large, with respect to the original DEM. A posting of 500 m results in a significant reduction in model skill, co-locating just one third as many lakes as SLInG simulations performed using a DEM of the standard resolution of 100 m. It is interesting to note that although the 1000 m resolution DEM reproduces much fewer lakes than the finer resolution models, it does successfully simulate 43 (18%) of them. It is likely that all 43 lakes which are successfully simulated at 1000 m resolution exhibit drainage behaviour; a lake of this size is certain to hold enough water volume to enable hydrofracture (Krawczynski et al., 2009). The correlation between simulated and observed lake onset day is high using a DEM at all four resolutions (r > 0.79). However, it is important to remember that this figure is based only on those lakes that are successfully located, the number of which reduces as the DEM resolution becomes coarser. These results suggest that reasonable results may be obtained using SLInG with a DEM posted at 300 m, which may be useful if SLInG is applied to large areas.

Table 2.1: Impact of DEM resolution on model skill. For the four metrics reported, only lakes larger than 0.125 km^2 are considered.

	DEM Posting (m)			
	100	300	500	1000
Maximum lake covered area (% total)	4.5	4.9	2.8	0.9
Observed lakes also modelled (number)	159	131	82	43
Observed lakes also modelled (%)	66	54	34	18
Correlation between simulated and observed onset dates.	0.83	0.79	0.79	0.87

2.4.3   *Temporal resolution of model*

Free surface gradients are found to be large between some cells and, using the SLInG model,

the maximum travel distance of the water is limited to one cell at each time-step. This imposes the requirement of a fine time-step in order to represent the full flow path of the water; with a coarse time-step, the flow is artificially retarded. However, computational expediency prevents the operation of the model at very fine, e.g. 1 second, resolution. In order to test the dependence of the model on choice of time-step, a simulation was performed for one day, day 196 (in the middle of the melt season), using a time-step of 60, 90, 120, 180, 210 and 600 seconds. The proportion of cells where all the water was displaced in each simulation was noted (Figure 2.7). Incomplete flow occurs in a greater proportion of cells when the time-step is increased. The use of a 600 second time-step meant incomplete flow was observed in over 20% of cells, which is unacceptable. Using 0.5% incomplete flow as an acceptable level of accuracy, 90 seconds was chosen as the standard time-step. The use of an RK4 approximation to integrate the flow rate equation, over an implicit solution, may also contribute to the development of incomplete flow.
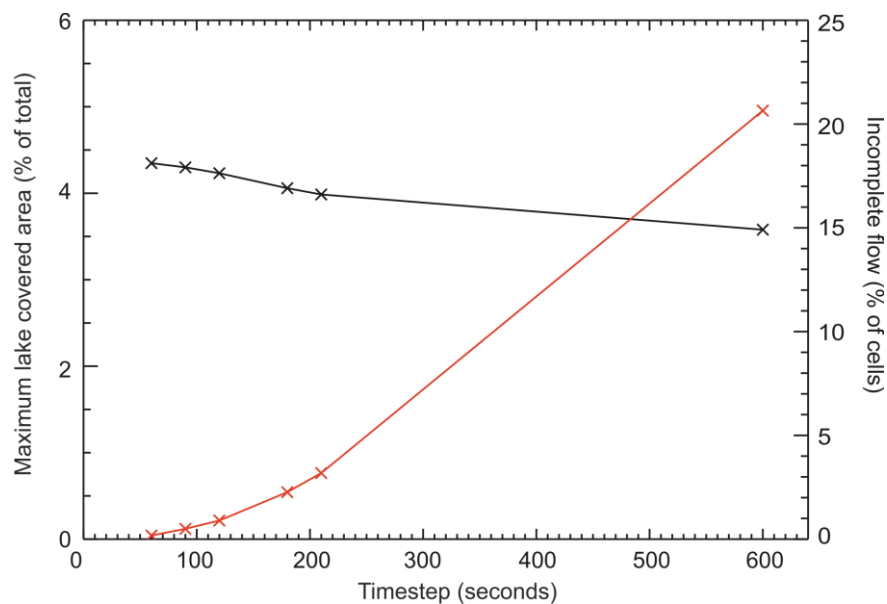
Figure 2.7: Maximum simulated lake covered area, as a percentage of the total area, with respect to time-step in seconds (black). The proportion of model grid cells exhibiting incomplete flow, with respect to timestep in seconds (red).

Simulations were performed for a full year with the time-step range indicated above in order to investigate the impact of the choice of time-step on the realisation of the flow path of the water (and consequently simulated maximum lake area, onset date and location). The model output was found to be generally insensitive to temporal resolution when locating and initiating lakes, with less than 5% difference between maximum (60 seconds) and minimum (600 seconds) values. All simulations reported the same number, and distribution, of lakes

and lake onset day showed no significant variation between simulations. The most significant impact of a coarser time-step is on the maximum cumulative area; a time-step of 600 seconds was found to have a maximum cumulative area 16% less that that simulated using a 60 second time-step (Figure 2.7). Using a time-step in the 60-120 second range made no significant difference to any of the metrics mentioned here and justifies the choice of 90 seconds as the standard time-step.

2.4.4   *Switch between Manning and Darcy type flow*

There are two principal methods by which runoff flows across the ice sheet surface via the supraglacial hydrological network, 1.) water flows through the snow pack, downhill from the point of production, by overland flow, 2.) the ice sheet is incised with both transient and perennial meltwater channels, which evolve according to the distribution of hydraulic potential in the system (Knighton, 1981, Lampkin, 2011). These channels are not represented explicitly in the SLInG model, since they are a sub-grid scale feature. Overland flow is parameterised in the model through the use of Darcy's law for flow through a porous medium and channelised flow is parameterised through the use of Manning's equation for open channel flow. The model switches between Manning- and Darcy-type flow, in order to calculate flux out of a given cell, based on the presence or absence of snow in that cell. This process is relatively simple for those cells where there is either no snow or snow depth is greater than runoff depth, where it is clear which type of flow applies. However, it is possible that snow is present in the cell but the runoff depth is greater than the depth of snow. Under these conditions in the real world, either a mixed flow-type regime occurs or the snow in the cell is removed by the passage of water (Banwell et al., 2012). In order to investigate model dependence on this, simulations were performed using SLInG where Manning-type flow was assumed unless the snow depth exceeded a fixed fraction of the runoff depth. If the snow depth exceeded this fraction, Darcy-type flow was assumed and flux out of the cell calculated accordingly. Simulations were performed with fractions of 0.2, 0.4, 0.6, 0.8 and 1 and for Manning-type flow only. Seasonal evolution of SGLs for each of these simulations was compared to observations (Sundal et al., 2009) and an optimal fraction chosen accordingly.

Using Manning-type flow only, lakes greater than 0.125 km^2 begin to appear 29 days earlier in the melt season (day 126) than when using both Manning- and Darcy-type flow (hereafter combination-flow) (day 155). The observations for 2003 of Sundal et al. (2009) first show signs of lakes on day 151. It is immediately apparent from Figure 2.8 that the two flow

regimes promote radically different maximum lake areas; Manning-type flow over-estimates the maximum lake area by 36% and combination flow overestimates maximum lake area by just 1.4%, for a switch fraction of 0.2. The Manning only regime outperforms the combination regime in simulating lake filling rate. The root-mean-square deviation between simulated and observed daily lake area during the filling period is found to be 8.20 km^2 when Manning-type flow is assumed and 28.45 km^2 when combination flow is assumed.

From Figure 2.8 it can be seen that the model is sensitive to the threshold applied for the Manning/Darcy switch. As the threshold proportion of snow depth to runoff increases, total lake area shows a corresponding increase. If more water is allowed to follow Manning-type flow, lakes grow larger. With a switch of 0.2, i.e. Darcy-type flow is imposed if snow depth is greater than 20% of the runoff depth, maximum lake coverage is 4.32% of the study area. With a switch of 1.0, i.e. Darcy-type flow is imposed if snow depth is greater than 100% of runoff depth, maximum lake coverage is 4.83% of the study area. In order to reproduce observed maximum cumulative lake area (Sundal et al., 2009), a switch value of 0.2 is required. Since combination flow with a switch value of 0.2 gives the most accurate results, simulating both onset day and maximum lake area in close agreement with the observations, this value is adopted as the standard threshold for the model.
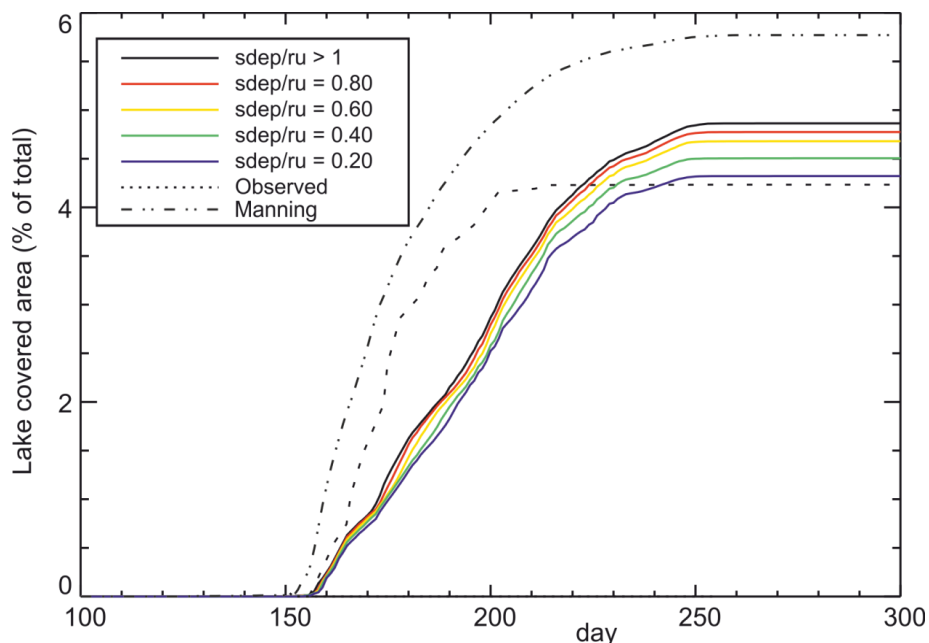
Figure 2.8: Simulated daily lake area using SLInG for instances where Darcy's law is applied once the snow depth (sdep) exceeds a given percentage of runoff (ru). Also shown is observed cumulative lake area for 2003 (Sundal et al., 2009) and simulated daily lake area using Manning-type flow only.

2.4.5   *Manning's 'n'*

In this thesis, an experimentally derived value for Manning's 'n' is used which, for ice, is found to be in the range 0.010-0.012 (Lotter, 1932). Model sensitivity is tested with respect to Manning's 'n' within this range and +/- a single order of magnitude: 0.11 and 0.0011. Within the range of values proposed by Lotter (1932), there is little variation in simulated SGL behaviour. If Manning's 'n' is increased or decreased by an order of magnitude, SGL evolution shows a significant departure from the results obtained using the experimental range proposed by Lotter (1932), particularly with regards to maximum lake area (Figure 2.9). When Manning's 'n' is higher lakes grow larger. A Manning's 'n' value of 0.11 is associated with very rough surface conditions; for example river flow over very dense brush or through trees, conversely an 'n' value of 0.0011 applies to a surface smoother even than polished brass (Chow, 1988). It is clear that flow over bare ice exhibits neither of these roughness characteristics and the choice of 0.011 as the value of Manning's 'n' in this study is reasonably justified.
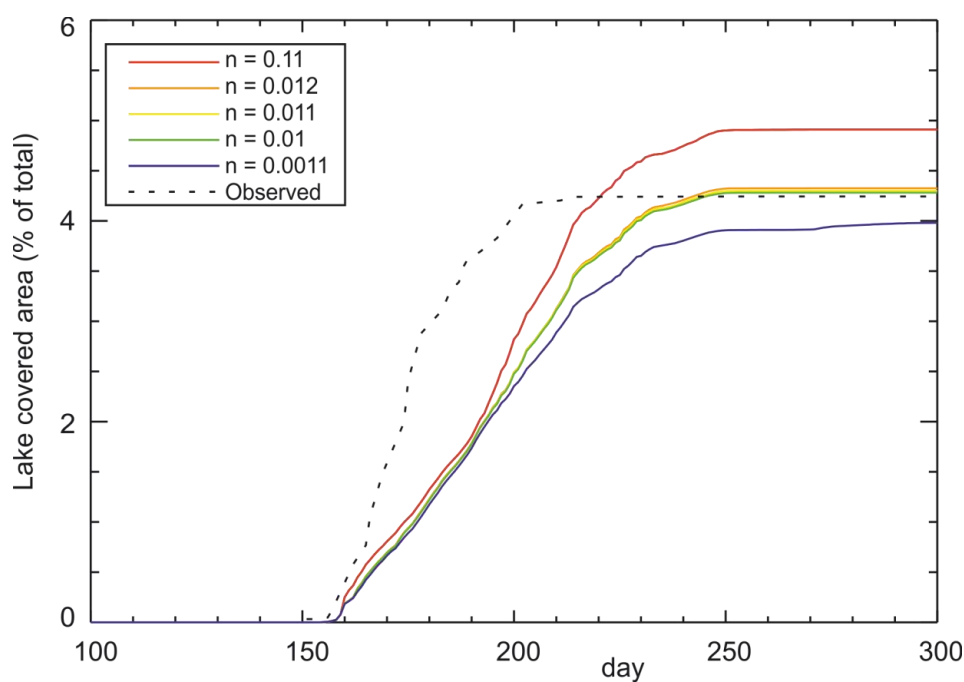
Figure 2.9: Lake area profiles, simulated using SLInG for a range of 'n' values (solid).
Also shown (dashed) is the observed cumulative lake area time series (Sundal et al., 2009)).

2.4.6   *Snow density and snow grain size*

In this study, snow density is used together with snow grain size in order to estimate snow pack permeability based on Shimizu's equation (Equation 2.6) (Shimizu, 1969). Snow density is an output of MAR and is calculated by a multi-layered thermodynamic snow-ice

model (Lefebre et al., 2003) which uses the snow metamorphism and albedo laws of the CEN (Centre d'Etudes de la Neige) snow model CROCUS (Brun et al., 1992). Snow grain size is an internal parameter in MAR and is imposed following the air temperature when snowfall occurs. Snow grain size is also allowed to evolve according to the conditions in the snowpack (i.e. melting, refreezing) again using CROCUS snow metamorphism (Brun et al., 1992). However, the grain size is only defined in MAR for non-dendritic (i.e. not freshly fallen) snow layers. The snow-ice model has been extensively validated for ETH Camp in west Greenland, situated ~252 km further north than the centre of the study area described in this thesis (Lefebre et al., 2003). However, this validation was performed with a focus on surface albedo, being of particular interest in climate simulation, rather than specific snow parameters.

Snow density across the region considered in this study ranges from ~74 kg m^{-3} to ~947 kg m^{-3} in the MAR output (Figure 2.10). There is a clear seasonal cycle in snow density; densification begins at the start of the melt season and continues throughout the spring/summer. Towards the end of the melt season, the compacted snow and firn either melts away or turns into ice, and fresh snowfall once more decreases the snow density. In the MAR output (Figure 2.10), very high snow densities are seen across the region, both above and below the equilibrium line, during the height of the melt season. These densities indicate very compact firn (Paterson, 1994). There are few observations of snow density in the ablation zone with which to make a comparison, however van den Broeke et al. (2008) have reconstructed the maximum snow density value in the ablation zone to be 500 kg m^{-3} by assuming that an energy balance model is correct and applying this to observations of snow depth. This suggests that a snow density of 947 km m^{-3} may be an overestimate. In order to investigate the impact that this may have on model results, a sensitivity analysis with respect to snow density was performed using SLInG.

The model was run with density as suggested by MAR, a fixed snow density of 500 kg m^{-3} throughout and fixed fractions of 0.5, 0.7 and 0.9 the MAR simulated snow density. No significant difference was found in simulated lake evolution using any of these values, indicating that the model is insensitive to snow density. The mean snow depth for cells with density greater than 500 is 0.02 m. This suggests that these densities occur in a very small layer of densified snow and thus their impact on model results is negligible. Maximum snow depth in the data obtained from MAR, is simulated to be 1.31 m in 2003, which corresponds to a simulated snow density of 282 kg m^{-3}. Since this value is simulated at the end of the melt season, it can be assumed that this is fresh snow, as such, the MAR

simulated density value is in good agreement with observed density values of freshly fallen snow (~300 km m^{-3}) (e.g. Lefebre et al., 2003, Greuell and Konzelmann, 1994).
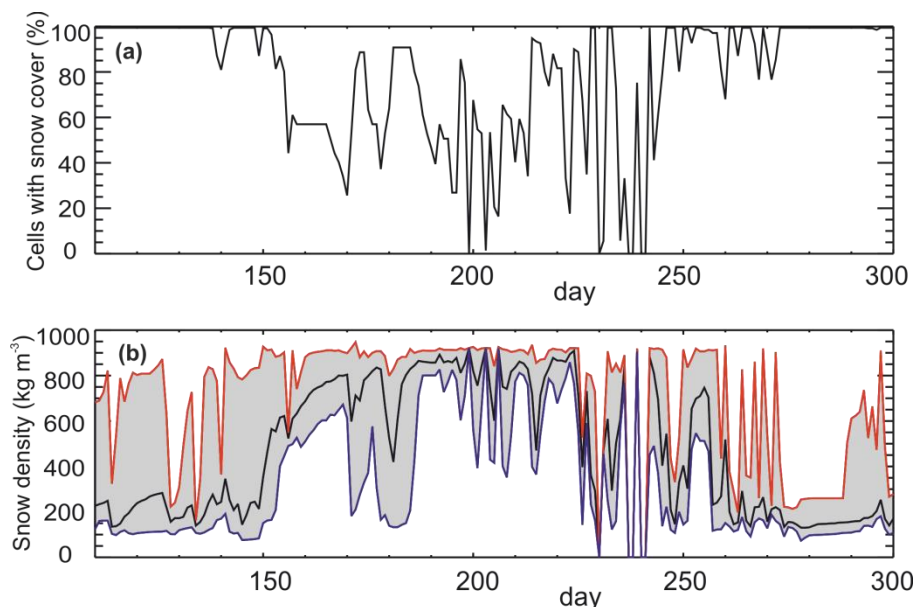
Figure 2.10: Snow pack variation throughout the melt season (days 110 to 300) for the study region, as simulated by MAR in 2003. Top: Snow cover in the study area. Bottom: Mean snow density (black), the shaded area shows the variability with the maximum snow density highlighted in red and the minimum in blue.

Typically, snow grain size takes a value in the range 0.2 to 1.0 mm, dependent on conditions in the snowpack (e.g. melting, refreezing) (Lyapustin et al., 2009, Shimizu, 1969). The SLInG model uses a value of 1.0 mm for snow grain size. In order to test the sensitivity of simulated SGL evolution to this grain size, model runs were performed for one year, 2003, with snow grain values of 0.2, 0.4, 0.6, 0.8, 1.2 and 1.4 mm. No significant difference was found in simulated lake evolution using any of these values, indicating that the model is also insensitive to snow grain size.

2.5 Limitations of the model

A new 2-dimensional transient hydrology model has been developed in order to simulate the initiation and growth of SGLs on the GrIS. This model uses hydrological equations to route runoff, calculated by a complex snow/melt model within an RCM, across a high resolution DEM of the ice sheet surface. While this model is sophisticated with respect to previously published models of SGL evolution, assumptions are made which may impose limitations on

the use of the model. These limitations are outlined here, their implications discussed in further detail and suggestions for future development to address them introduced.

2.5.1   *Pre-existing surface-englacial conduits*

The SLInG model does not include, or parameterise for, sub-grid scale features of the supraglacial hydrological network. This includes crevasses and moulins, which are common features on the GrIS, particularly near the margin. Crevasses, moulins and other pre-existing surface-englacial conduits hinder the formation of lakes by draining runoff from the surface before it is allowed to accumulate sufficiently to pool into topographic depressions. Crevasses are abundant at low elevations where ice sheet velocity is high, relative to the interior, resulting in tensile stress regimes (Lampkin, 2011). Moulins are more commonly found at lower elevations also, with a peak density between 200 and 700 m a.s.l. (Phillips et al., 2011). SGLs are principally of interest due to their potential to affect ice dynamics through hydrofracture and drainage. This is most significant in regions where pre-existing surface-bed conduits are rare, such as high elevations. Restricting the applicability of the SLInG model to regions where crevassing and moulins are rare has little impact on the ability of the model to address this area of interest.

2.5.2   *Temporal variations in topography*

A fixed DEM forms the surface of the GrIS in the SLInG model. Although an InSAR DEM is typically derived from observations made over a single winter, SLInG assumes that a single high resolution DEM is sufficient to represent the surface of the ice sheet in any year. This assumption is made on the basis that surface topography is largely controlled by the transmission of basal conditions through the ice (Lampkin and VanderBerg, 2011, Gudmundsson, 2003) and so inter-annual variability of surface topography is not significant. It has been observed that many supra-glacial lakes are intransient features (Echelmeyer et al, 1991, Selmes et al 2011) which supports this assumption. However, this observation is based on years of data, and it is unlikely that the hypsometry of the ice sheet would be sensitive to climate forcing at this timescale. This uncertainty would need to be reconsidered if the model were to be used to make forward projections for, for example, tens of years.

2.5.3   *Initial condition*

SLInG assumes that the ice sheet is 'empty' at the start of the melt season; i.e. that local

depressions in the surface contain no water. It is known from observations that lakes that have not drained, freeze over at the end of the melt season (Sundal et al. 2009; Selmes et al. 2011). If lakes do not freeze completely then there must be an ice 'lid' covering the lake. An InSAR DEM of an ice sheet surface represents a scattering horizon at depth rather than the true surface. Rignot et al (2001) showed that for ice, the radar penetration can be as shallow as 0 m (typically 1 m (+/-2 m)). For firn, this depth was found to be closer to 10 m, however much of the DEM (95%) lies below the permanent snowline (~1600 m a.s.l. in MAR). If the ice lid is thick (1-3 m), the surface of the lake and the surrounding ice in the DEM will be slightly below their absolute value, but the gradient between them will be the same. If the ice lid is thin, the radar is reflected at the lid/lake boundary; radar cannot penetrate water, and the gradient between lake/surrounding ice will be artificially shallow by up to 3 m.

It is clear therefore, that a DEM derived from InSAR data collected in a single winter will include existing supra-glacial lakes, although their surface elevation may be 1-3 m below the absolute value. In order to ascertain which of the sinks in the DEM contain frozen lakes, observations of lakes from the preceding melt season are needed, including a record of which lakes drained and which re-froze. Observational datasets of sufficient temporal resolution to verify this information are obtained from MODIS imagery (which is only available from 2001). As such, this uncertainty is unable to be quantified for DEMs derived from data collected before this period. This uncertainty could be minimised by the use of a DEM that has been derived by stacking elevation data from multiple years, e.g. the Advanced Spaceborne Thermal Emissions and Reflection Radiometer (ASTER) global Digital Elevation Model (GDEM). However, the ASTER GDEM is unsuitable for use in studies of the GrIS due to large uncertainties in reported elevation for perennially ice-covered areas (Meyer et al., 2011).

2.5.4   *Channelised vs. overland flow*

The model uses a parameterisation for channelised and overland flow whereby, if snow depth in the cell exceeds 20% of the runoff depth, flow is calculated using Darcy's law for flow through a porous medium as opposed to Manning's equation for open channel flow. Section 2.4.4 discussed this approach in more detail and tested the model sensitivity to this threshold value. It was determined that, while a reasonable degree of agreement with observations of SGL evolution is achieved using this method, none of the threshold values, nor Manning-type flow only, is able to capture lake filling rate exactly. This suggests that

there are processes not accounted for in this method. One of these processes could be the removal of snow; in reality, the passage of water in supraglacial channels would displace any snow therein. Using the method outlined in section 2.2.2.1, snow remains in the cell until no longer present in the MAR simulation. Since supraglacial channels are a sub-grid scale feature, they cannot be modelled realistically; however, it would be possible to create a pseudo-channelised system within the model. This could be calculated as a network of cells, following the lowest contours of hydraulic potential. These cells would be assigned as 'channel cells' and all snow in these cells would be assumed to be washed away in the course of the day's water routing. This would be a significant development of the model however and it is unclear how much, if any, of this uncertainty this process would remove. It is recommended that any such development be deferred to a future time and the current model setup be retained.

2.5.5 *Enhanced melting at the lake/bed interface*

The SLInG model does not account for enhanced melting at the lake/ice interface at this time. This is because the contribution of enhanced melting to water volume held in lakes is found to be roughly an order of magnitude less than the contribution of hydrological routing to lake water volume. The water depth in SLInG simulated lakes (with no enhanced melting) grows on average at a mean rate of 0.29 m day^{-1}, and SGLs have been observed to contribute an additional 0.03 m day^{-1} of water volume through enhanced ablation at the lake bottom (Tedesco et al., 2012). The absence of this process suggests that lake volume may be underestimated slightly by SLInG, particularly since the bathymetry of the lake is not allowed to evolve in response to this enhanced ablation.

2.5.6 *End of life processes not included in the model*

The SLInG model simulates only lake growth, and at present does not incorporate end of life processes including refreezing and processes leading to rapid lake drainage. Since neither the patterns of, nor processes contributing to, rapid lake drainage are well understood, it is inappropriate to include end of life processes in the SLInG model at this time. As a consequence, SLInG may only be used in time slice mode; the boundary condition of an empty DEM is re-enforced at the start of every melt season and residual lake volume is not carried over into the next. At this time, the SLInG model may be used to obtain valuable information about the location, onset, and cumulative area of SGLs in any given year, but not the timing of or mode of demise. Since these processes are essential in order to

reproduce the full seasonal cycle of lake evolution, the model ought to be adapted to include end of life processes once this behaviour is better understood.

2.6 Summary

In this chapter, a novel 2-D transient hydrology model (SLInG) which initiates and grows SGLs on the GrIS has been described. The model architecture consists of three algorithms, flow direction, water displacement and lake accumulation. The model calculates flow direction on a cell-wise basis based on the path of steepest descent. Water displacement is calculated either using Darcy's law for flow through a porous medium or Manning's equation for open channel flow. Water is accumulated into lakes by allocating water that has been transported to topographic sinks to become fixed and unable to flow. The model operates with a 90 second time-step and produces daily maps of SGL distribution.

The model setup has been justified and model output has been tested for sensitivity to model configuration. The optimal temporal resolution of the model has been found to be 90 seconds in a trade-off between accuracy and computational expediency. The model is forced by runoff generated at a constant rate throughout the day; in actuality runoff quantity exhibits diurnal variation. The impact of this on simulated SGLs was tested and the accumulation and routing of meltwater was found to dampen this signal; the evolution of SGLs does not exhibit diurnal variability in the SLInG model. The model is found to be sensitive to runoff amount, which suggests that it can be used to simulate the response of SGLs to changes in climate. The model is also found to be sensitive to DEM resolution and it is recommended that SLInG be operated at as fine a resolution as the DEM will allow. However, reasonable results may be obtained up to DEM postings of 300 m, which may prove useful if simulations are performed over a large area. The model was found to be sensitive to a parameterisation of overland and channelised flow. Testing against observations of SGL evolution suggests that when snow depth is equal to or greater than 20% runoff depth, flow should be assumed to be overland flow and calculated using Darcy's law. Otherwise, flow should be assumed to be channelised and calculated using Manning's equation. The model was found to be insensitive to values of Manning's 'n', within a reasonable range derived experimentally for ice. A Manning's 'n' value of 0.011 is used within the model. The model was also found to be insensitive to values of snow density and snow grain size. MAR produced snow density and a constant snow grain size of 1 mm were chosen for use within the model.

SLInG is the most physically based SGL evolution model to date. However, limitations have been identified. First, due to a relative abundance of moulins and crevasses, for simulations based on the GrIS, the model may not be applied at low elevations. This has little impact on the usefulness of the model since the impact of SGLs on ice dynamics is likely to be most significant at high elevations. Second, a fixed DEM is used to represent the ice surface in the model in all years of interest. This is valid due to the intransient nature of surface topography in general and the depressions in which lakes form in particular. However, assuming that the DEM is empty of lakes is also source of uncertainty in the model output. The magnitude of this uncertainty is difficult to quantify, given the lack of contemporaneous observations. Third, lake filling rate is underestimated by the model, this is attributed to the lack of explicit representation of the removal of snow by meltwater channels. Finally, the model at present does not include end of life processes including re-freezing and drainage. At this time, insufficient knowledge exists regarding the mechanisms and patterns of drainage for these end of life processes to be included in SLInG in any robust way.

The SLInG model, the first 2-D fully transient hydrological model, is a useful research tool and, as it is physically based, allows the processes that control the evolution of SGLs to be studied. The framework of SLInG allows for a continuous temporal record of SGL evolution over many years to be obtained, where/when observations are unavailable. The model is forced by runoff produced by an RCM with a comprehensive ice and snow model, giving a high degree of confidence in runoff quantities. In addition, by optimising the model for forcing by an RCM, it has been made possible to use SLInG for forward projections, assuming little future variation in ice sheet topography. However, before the model can be used to investigate the evolution of SGLs, in present times or in the future, extensive evaluation against a range of observations is needed. Such an evaluation is performed in the following chapter.

Chapter 3

On the simulation of supraglacial lake evolution using the SLInG model

3.1 Introduction

Supraglacial lakes (SGLs) form annually in intransient depressions on the Greenland ice sheet (GrIS) and are known to form in the same locations year-on-year (Echelmeyer et al., 1991, Selmes et al., 2011). These lakes have been observed to drain rapidly, presumably through hydrofracture (van der Veen, 2007), delivering large volumes of meltwater to the base of the ice sheet (Das et al., 2008, Doyle et al., 2013). This can lead to seasonal and shorter-term variations in the velocity of the ice sheet flow (Bartholomew et al., 2012, Shepherd et al., 2009, Joughin et al., 2008, Zwally et al., 2002). Although it is uncertain at present, what the long term implications of these perturbations of ice dynamics may be, SGLs remain of interest due to their influence on ice sheet albedo (Greuell et al., 2002) and their ability to enable surface-to-bed connections where conduits such as moulins and crevasses are rare; i.e. at high elevations (Phillips et al., 2011). Observations of SGLs cover short time periods and are temporally sparse (e.g. McMillan et al., 2007, Johansson et al., 2013). This thesis aims to address uncertainty in the observational record of SGLs, by modelling their initiation and growth and thus enhancing current scientific understanding regarding their evolution.

The supraglacial lake initiation and growth (SLInG) model, a new model which has been specifically written for this thesis, was introduced in Chapter 2. SLInG can be used to simulate the initiation and growth of SGLs. These processes are a necessary precursor to drainage, which is not included in the model at present. In Chapter 2, the SLInG model was extensively described and evaluated scientifically. In this chapter, SLInG is evaluated operationally, i.e. against observations, for a region of the west GrIS in the vicinity of the Russell Glacier. In this region, SGLs are abundant and seasonal and shorter-term variations in ice sheet velocity, which have been attributed to meltwater availability, are well documented (e.g. Bartholomew et al., 2012, Shepherd et al., 2009, Palmer et al., 2011). In order to verify the usefulness of the model as an SGL simulation tool, three

subsections of simulated SGL evolution have been chosen against which to evaluate model performance. These are: lake location, lake temporal evolution (onset and filling) and lake spatial evolution (area and volume). The location of SGLs indicates where surface-bed conduits initiated by rapid drainage may appear. Onset day can be considered a proxy for the onset of drainage because lakes can drain as soon as 4 days after they appear (Johansson et al., 2013). Also, knowledge of SGL volume is desirable in order to constrain the amount of water available for hydrofracture, and subsequent rapid delivery to the base of the ice sheet (Leeson et al., 2012). These simulated SGL characteristics are comprehensively evaluated with respect to the observations of Sundal et al. (2009) using various statistical methods. Section 3.2 describes these methods, Section 3.3 evaluates model skill in reproducing the seasonal cycle of lakes during 2003; the year in which the sampling of the satellite observations is most dense. Section 3.4 evaluates model skill in reproducing inter-annual variability for the 2005-2007 period and Section 3.5 provides a summary of this chapter. The majority of the work contained in this chapter has been published in the journal The Cryosphere (TC) (Leeson et al., 2012).

3.2 Evaluation methods

In this chapter, a range of different metrics will be used to evaluate the performance of SLInG against observations of lakes. Here, these methods are described with respect to lake location, temporal (onset, filling rate) and spatial (lake covered area and volume) evolution.

3.2.1 *Observations of supraglacial lake evolution*

Observations from the dataset of Sundal et al. (2009), which were described more fully in Chapter 1, are used to assess the skill of the model in simulating the evolution of SGLs. These data are derived from Moderate-resolution Imaging Spectroradiometer (MODIS) imagery using an automated method. Sundal et al. (2009) used an object-oriented segmentation and classification system to identify possible lakes in a MODIS image, using fuzzy logic to assign objects lake/not-lake status based on their degree of membership to the lake or not-lake class. By this method, Sundal et al. (2009) were able to produce daily lake distributions using cloud-free MODIS images for 28 separate days during the 2003 melt season and 12 separate days each for the 2005-2007 melt seasons (e.g. Figure 3.1).

The spatial resolution of the MODIS instrument is 250 m. SGLs of smaller area are therefore not resolved. It is estimated that total SGL area is underestimated by 12% when using the relatively coarse-resolution MODIS data, as compared to a manual classification of

fine- resolution (15 m) ASTER imagery (Sundal et al., 2009). Because of this, and because small lakes do not hold enough water to drain rapidly, lakes which are smaller than 0.125 km^2 are masked out of simulated lake distributions, which are described in this chapter. This value corresponds to the minimum water volume required for hydrofracture through 1 km thick ice (Krawczynski et al., 2009). There is also an error (~14%, but temporally variable) associated with the mis-categorisation of ice-covered lakes as bare ice using this automated classification method (Sundal, 2009). The observations used in this study have been manually corrected for this error.
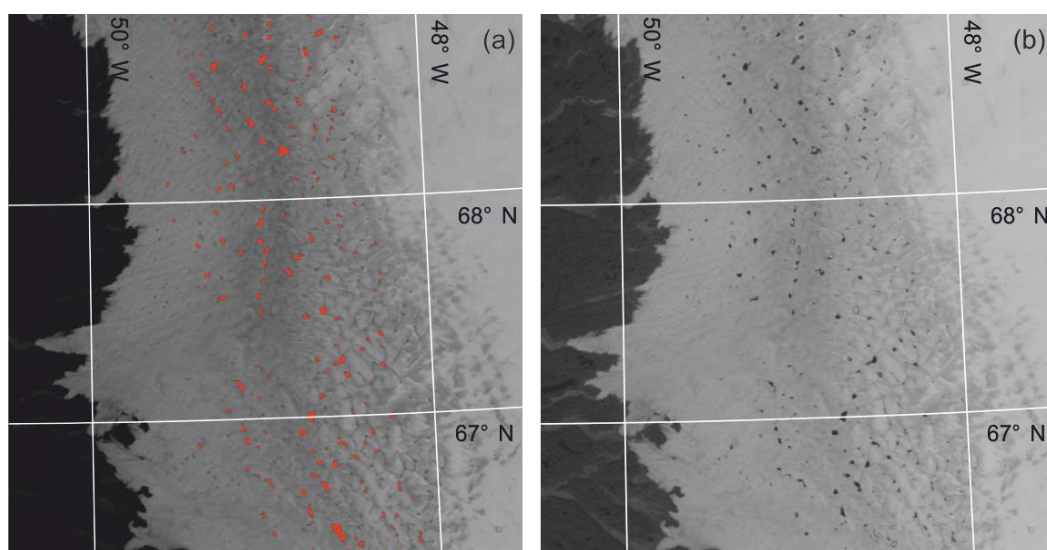
Figure 3.1: Automatically delineated lake distribution for day 196, 2003. (a) MODIS image with automatically delineated lakes superimposed in red. (b) Original MODIS image.

3.2.1.1 A cumulative record of supraglacial lake initiation and growth.

The SLInG model simulates the initiation and growth of SGLs. As such, it may only be used to model SGLs up to the observed date of drainage. However, in order to assess model performance, it is appropriate to refer to a time series of cumulative observed lake covered area; which is assumed to represent the evolution of SGLs, should drainage not occur. It is also assumed that this cumulative distribution includes all possible lakes that are larger than the resolution of the MODIS instrument.

For each of the observation days, a 2-dimensional map of lake distribution is available. A time series of cumulative lake observations is constructed by superimposing the lake distribution on each observation day onto all preceding observations (e.g. Figure 3.2). For example, the cumulative distribution of lakes on observation day 3 consists of the reported distribution of lakes on day 3, superimposed onto the reported distribution of lakes on

observation day 2, and onto the reported distribution of lakes on observation day 1. Thus, lakes that form, and then drain, are included in the cumulative distribution and are available for comparison with simulated lakes that form, but do not drain. In order to investigate lake location, the cumulative distribution of lakes on the final observation day is used. If a pixel in the model grid is observed to be part of a lake at any point during the observational record, it is included in this distribution.
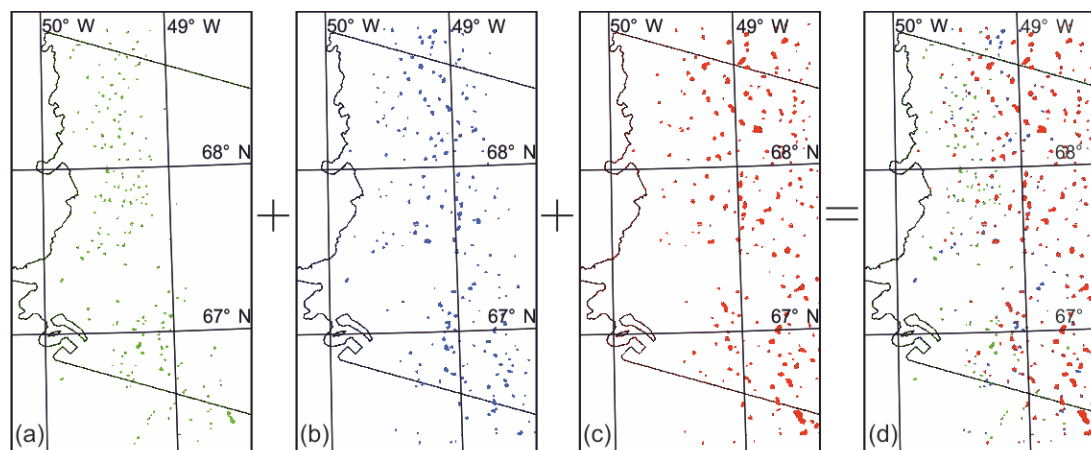
Figure 3.2: Example of method of creating cumulative SGL distributions from the dataset of Sundal et al. (2009). (a) day 157, 2003, (b) day 166, 2003 (c) day 175, 2003 (d) cumulative distribution on day 175, 2003.

3.2.2   *Lake location*

In order to assess the skill of the model in predicting lake location, cumulative spatial distributions of simulated and observed lakes are analysed. Since SGLs predicted by the model do not drain, the simulated lake distribution at day 300 (after the last day for which positive runoff is generated) can be used to represent the cumulative distribution of all lakes simulated by the model throughout the melt season.

The observed and simulated lake distributions may be compared qualitatively or quantitatively. Quantitative methods take two different forms. 1.) A simple lake-by-lake comparison, which analyses the number of observed lakes which are also modelled, and 2.) a somewhat more complex cell-wise method using statistical approaches suggested by Stephenson (2000). For the first case, the observed lake distribution is superimposed on the simulated lake distribution and the number of lakes that are 1) observed only, 2) simulated only and 3) both observed and simulated, are counted. It can be considered a perfect result of the model if all of the observed lakes are simulated; model skill is represented as that percentage of observed lakes that the model co-locates. The statistical methods suggested

by Stephenson (2000) are implemented with particular reference to the 'odds ratio' and the Heidke skill score (HSS), which both require the assembly of a contingency table. A contingency table is a matrix that displays the frequency distribution of two variables; in this case observed lake pixels and modelled lake cells. In this instance, the contingency table consists of a.) 'Hits'; cells which are both observed and simulated to contribute to a lake, b.) 'False alarms'; cells which are predicted to be part of a lake but not observed to be so, c.) 'Misses'; cells observed, but not predicted, to be part of a lake, and d.) 'Correct rejections'; cells which are neither simulated nor observed to be lake cells (e.g. Table 3.1).

Table 3.1: Standard configuration of a two variable contingency table.

		Event observed		
		Yes	No	
	Yes	a	b	
Event forecast	No	c	d	
	Total			n

The 'odds ratio', θ, is defined as being the ratio of the odds of successfully predicting that a cell is a lake (a hit) or not (a correct rejection) to the odds of making an incorrect prediction (false alarms + misses) and is calculated using Equation 3.1 (Stephenson, 2000).

$$\theta = \frac{ad}{bc} \qquad\qquad 3.1$$

Where a, b, c, d are as indicated in Table 3.1. The odds ratio can be positively skewed by a low event to non-event ratio (Stephenson, 2000) and these data presented here apparently exhibit this rare event bias, given that there are many more cells which do not form part of a lake than there are cells which do. In this case however, a correct rejection is considered to be a positive result of successful water routing and ponding. The Heidke skill score (HSS) provides a means of assessing model skill when compared to a random assignment of lake/not-lake cells by calculating the proportion of correct forecasts to that which would be obtained by chance. The HSS can be calculated using Equation 3.2.

$$HSS = \frac{2(ad - bc)}{(a+c)(c+d) + (a+b)(b+d)} \qquad\qquad 3.2$$

Where a, b, c, d are as before. Neither the HSS nor the odds ratio take into account any degree of spatial autocorrelation, i.e. where many cells are clustered together into a lake.

3.2.3 *Temporal evolution*

The extent to which the model was able to reproduce the temporal evolution of SGLs, both in terms of onset day and subsequent growth, was investigated. Since it is desirable that the model simulates the initiation of lakes effectively, lake onset day is used to assess model skill in timing the appearance of lakes. The onset day is calculated for each individual lake, and is defined as the first day in the year when that lake can be seen in the observations or simulation results as appropriate. In order to compare observed and simulated lake onset day; first, coincident lakes (both observed and simulated) are identified in the cumulative observed lake distribution, and the simulated lake distribution. Then, a simulated and an observed onset day are assigned to each lake based on its first appearance in the simulated and observed record. Finally, the Pearson correlation co-efficient (PCC) is calculated between the simulated and observed onset days. The PCC is a measure of linear dependence between two variables (in this case simulated onset day and observed onset day). The PCC takes a value between -1 and 1 where 1 indicates perfect correlation, -1 indicates perfect anti-correlation and 0 indicates no relationship between the two variables. If the PCC between simulated and observed onset day were found to be 1, this would be interpreted as the model being certain to reproduce the observed onset day. Qualitative interpretation of the strength of correlation based on the PCC is somewhat arbitrary. In this thesis the interpretation of Bluman (2004) is used; a relationship can be said to be 'strong' if the PCC exceeds 0.69. Also, the PCC can be tested for statistical significance using the t-test (Bluman, 2004). The PCC is accepted as evidence of model skill if it is found to be significant at the 99th percentile.

The lake filling period is defined as the period during which SGLs fill, from onset to maximum capacity. This can be assessed on an area-averaged and lake-by-lake basis. Because observed lakes exhibit rapid drainage behaviour, a process not currently included in the model, a cumulative lake covered area estimate is used (section 3.2.1.1). In this chapter, model skill in filling rate is evaluated on an area-averaged basis i.e. considering all lake cells together rather than resolving individual lakes. This evaluation is performed by calculating the root-mean-squared deviation (RMSD) (Equation 3.3), between modelled and observed values, for total number of grid cells/pixels which form part of a lake during the filling period. The RMSD is a measure of the average magnitude of the difference between two datasets (Willmott et al., 1985). Because it is also useful to know the direction of the difference, mean bias, $\overline{B}$ is also calculated (Equation 3.4).

$$RMSD = \sqrt{\frac{1}{n}\sum_{t=1}^{n}\left(O_t - M_t\right)^2}$$

  3.3

$$\overline{B} = \frac{1}{n}\sum_{t=1}^{n}O_t - M_t$$

  3.4

Where O_t and M_t are the observed and modelled value of lake covered area at time, t.

3.2.4   *Maximum lake covered area*

Maximum lake covered area may be used to constrain the maximum amount of meltwater that may be available, through hydrofracture, for rapid delivery to the base of the ice sheet. Total lake covered area, on a given day, is defined as the sum of the area of all pixels/grid cells which are observed/simulated to form part of a lake on that day. In the observational record of SGL evolution, maximum total lake covered area occurs prior to the onset of widespread drainage (Shepherd et al., 2009). In the simulation, maximum total lake covered area occurs towards the end of the melt season, when either depressions are brim-full or insufficient runoff remains available to fill them. Because of this difference, once more the cumulative time series of lake distribution, described more fully in section 3.2.1.1, is used in order to assess model skill in simulating maximum lake covered area. Model skill is expressed as a percentage overestimate or underestimate of the simulated maximum lake covered area with respect to the observed maximum lake covered area.

3.3 Model performance in 2003

Due to the dense temporal sampling available, 2003 is a notable year in the observational record of SGL evolution. Observations are available on 28 separate days in 2003 (Sundal et al., 2009), the next densest available sample (of daily distributions of SGLs) is 23 separate days in 2010 (Johansson et al., 2013). This is primarily due to the lack of cloud cover in MODIS observations in that year. SLInG is operationally evaluated against the 2003 observational record of Sundal et al. (2009). Simulated values are obtained by running the SLInG model for 2003, forced by runoff and snow characteristics generated by the MAR (Modèle Atmosphérique Régional) regional climate model (RCM) (Lefebre et al., 2005), and using the high-resolution digital elevation model (DEM) of Palmer et al. (2011).

3.3.1   *Experiment design*

Simulations for 2003 were performed using the model set-up detailed in Chapter 2. A

summary of the model set-up is provided here. The model was again run with a resolution of 100 x 100 m in a 6,753 km^2 region of western Greenland, in the vicinity of Russell Glacier (Figure 3.3). SLInG is run with a 90 second time-step and lake distribution is reported every model day. Simulations were forced by runoff, snow depth and snow density, generated by the MAR RCM run at 25 km resolution. MAR is forced at the boundaries by the European Centre for Medium Range Weather Forecast (ECMWF) ERA-Interim reanalysis. The high resolution DEM of Palmer et al. (2011) forms the surface of the ice sheet in the simulations. This DEM was created from Interferometric Synthetic Aperture (InSAR) data acquired in 1996 by the European Remote Sensing satellites. In this region of the GrIS, elevation ranges from 1100 m a.s.l. to 1752 m a.s.l., 1100 m a.s.l. is chosen as the lower bound in this experiment because the spatial resolution of the (forcing) runoff data limits the ability of the RCM output to adequately resolve surface mass balance in regions of steep elevation gradient (Franco et al., 2012). In addition, the distribution of crevasses, moulins and other pre-existing surface-englacial conduits below this elevation, are able to drain water from the surface directly into the englacial environment, thereby rendering it unavailable for lake formation.

3.3.2   *Lake location*

The skill of the SLInG model in predicting lake location is assessed on a cell wise basis and on a lake-by-lake basis across the study area. In order to quantify model skill in predicting the presence or absence of lakes on a cell wise basis, the number of simulated lake cell hits (predicted and observed), false alarms (predicted but not observed), misses (observed but not forecast) and correct rejections (neither predicted nor forecast) are presented in the form of a contingency table (Table 3.2). Using this contingency table, the odds ratio is calculated to be 18.93; indicating that the model is ~19 times more likely to predict a cell to be part of a lake or not than to make an incorrect prediction. The HSS is found to be 0.32, which suggests that the model performs 32% better than a random assignation of lake/not-lake cells over the study area.

Table 3.2: Contingency table detailing the number of predicted and observed lake cells in this study area.

		Lake cells observed		
		Yes	No	Total
	Yes	9 956	18 701	28 657
Lake cells simulated	No	18 238	648 393	666 631
	Total	28 194	667 094	695 288

Figure 3.3 shows a comparison between observed (red) and simulated (blue) lake distribution, with coincident lake area highlighted in purple, within the study area. There are simulated and observed lakes that are in close proximity, but that are not coincident. There are also a number of incidences of one large observed lake coinciding with several smaller modelled lakes. However, in general, there is good agreement between the model and observations in terms of locating lakes; the location of 66% of lakes greater than 0.125 km^2 is correctly simulated.
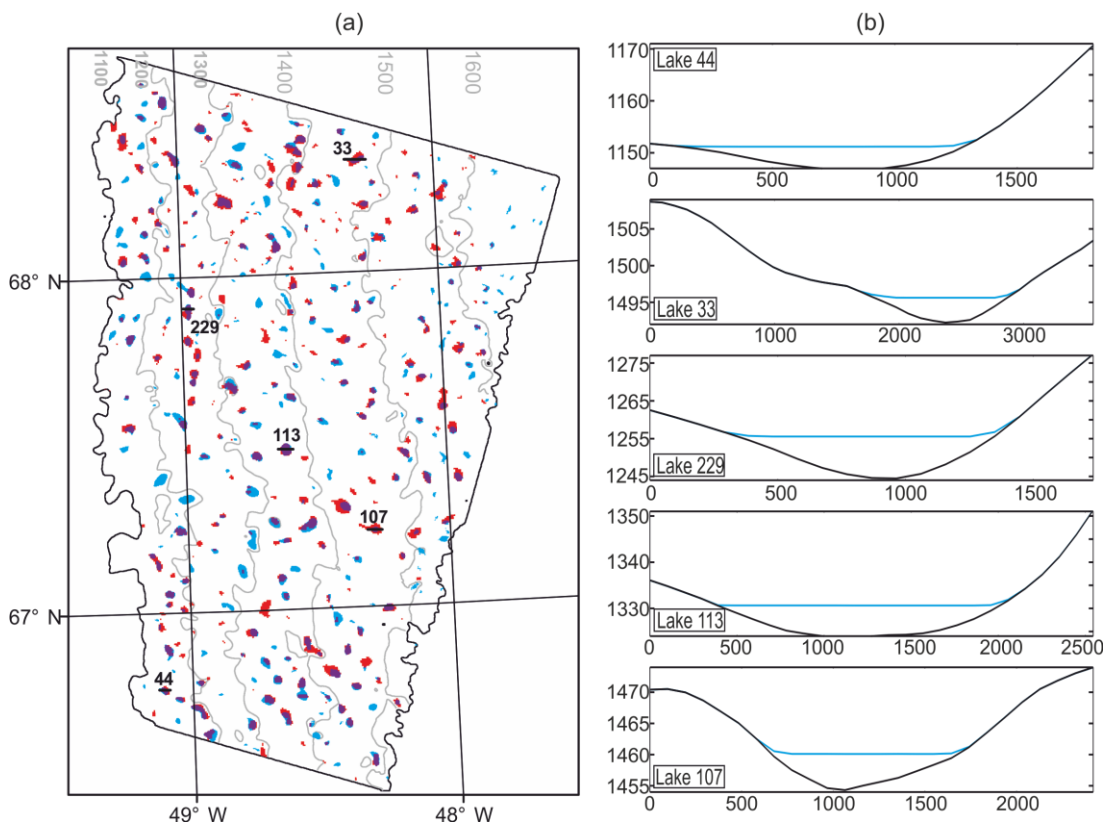
Figure 3.3: Simulated vs. observed lake distribution. (a) Composite map of all MODIS observed lakes (red) and all lakes simulated using SLInG (blue) during the 2003 melt season. Coincident lake area is shown in purple. (b) East-west lake surface (blue) and bed (black) profiles for modelled lakes indicated by number in (a). The transect taken is shown in black in (a).

These results are encouraging as they support the use of the model described in this thesis as a tool for pin-pointing the location of lakes. This is useful, as SGLs are known to drain rapidly through hydrofracture and enable the rapid delivery of large amounts of meltwater to the base of the ice sheet (Doyle et al., 2013, Das et al., 2008, Krawczynski et al., 2009). This supraglacial perturbation of the subglacial environment is particularly important at higher elevations where existing surface-bed conduits, such as moulins and crevasses, are rare (Howat et al., 2013, Phillips et al., 2011). It is reassuring therefore that SLInG performs

well in this region. The successful location of observed lakes is primarily attributed to DEM accuracy. However, realistic water routing is also a major factor. The skill this model displays in predicting SGL location is a result of uniting these factors.

3.3.3   *Lake covered area and volume*

Since the processes of lake drainage and refreezing are not incorporated within the model at this time, results are restricted to comparisons of lake filling and are meaningful only until the date of drainage/commencement of refreezing. However, model skill in simulating cumulative lake covered area, assuming no drainage, can be investigated by comparing model output for daily lake covered area with an estimate of cumulative lake covered area derived from satellite observations (Figure 3.4). The model predicts the maximum cumulative lake covered area, between 1100 and 1700 m a.s.l., very well, with an overestimation of just 1.5% of the maximum value. The maximum cumulative area occupied by lake pixels/cells is reached around day 203 (21st July) in the observations, about one week later than the maximum daily runoff amount in the MAR data which occurs at day 196 (15th July), and reached around day 245 (September 2nd) in the simulation.
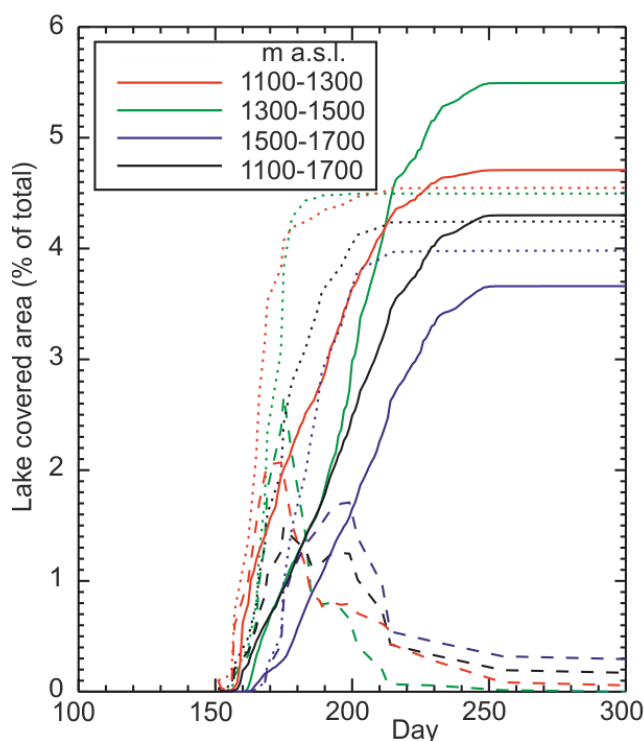
Figure 3.4: Comparison between SLInG simulated (solid), observed (dashed) and cumulative observed (dotted), fractional lake covered area in 2003 for three elevation bands in the Russell Glacier catchment of the Greenland ice sheet.

Luthje et al. (2006b) model the routing and ponding of runoff in a similar region of the GrIS to that investigated in this thesis, using empirical methods. In their study, Luthje et al. (2006b) model the maximum lake covered area to be around 6%. They also propose that this is a topographic limitation, i.e. that once this area has been reached, the lakes are brim-full and can grow no more. In order to find the maximum possible lake covered area for the DEM that is used by SLInG to route runoff in this study, ArcGIS was used to fill the sinks in the DEM to their maximum capacity. The maximum possible lake covered area, was found to be 6.4% of the ice sheet above 1100 m a.s.l., in agreement with the findings of Luthje et al. (2006b). The maximum volume of water that can possibly be stored in SGLs in this sector of the GrIS is therefore estimated to be 1.49 km^3, or 12% of all runoff produced in 2003. This suggests that the vast majority of runoff passes through or over the ice sheet without being stored for long periods in lakes. Lake area coverage of 6.4% is never reported by observations derived from MODIS imagery. Neither is 6.4% lake area coverage ever simulated using the SLInG dynamic hydrology model, even when double the MAR simulated runoff is supplied (see Chapter 2). Although simulated lake area coverage stabilises, not all lakes are brim-full by the end of the melt season with respect to the sink in which they are located, especially at the higher elevations where melting begins later and ends sooner. If the ablation season were to lengthen, particularly at these higher elevations, it is possible that this topographic limit could be reached.

Although the model does not include drainage it is reasonable to conclude that runoff, extraneous to that ponded in lakes by the observed date of drainage or refreezing, has passed into the ice sheet though englacial channels (e.g. crevasses or moulins). Crevasses are abundant at lower elevations, where velocity gradients relative to the interior result in high tensile stress regimes (Lampkin, 2011). In addition, moulin density is typically 1 moulin per 1-2 km^2 for ice sheet elevations below 1000 m a.s.l in west Greenland (Phillips et al., 2011). Above 1100 m a.s.l., up to the date of observed maximum simulated lake covered area (day 245, September 2nd), 11.89 km^3 of runoff is produced, according to the MAR model. A maximum of 12% of this runoff is estimated to be stored in observed lakes when considering a cumulative lake covered area, a conical lake and a diameter-depth ratio of 100:1 (Box and Ski, 2007). By comparison, a previous study of the nearby Swiss Camp region of the GrIS estimated, using observations of lake area and mean depth, that 17% of total meltwater volume produced had been stored in lakes by August (McMillan et al., 2007). By day 245, according to SLInG simulated SGL volume estimates, just 6% of total runoff to date is stored in lakes. However, using SLInG simulated SGL area estimates, together with a conical approximation, 11% of total runoff is estimated to be stored in lakes by day 245, a

value more consistent with observations. These results, together with the fact that 34% of the MODIS observed lakes in 2003 are not simulated, suggests that the DEM used in this study underestimates the amplitude of the short period variations in the ice sheet surface that lead to the formation of lakes. This could arise from the DEM smoothing process, or indicate the presence of refrozen lakes mis-interpreted as part of the ice sheet surface. This also provides an explanation for a number of lakes which are simulated slightly offset from observed locations. As a result, the 12% estimate for maximum storage volume should be taken as a lower bound, given a 6.4% maximum lake covered area.

3.3.4   *Temporal evolution*

The temporal evolution of SGLs is investigated using the methods outlined in section 3.2.3. The simulated onset day, of the 66% of observed lakes successfully placed by the model, is found to be correlated with the observed onset of these lakes with a PCC of 0.76 (Figure 3.5). This may be considered a strong correlation (Bluman, 2004). A mean lead in the observations of 4 days is calculated when considering all 159 lakes. Lakes initially form at lower elevations, and subsequently form progressively further inland over the course of the melt season (Figure 3.4). This pattern can also be seen in the MODIS data. Simulated lake initiation is contemporaneous with observations in the upper two elevation bands at days 155 and 162 for 1300 to 1500 m a.s.l., and 1500 to 1700 m a.s.l. respectively, however observed lakes begin to appear 4 days earlier than simulated between 1300 and 1500 m a.s.l..
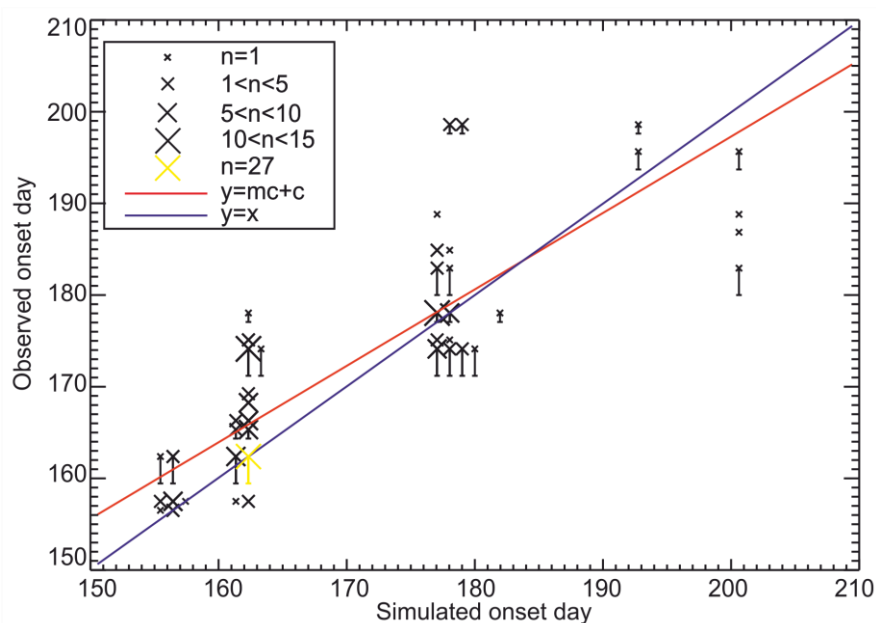
Figure 3.5: Correlation between simulated and observed onset day for 159 successfully located SGLs. Vertical error bars indicate uncertainty in observed onset day due to non-uniform temporal sampling. Size and colour of symbol indicate number of points, n, with indicated value. Also shown: line of best fit (red), 1:1 correlation (blue).

Simulated lake filling rate is much slower than that observed; in this experiment, the model underestimates cumulative lake covered area and exhibits an RMSD from observed values of 28.45 km^2 during the filling period. One possible explanation for this is the method by which channelised flow is parameterised in the model; when a snow depth greater than 20% of runoff depth is present, Darcy-type flow is assumed. Snow depth is varied in SLInG according to MAR simulated values and there is no feedback between flow through a cell and snow depth within it. It is likely that small amounts of snow would be washed away by the passage of water, a process not currently included in SLInG.

3.4 Model performance at the inter-annual timescale

The model was run with a resolution of 90 seconds for 2005, 2006 and 2007 (in addition to 2003) to investigate the performance of the model in capturing inter-annual variability and to provide a more robust validation.

Table 3.3: Observed SGL data availability, characteristics of runoff and statistical description of model skill in predicting lake locations in 2003, 2005-2007. Daily mean runoff relates to the melt season (day 130 to 250). Also shown is the number of observations available in each year, the maximum observed and modelled lake covered area, as a percentage of total area and the PCC calculated between observed and simulated lake onset day.

Year	2003	2005	2006	2007
Total Runoff (km^3)	12.34	6.93	7.93	12.99
Daily Average Runoff (mm)	16.52	11.55	15.32	20.77
Number of Satellite Images available	29	12	12	12
Percentage (%) of observed lakes modelled	66	57	64	70
Odds ratio	19	21	17	18
Heidke skill score	0.32	0.28	0.25	0.22
Maximum Modelled Lake covered area (%)	4.30	3.19	4.08	5.15
Maximum Observed Lake covered area (%)	4.24	2.67	2.54	1.93
Onset day correlation	0.76	0.62	0.73	0.30

These years were chosen because they were the years for which observations were available, using the same method as those for 2003 (Sundal et al., 2009). Of these years, 2003 and 2007 were particularly warm, resulting in a total runoff amount over the whole of this sector of the ice sheet of 12.34 km^3 and 12.99 km^3 (Table 3.3) according to the MAR RCM (Lefebre et al., 2005). This corresponds to a daily mean runoff depth of 16.52 and 20.77 mm. The 2005 and 2006 melt seasons have over 30% less runoff than the other two years at 6.93 km^3 and 7.93 km^3, respectively.

The model performs consistently well in locating lakes in 2005, 2006 and 2007 with odds ratio values of 21, 17 and 18 (Table 3.3). These results confirm that the locations of SGLs coincide with intransient depressions in the ice surface topography and, with the current model set-up, it is not essential to have contemporaneous surface elevation and runoff observations to predict where lakes form. Both Echelmeyer et al. (1991) and Selmes et al. (2011) observed that SGLs appear in the same locations on different years, in agreement with the findings of this modelling study. Figure 3.6 shows the cumulative lake covered area, as a percentage, both as simulated (solid) and observed (dashed). The best agreement between modelled and observed maximum cumulative lake covered area occurs in 2003. The model overestimates this value slightly in 2005, and significantly more in the other years considered.

SLInG shows closest agreement with observations of cumulative lake covered area described by Sundal et al. (2009) in 2003 and 2005. SLInG also simulates a positive correlation between runoff production and lake size, particularly between mean daily runoff and maximum cumulative lake covered area. SLInG simulates similar maximum modelled lake covered areas in 2003 and 2006, which also have similar runoff amounts of 16.52 and 15.32 mm per day on average. However, the observations do not confirm this correlation; maximum lake covered area in 2007, the year of most abundant runoff is smaller than in the other three years. This could be attributed to the role that drainage plays in regulating SGL area. However, there are 28 days of observations for 2003 and only 12 per year for the period 2005-2007, in addition to which, the observations taken in 2007 are highly clustered (Figure 3.7). The sparseness of observations in 2005-2007 relative to 2003, and the clustering of observations in 2007, suggests that observations in these years may not be able to capture a comparable degree of variability in runoff forcing of daily lake covered area.
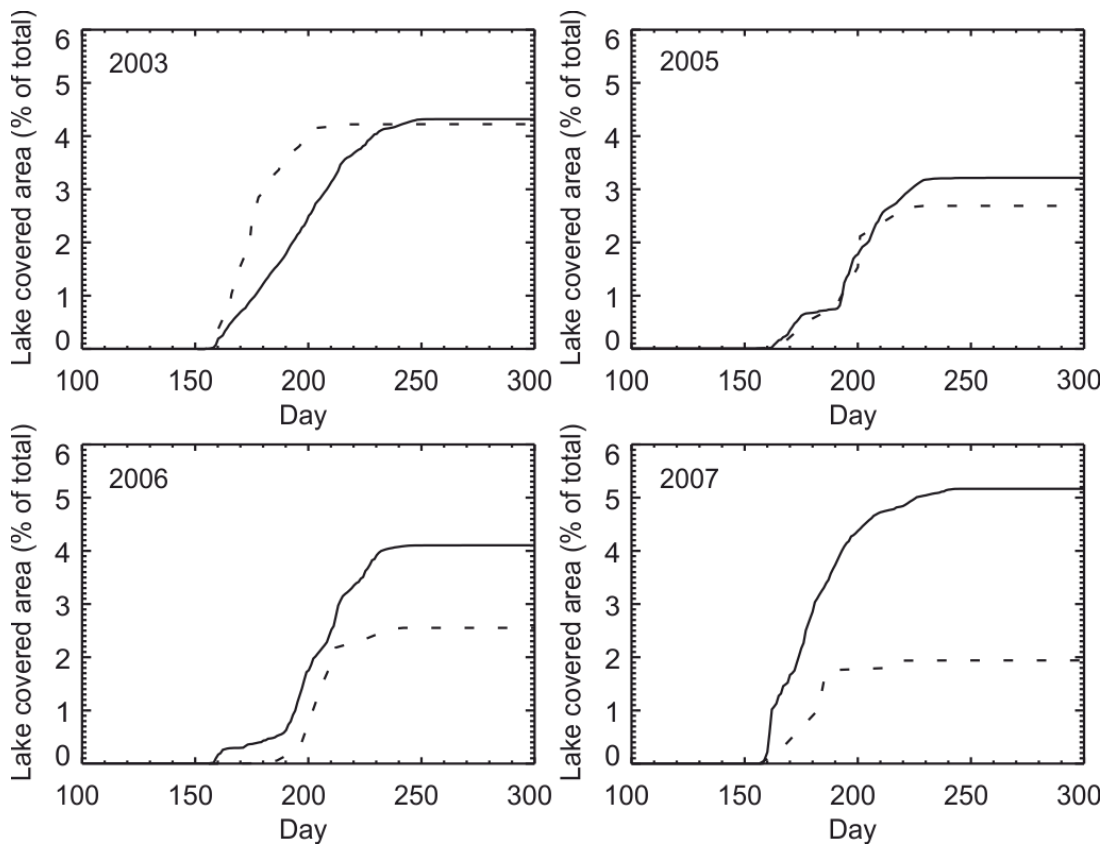
Figure 3.6: Multi year comparison of cumulative lake covered area (1100m to 1700 m a.s.l.) as a percentage of total area. Modelled values are given with solid lines and the observed values of Sundal et al. (2009) are given with dashed lines.

Although cumulative lake covered area is over predicted, the variability of cumulative lake covered area is reproduced well for 2005 and 2006; the simulated and observed cumulative area profiles show the same shape (Figure 3.6). This is particularly evident in 2005 where the mean bias between the model and observations during the filling period is just 2.19 km^2. Mean bias values are found to be -66 km^2, 52 km^2 and 130 km^2 for 2003, 2006 and 2007, respectively. In 2005, the direction of the bias is variable; the RMSD is calculated to be 14.75 km^2. Again, there is a reasonable correlation between simulated and observed onset day (Table 3.3), with the exception of 2007 where correlation is 0.30, which may be considered insignificant. Uncertainty in the observations is highest for this year. It is clear that an investigation into the uncertainty associated with observations of SGLs is needed, particularly with regard to the impact of sample size and density on reported SGL evolution. Additional observations may be required to fully evaluate model performance at the inter-annual timescale.
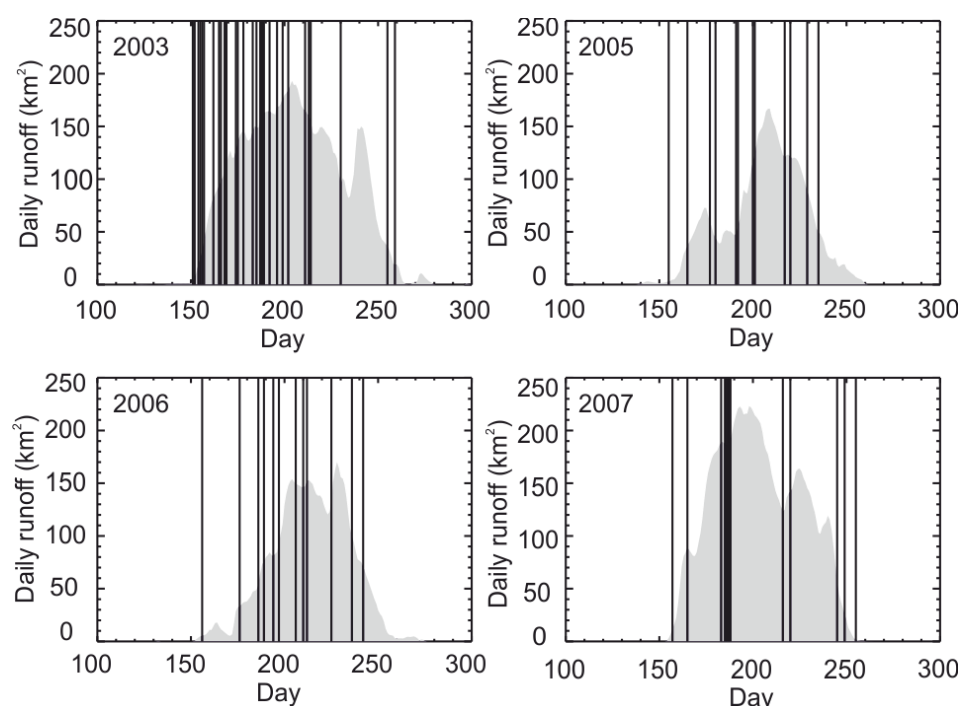
Figure 3.7: Runoff variability and temporal sampling of the observations of Sundal et al. (2009) for 2003, 2005-2007. Shaded region indicates total runoff integrated over the study region. Vertical lines indicate days for which an observed daily lake distribution is available.

3.5 Summary

In this chapter, a new method of modelling SGL evolution has been evaluated (the SLInG model). This model has been used to simulate the onset and growth of SGLs in the Russell Glacier catchment in western Greenland. Using data acquired during the 2003 melt season, the model has been demonstrated to be 19 times more likely to correctly predict the presence (or absence) of lakes than to make incorrect predictions, within an elevation range of 1100 to 1700 m a.s.l., when compared with MODIS satellite imagery. Of the 66% of observed lake locations, which the model correctly reproduces, the simulated lake onset day is found to be correlated with that observed with a PCC of 0.76. The model predicts a progression of lake initiation inland as the melt season progresses, a pattern also previously reported in numerous satellite surveys of SGLs (e.g. Sundal et al., 2009, McMillan et al., 2007, Sneed and Hamilton, 2007a). SLInG accurately simulates maximum cumulative lake covered area with only a 1.5% overestimate. However, because the model does not simulate processes leading to lake stagnation or decay, such as refreezing or drainage, absolute daily lake covered area is not simulated. The maximum potential lake-covered ice sheet area is limited by topography to 6.4%. This corresponds to a volume of ~1.49 km^3, 12% of the runoff produced in 2003. This can be taken as an upper bound given uncertainty in the DEM.

SLInG has been evaluated at the inter-annual time scale and found to reproduce lake location successfully in 2003 and 2005-2007. This confirms the assumption that ice sheet topography is the dominant driver of SGL location. This is in agreement with the findings of Echelmeyer et al (1991) and Selmes et al (2011), who used a range of observational techniques to investigate the inter-annual distribution of SGLs on the GrIS. Both studies observed that SGLs appear in the same locations on different years, also indicated in this modelling study. However, the agreement between model and observations in terms of lake covered area and volume and temporal evolution is much less convincing. This may be the result of drainage, potentially influencing the observational record but not included in SLInG simulations. However, it may also possibly a data artefact, as the days on which observations are available in 2005-2007 are few and sparse. An investigation into the impact of sample size and spacing on reported lake evolution is required and will be addressed in Chapter 4.

It is important to note that the SLInG model simulates only lake growth, and at present does not incorporate processes leading to rapid lake drainage, which is known to be an aspect of the seasonal cycle of some lakes (e.g. McMillan et al, 2007; Georgiou et al. 2009, Sundal et al. 2009, Selmes et al. 2011). In consequence, while the model provides information about the location, onset, and cumulative area of SGLs, it cannot fully simulate the evolution of lakes that drain. On the other hand, differences between modelled and observed lake volumes can provide useful information as to the quantity of water that has drained from lakes. In future work, processes such as drainage and refreezing may be investigated in the context of this model. This chapter has shown SLInG to be a good first step towards capturing the variability of SGL evolution with a numerical model. These initial results are promising and suggest that the model is a useful tool for use in analysing the behaviour of SGLs on the GrIS in the present day and potentially beyond.

Chapter 4

A comparison of observations of supraglacial lake evolution at the western margin of the Greenland ice sheet

4.1 Introduction

Supraglacial lakes (SGLs), formed from the pooling of runoff in topographic depressions, are an annual feature on the Greenland ice sheet (GrIS) during the melt season. SGLs locally decrease the surface albedo with respect to the neighbouring bare ice area, accelerating melting as a result (Greuell et al., 2002). However, in recent years, SGLs have been the subject of both observational (e.g. Doyle et al., 2013, McMillan et al., 2007) and modelling studies (e.g. Banwell et al., 2012, Luthje et al., 2006b) due to their supposed ability to impact ice sheet dynamics. SGLs may drain rapidly through hydrofracture (Krawczynski et al., 2009, van der Veen, 2007), and this drainage has been observed to affect the local dynamics of the ice sheet (Das et al., 2008). The timing of peak lake drainage has also been linked to seasonal speed-up of the ice sheet (Shepherd et al., 2009). The role of SGL drainage in a potential net acceleration of the ice sheet is uncertain (Sundal et al., 2011, Schoof, 2010). However, SGLs remain of interest due to their role in the supraglacial hydrological network. In particular, the location of SGLs is of interest because they can enable surface-to-bed connections at high elevations; where conduits such as moulins and crevasses are rare (Bartholomew et al., 2011b, Howat et al., 2013). Additionally, knowledge of SGL volume is desirable to constrain the amount of water available for hydrofracture, and delivery to the base of the ice sheet (Leeson et al., 2012).

Observations of lake behaviour have traditionally been made in-situ or obtained remotely using satellite instruments such as the Advanced Spaceborne Thermal Emission and Reflection Radiometer (ASTER), the Moderate-resolution Imaging Spectroradiometer (MODIS) and the Landsat-7 Enhanced Thematic Mapper plus (ETM+) (e.g. Georgiou et al., 2009, Sundal et al., 2009, Tedesco and Steiner, 2011). SGLs have been identified in satellite images obtained using these optical remote sensing instruments by manual interpretation, where each lake is digitised by hand (e.g. Georgiou et al., 2009, McMillan et al., 2007), and by semi- or fully-automated methods (e.g. Sundal et al., 2009, Liang et al., 2012). Automated mapping of lakes enables a number of images, containing numerous lakes, to be

processed efficiently. Both ASTER and ETM+ images have a high spatial resolution (of the order ~10 m) conducive to accurate lake delineation. However, the MODIS image record has a far higher temporal sampling –at least once a day, rather than bi-weekly and is better able to resolve the evolution of lakes. Typically, studies of seasonal and inter-annual variability in modes of SGL evolution are investigated using MODIS (e.g. Johansson et al., 2013, Selmes et al., 2011). This is due to this relatively dense temporal sampling, even once cloud-covered days have been removed. However, in years of abundant cloud cover, the record consists of as few as 12 cloud free images per year (Sundal et al., 2009). SGLs are abundant in the Russell Glacier catchment on the GrIS and the impact of rapid lake drainage on seasonal and shorter-term ice sheet dynamics in this region is well documented (Palmer et al., 2011, Shepherd et al., 2009). Three independent observational studies of SGL evolution in the Russell Glacier region have been performed (Sundal et al., 2009, Selmes et al., 2011, Johansson and Brown, 2013), each using a different semi-automated lake classification system to report the daily distribution of lakes.

In Chapter 2, a new model of SGL initiation and growth (the SLInG model) was described and in Chapter 3, the performance of this model was evaluated. Although the performance of SLInG was validated at the seasonal timescale, data limitations prevented the evaluation of SLInG at the inter-annual timescale. In this chapter, a new inter-comparison of automatically derived observations of SGL evolution is performed, using the data of Sundal et al. (2009), Selmes et al. (2011) and Johansson and Brown (2013). Ultimately, these data are combined to form a new, robust SGL index for 2005-2007. The 2005-2007 period encompasses one high (2007), one low (2005) and one moderate (2006) runoff year according to runoff values simulated at a resolution of 25 km by the regional climate model (RCM) MAR (Modèle Atmosphérique Régional) (Fettweis, 2007) forced by ERA-Interim reanalysis. The remainder of this chapter is structured as follows. In Section 4.2, the three observational datasets are described, and methods used to inter-compare them are outlined. In Section 4.3, the effect of temporal sampling on reported SGL characteristics is investigated. In Section 4.4, reported daily SGL distributions in each of these three datasets are independently evaluated using a new subset of manually delineated lakes, and a sample of manually derived daily lake distributions. Both samples were derived from MODIS imagery. In Section 4.5, a new, robust dataset is assembled for 2005, 2006 and 2007 by combining the three individual datasets in a hierarchical manner. Finally, Section 4.6 provides a summary of the work described in this chapter. The majority of the work contained in this chapter has been accepted for publication in the Journal of Glaciology (Leeson et al., 2013).

4.2 Data and Methods

This study focuses on a 16,000 km^2 area of the west GrIS, ranging from the margin to ~1750 metres above sea level (m a.s.l.) in the region of Russell Glacier (Figure 4.1). In this region, three different sets of observations of SGL evolution are available. These data include firstly, the daily SGL distributions for 2003 and 2005-2007 of Sundal et al. (2009) (hereafter 'Sundal09'). Secondly, daily SGL distributions for 2001-2010 reported using the method of Johansson and Brown (2013) (hereafter 'Johansson13'). Thirdly, daily SGL distributions, on days visually identified as cloud-free, for 2005-2007 were mosaicked together, from time series' of evolution for 231 lakes, a subset of those described in Selmes et al. (2011) (hereafter 'Selmes11'). Although each of these datasets is derived from the same set of MODIS images, each dataset has a different record length and temporal sampling is not consistent between them. Table 4.1 indicates the temporal sampling of each dataset on each year for which observations are available. Generally, Selmes11 has the highest sampling density (22-27 days) and Johansson13 has the longest temporally contiguous dataset (2001-2010). Each dataset includes observations for years of high and low runoff availability, indicated in red and blue in Table 4.1. These data are referred to collectively as the 'automatically derived datasets' from here onwards. A brief description of each method is provided here; the respective publications should be referred to for more detail.
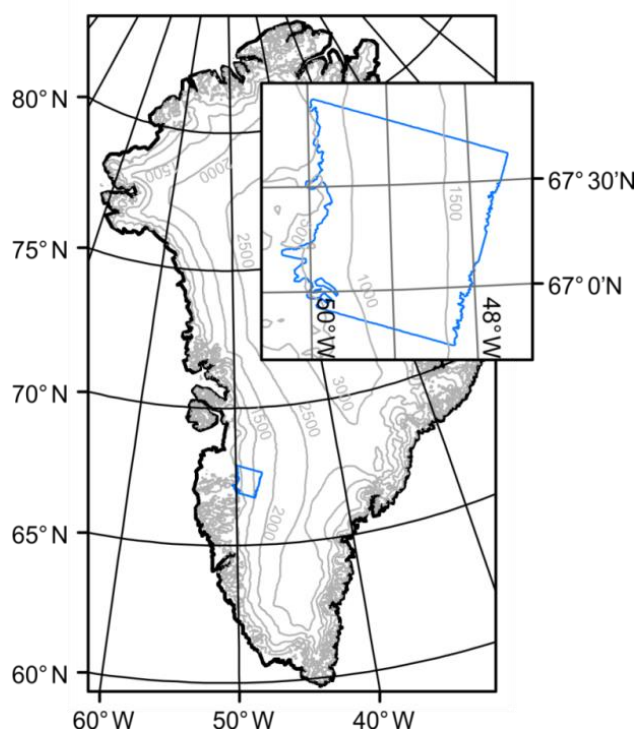
Figure 4.1: Map of Greenland indicating location of study area (bounded in blue). Shown are elevation contours, taken from Bamber et al. (2001), at 500 m intervals from 500 m a.s.l.

Table 4.1: Number of SGL observations in each dataset, in each year. Also shown is the runoff availability for that year, where high runoff, relative to the 2001-2010 mean, is highlighted in red, and low runoff, relative to the 2001-2010 mean is highlighted in blue.

	2001	2002	2003	2004	2005	2006	2007	2008	2009	2010
Johansson13	14	9	11	10	10	13	14	20	19	23
Selmes11	-	-		-	22	27	22	-	-	-
Sundal09	1	-	28	-	12	12	12	-	-	-

Sundal et al. (2009) used MODIS imagery to investigate differences in the seasonal evolution of SGLs across three climatologically distinct regions of the GrIS. In their study, objects are assigned a "lake" or "not-lake" status based on the degree to which they belong to the lake or not-lake class, in terms of reflectance. Sundal et al. (2009) use 268 band 1 (red, 0.620-0.670 μm) MODIS images for the 2003, 2005-2007 period to chart the seasonal evolution of SGLs in three climatologically distinct regions of the GrIS, including the Russell Glacier region. Lake distribution on cloud-free days each year was automatically derived using an object-oriented segmentation and classification method. The classification of lake or not-lake objects was achieved using fuzzy logic membership functions, which assign lake or not-lake status, based on the degree of membership to the lake or not-lake class, rather than using a fixed threshold of a given parameter, e.g. reflectance.

Johansson and Brown (2013) presented and evaluated a new, improved, adaptive lake classification algorithm. This algorithm has been designed in order to report more lakes which are difficult to automatically identify in satellite imagery, such as deep lakes, than previously developed methods. They employ a similar method to Sundal et al. (2009); however they extend the method of classification to include five predefined categories describing early, mid and late season lakes along with small and deep lakes. These categories were based on multiple parameters such as lake length, reflectance and shape. The categories were developed through modelling of statistical distributions of these parameters using 15 manually delineated MODIS images taken in 2007. The categories were designed to address previously identified uncertainty in a reflectance-only method of classification, i.e. small lakes (< 0.1 km^2), lakes covered by an ice 'lid', deep lakes and lakes within cryoconite covered areas. These data include up to 586 individual lakes derived from band 2 (near infra-red, 0.841-0.876 μm) and band 4 (green, 0.545-0.565 μm) MODIS images; SGLs are identified in ~10 images in each year.

Selmes et al. (2011) investigate the distribution of fast draining lakes on the GrIS between 2005 and 2009. In their study, band 1 MODIS images covering the whole of the ice sheet area are used. Selmes et al. (2011) do not use object oriented segmentation. Instead, they devise an a-priori assumed lake distribution, determined from a supervised classification of a subset of images, in order to track the onset, evolution and demise of individual lakes, which exhibit a maximum area greater than 0.125 km^2. Each known lake location is considered in turn; at each location, pixels are assigned lake or not-lake status based on a threshold reflectance value of 65% of a standard reference window (derived from 15 m resolution ASTER imagery). By tracking individual lakes, rather than considering a wide area, this approach enables greater exploitation of the MODIS image library as cloud cover is not considered a limitation, provided at least one lake is visible in each image. An example of lake delineation using each of the methods described here is given in Figure 4.2.
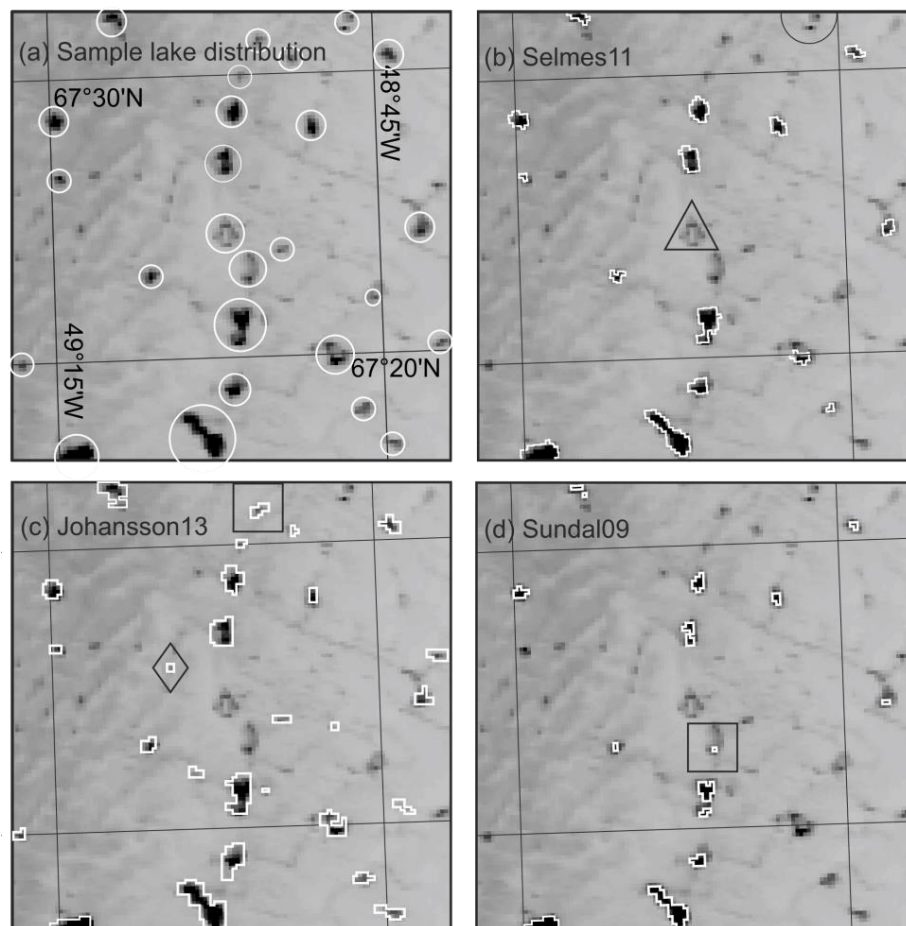
Figure 4.2: Comparison of manually and automatically derived lake distributions on 14th June 2005 (day 165). Background is the original MODIS image. In a) circles surround SGLs identified manually. In b) the triangle indicates an ice covered lake, and the semi-circle indicates an ice-free lake, both are not reported in the automatically derived lake distributions. Squares illustrate lakes reported in a single dataset. Diamond indicates a reported lake that has been identified as a false positive.

The performance of these automated classification algorithms have previously been evaluated by comparing a sample of automatically delineated lakes from a MODIS image, against a sample of lakes manually delineated from high-resolution ASTER or ETM+ imagery. Sundal et al. (2009) perform this evaluation using manually delineated lakes from 15 m ASTER scenes from a single day, 1st August 2001, and automatically delineated lakes from a MODIS image taken on the same day. Selmes et al. (2011) evaluate their method using 15 m ASTER scenes over a three year period across two regions of the ice sheet; one hundred manually-delineated lake images are used in total. Johansson and Brown (2013) validate their method using seven Landsat (ETM+) images acquired between two to six days prior to/after the acquisition of four MODIS images, over two years. The relative scarcity of cloud free MODIS, ASTER or ETM+ images means few days exist where an in-depth evaluation may be made using contemporaneous data.

Each method is known to exhibit unique sources of uncertainty; Sundal09 found that their algorithm had difficulty resolving ice covered lakes and that their method may underestimate lake covered area by as much as 21.1% accordingly (Sundal, 2009). They also estimate that their method may underestimate lake covered area, due to the presence of lakes that are smaller than the resolution of the MODIS instrument, to be 12%. Johansson and Brown (2013) report that as many as 18% of reported SGLs are likely to be false positives. False positives are defined as objects which are initially categorised as lakes, but which may be re-assigned to the not-lake category upon further inspection, e.g. by reference to an image with higher spatial resolution. Johansson and Brown (2013) suggest that the uncertainty associated with the absence of sub-resolution lakes in the dataset is around 11%; in agreement with the similar assessment performed by Sundal et al. (2009). Because Selmes et al. (2011) operate from an a-priori lake distribution, any lake either not available for inclusion in this distribution, or smaller than 0.125 km^2 does not feature in the dataset. The method of Selmes et al. (2011) has also been estimated to under-predict the area of individual lakes by around 1.77% in comparison with higher-resolution ASTER imagery (Selmes et al., 2011).

Although SGL evolution exhibits short-term variability (Das et al., 2008, Doyle et al., 2013), the temporal sampling of satellite datasets is typically sparse by comparison (see Table 4.1). To investigate the impact that temporal sampling has on assessments of SGL evolution, the most populous lake dataset was systematically sub-sampled and key metrics were computed from successively smaller samples. For this exercise, the Sundal09 dataset acquired in 2003 was used, as this was the most densely sampled with 28 separate observations. For each

sample size ranging from 5 to 27 images, 1000 sub-samples were randomly selected from this dataset. The mean, standard deviation and range of values of four key SGL characteristics among each set of sub-samples were then calculated and compared. The SGL characteristics selected for this analysis were the maximum total daily area covered by lakes (the maximum area, in km^2), the date of first appearance of any lake in the dataset (the onset day), the maximum elevation that lake covered area reaches (the maximum extent, in m a.s.l.), and the total number of times any lake is observed during a one year period (the number of lake appearances).

SGL retrieval algorithms exhibit differences in performance. To assess this difference, the size and number of SGLs reported in each automated dataset were compared to estimates derived from manual classifications. The manual classifications were developed from MODIS data acquired in the early, mid and late melt season in each year of overlap between the three automated datasets (2005, 2006 and 2007). First, maps of SGL distribution were created by three people, each on 9 separate days. Features reported as lakes in two or more of these manual distributions were identified as SGLs (Figure 4.3). This corresponds to 78% of all features identified.
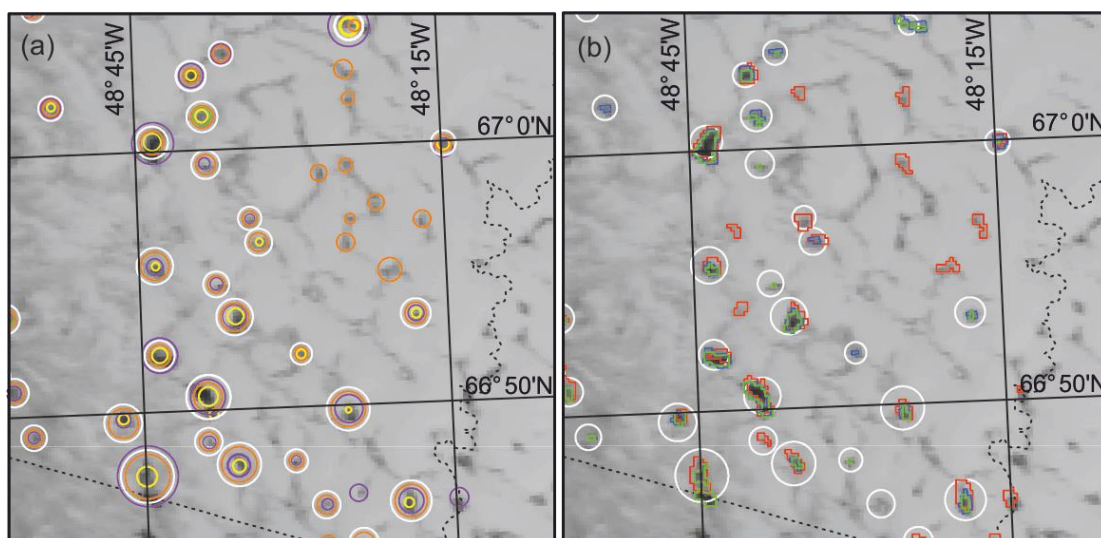
Figure 4.3: Example distribution of SGLs in the study area. (a) Manually delineated lake distribution according to three independent sources (purple, yellow and orange). Sample compiled from two or more of these sources is indicated in white. (b) Automatically delineated lake distribution according to Selmes11 (blue), Sundal09 (green) and Johannsson13 (red). Again, white circles denote lakes that have been positively identified manually (as in (a)).

Secondly, the areas of 10 lakes, exhibiting a range of size and shape (Figure 4.4), were delineated by three individuals using satellite images acquired on two different days in each

year. To be included in this sample, SGLs were required to be reported by all three of the automatically derived datasets, and in two or more images, and in each of the three years. Pixels reported to be lakes in two or more of the manual delineations were identified as SGLs. Because MODIS imagery has a coarse spatial resolution (250 m), the relative performance of this method of manually classifying MODIS imagery was assessed by comparison with ASTER data. A sample of 45 lakes, from imagery acquired on the 1st August 2001 was used; this was the only day for which ASTER data were available, and which featured in two or more of the automated datasets. No ASTER data were available for common days between all three datasets.

In order to combine the three automatically derived datasets, a performance score for each dataset was computed. This was calculated as a linear sum of the relative performance of each dataset in terms of describing the area of individual lakes and lake frequency, when compared to manually delineated data. Relative performance, P, between datasets, j, was calculated using the RMSD from the manually derived data (Equation 4.1) and Equation 4.2:

$$RMSD = \sqrt{\frac{1}{n}\sum_{t=1}^{n}\left(R_t - O_t\right)^2} \qquad\qquad 4.1$$

$$P_j = \frac{RMSD_j^{-1}}{\sum_{j=1}^{3} RMSD_j^{-1}} \qquad\qquad 4.2$$

Where R is the lake size or daily lake number according to the manually derived sample, and O is the lake size or daily lake number according to the observations of Sundal09, Selmes11 or Johansson13. The three datasets were combined hierarchically based on relative performance in reporting lake area and distribution to form a single robust SGL index for the period 2005-2007. In this dataset, lakes are mapped on each date when two or more observations were available. Firstly, lakes from the dataset with the highest performance are incorporated. Next, lakes from the dataset with the second highest performance, and which do not feature in the dataset with the highest performance, are included. Finally, lakes from the dataset with the lowest overall performance are similarly incorporated into the combined record. Because automatic methods of identifying SGLs in satellite imagery are known to produce false positives (Johansson and Brown, 2013), the frequency of false positives in each dataset was also estimated by comparison to a sample of manually classified SGLs.
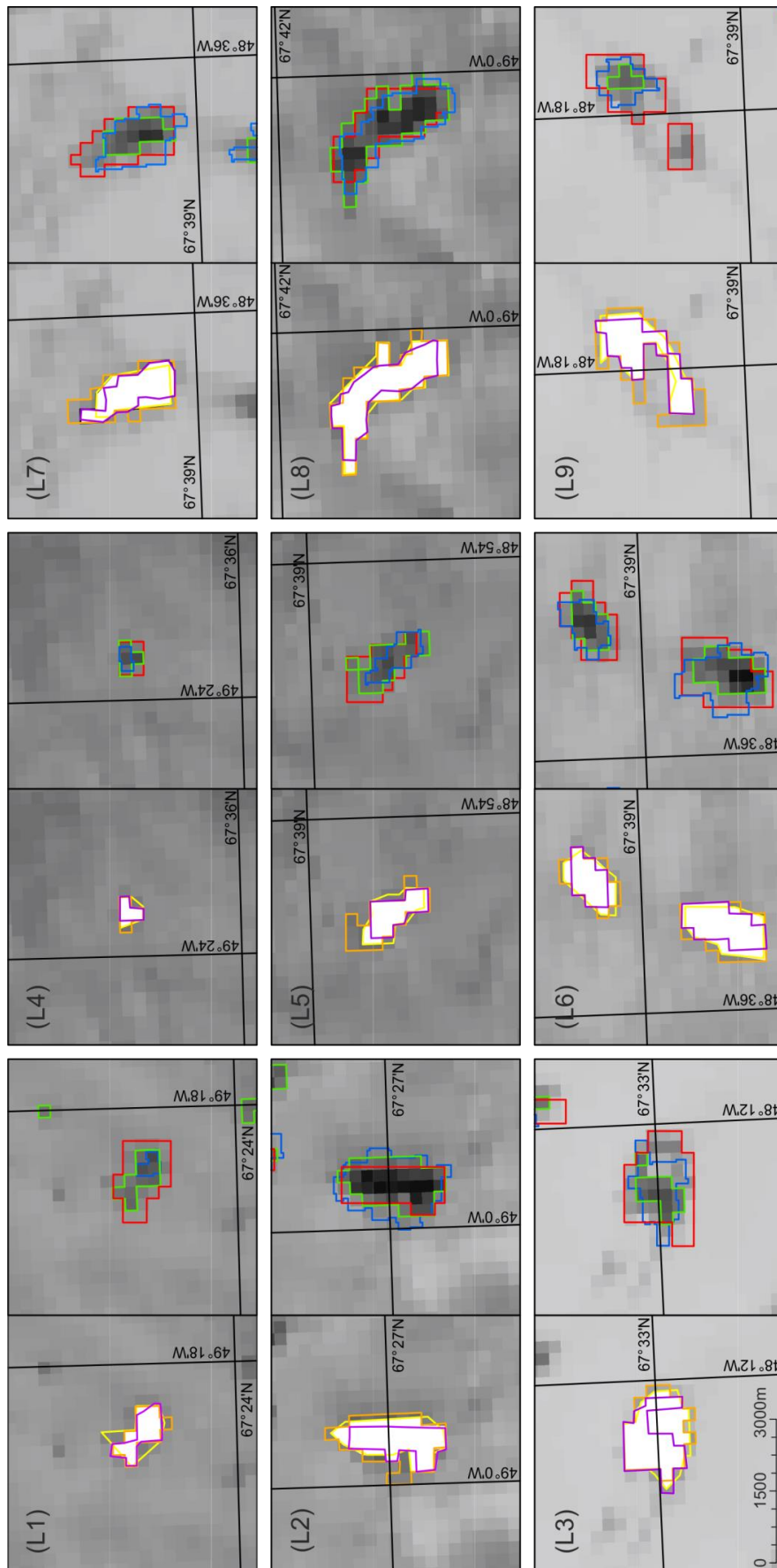
Figure 4.4: Lakes used to create the manually delineated sample. The three different manual delineations are given in yellow, orange and purple. The coincident area, used to create the sample is given in white. Automatically delineated lake area is given in blue (Selmes11), red (Johansson13) and green (Sundal11). All lakes are shown at the same scale.

4.3 Impact of temporal sampling on reported lake evolution

Sub-sampling of the satellite imagery shows that sparsely sampled datasets can fail to capture key aspects of SGL evolution (Figure 4.5).
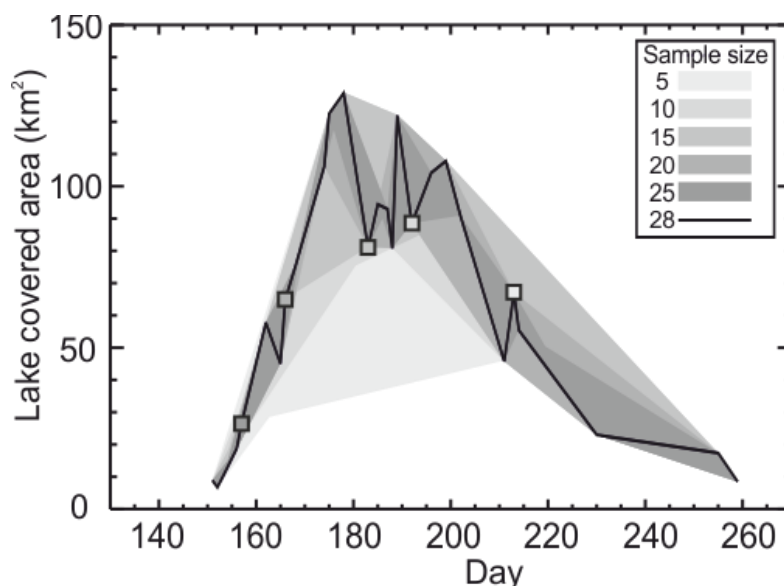
Figure 4.5: Impact of temporal sampling of the Sundal et al. (2009) dataset on reported SGL evolution. Lake covered area is reported daily using sample sizes of 5, 10, 15, 20, 25 days and the full data record of 28 days. Shaded regions indicate the spread of values associated with each sample size, using 1000 random samples. Shaded squares indicate the latest possible onset day using that sample size. Point data is connected by linear interpolation.

If the sample size is limited to 10 days (the smallest sample size featured in the automatically derived observational datasets), the estimated onset date can be delayed by up to 41 days, the estimated maximum daily lake covered area can be underestimated by up to 287%, the maximum altitudinal extent can be underestimated by as much as 180 m a.s.l., and the total number of lakes can be underestimated by as much as 60% (Figure 4.6). These statistics are not surprising, because in this region of the GrIS approximately half of all lakes have a lifespan of less than ten days (Johansson et al., 2013). These extreme deviations from true values arise as a result of clustering within a sample. On average, a sample size of 10 days underestimates the maximum area, onset date, maximum extent and the number of lake appearances by 16%, 4 days, 3 m a.s.l. and 23%, respectively (Table 4.3). In order to produce a reliable record of seasonal SGL evolution from daily observations, i.e. such that maximum lake covered area, onset day, maximum extent and number of lake appearances are all reported, on average, to within 5% of the value reported using 28 days of observations, 20 or more images are required (Figure 4.6). In addition, in order to minimise the possibility that extreme (misleading) values are reported for one or more of these metrics, these images ought to be uniformly distributed throughout the year.
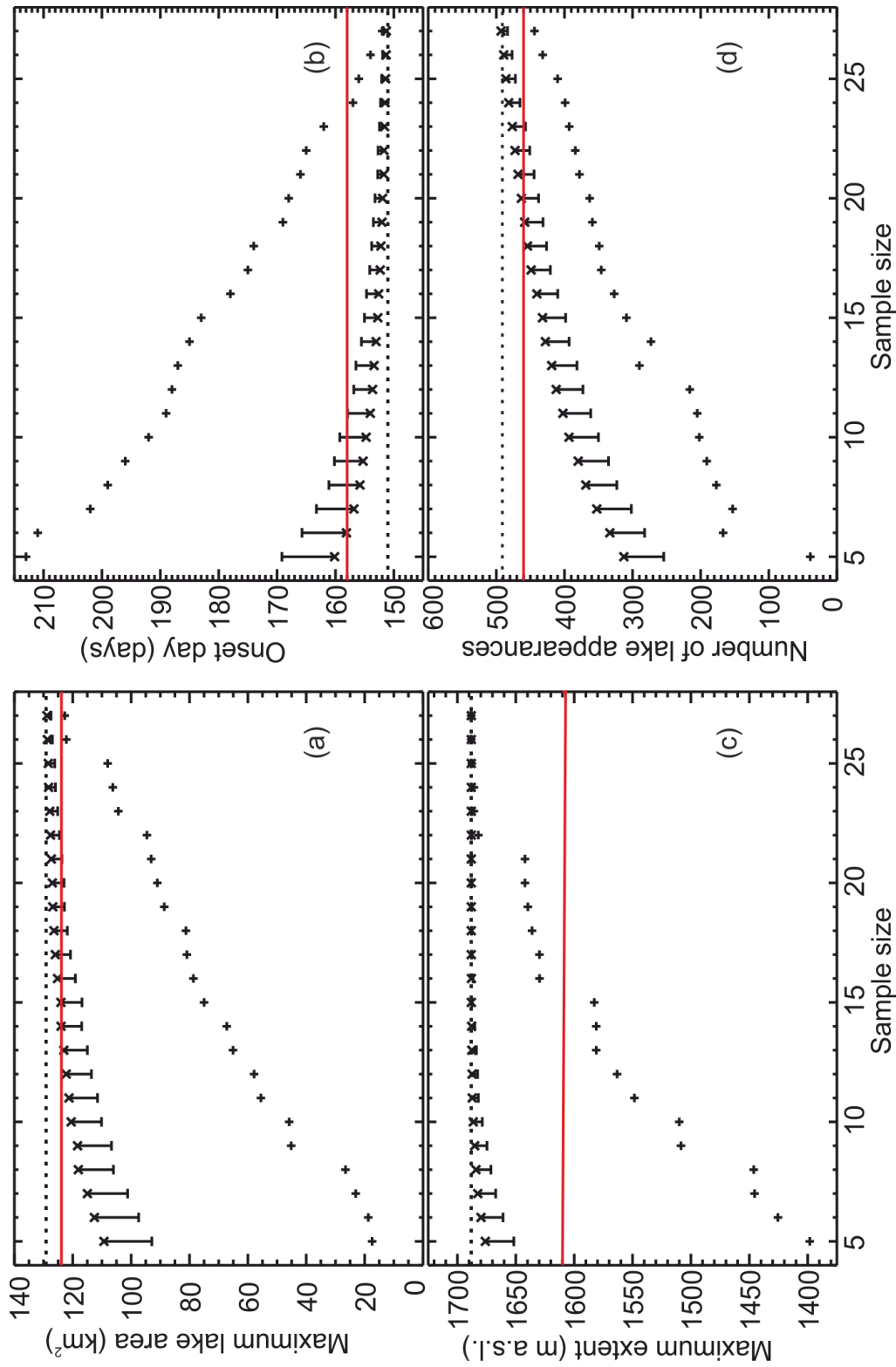
Figure 4.6: *Detailed impact of temporal sampling on reported SGL evolution in the Sundal et al. (2009) dataset. (a) Range of maximum lake covered area reported by taking 1000 samples of each size 5-27 days, from a 28 day dataset. 'x' indicates mean value, error bars refer to 1 σ, '+' indicates the most extreme value. (b) As (a) but for onset day; the day of first appearance of any lake in the entire record. This value is overestimated when small samples are used. (c) As (a) but for maximum elevation on the ice sheet where lakes are reported. (d) As (a) but for number of lake appearances. Also shown is the value reported using a 28 day sample (black dashed) and 5% above or below this value, as appropriate (red).*

However, given the scarcity of cloud free MODIS images, particularly prior to 2008, it may be appropriate to use a model (such as SLInG, described in Chapter 2) in conjunction with temporally sparse observations to investigate problems requiring a high degree of accuracy.

Table 4.2: Mean and standard deviation, associated with sample size, of reported maximum lake covered area, onset day, maximum extent and number of lake appearances in the Sundal et al. (2009) dataset.

Sample size	Maximum lake covered area (km^2)		Onset day (days)		Maximum extent (m a.s.l.)		Number of lake appearances	
	$\bar{x}$	σ	$\bar{x}$	σ	$\bar{x}$	σ	$\bar{x}$	σ
5	109	16	160	9	1675	24	302	48
10	121	11	155	4	1685	7	390	41
15	123	6	153	3	1687	1	431	34
20	127	4	152	2	1688	0	447	12
25	128	2	151	1	1688	0	485	15
28	129	-	151	-	1688	-	509	-

4.4 Inter-comparison of supraglacial lake evolution as reported in three datasets

Each of the three automatic SGL classification methods leads to slightly different distributions (e.g. Figure 4.2), potentially because each method was developed in order to address a different motivation. For example, no single method reports all of the lakes identified manually, tracking ice covered lakes is a problem for all three methods, and each dataset includes false positives. The total number of lakes reported in each year using combinations of the individual datasets were calculated (Figure 4.7). For example, when combined, the Johansson13 and Selmes11 datasets report up to 70% more lakes than the Selmes11 dataset (the dataset of lowest reporting frequency). Combining all three datasets leads to the maximum number of lakes being reported.

When compared to the manually-delineated SGL dataset, the Selmes11, Sundal09 and Johansson13 datasets feature 27 (5%), 61 (9%), and 322 (33%) false positives, respectively (Table 4.3). This equates to 1.66 km^2 (4%), 1.71 km^2 (4%) and 26.5 km^2 (26%), of lake covered area for the three datasets, respectively. For comparison, Johansson and Brown (2013) estimate that their data contain up to 18% false positives. Possible explanations for the ~twofold increased rate of false positives reported here include the relatively coarse

temporal separation of the evaluation data used by Johansson and Brown (2013), and the relatively coarse spatial resolution of the evaluation data used here.
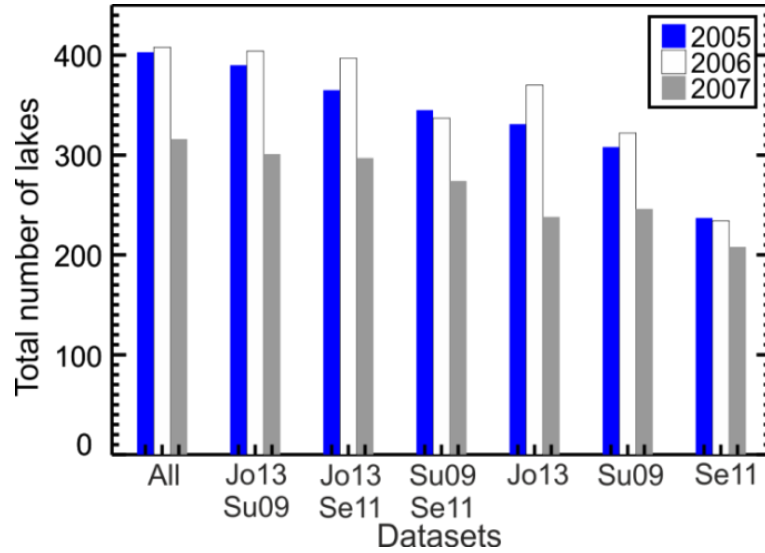
Figure 4.7: Number of lakes reported in each year, using combinations of datasets. Jo13, Se11 and Su09, refer to Johannson13, Selmes11 and Sundal09 respectively.

When false positives are excluded, the Selmes11, Johansson13 and Sundal09 datasets report 52%, 59%, and 71% of the manually identified lakes, respectively. The Selmes11 dataset reports the lowest proportion of lakes. A possible explanation for this under-reporting is the fact that the Selmes11 procedure excludes lakes that are small and that do not feature in a pre-defined target distribution. The RMSD between the number of positively identified lakes reported on each day in the automatically- and manually-derived datasets ranged from 40 lakes (Sundal09) to 64 lakes (Selmes11) (Table 4.4).

Table 4.3: Inter-comparison of lake appearances and false positives between automatically derived observations of SGLs on three days each year for 2005-2007. False positives are determined with reference to manually derived daily lake distributions. These data refer to days 165, 200 and 235 in 2005, days 176, 206 and 225 in 2006 and days 165, 186 and 216 in 2007.

	Johansson13			Sundal09			Selmes11		
Year	2005	2006	2007	2005	2006	2007	2005	2006	2007
All lake appearances	197	475	262	228	322	246	173	228	165
False positives	60	182	75	5	28	28	3	11	13
False negatives	203	103	119	117	102	88	170	179	154
All lake area (km^2)	207	442	266	88.5	149	99.1	136	172	126
False positive area (km^2)	43.2	135	60.4	0.93	7.44	6.57	2.40	6.27	6.71

Lake size, as reported in Johansson13, Sundal09 and Selmes11, is compared with a sample of manually delineated lakes and a mean bias in reported lake area is found of +55%, -27% and -4%, respectively. This is in good agreement with Selmes et al. (2011), who estimate that their method under predicts individual lake area by 1.77%. The variability in all cases is high; neither Selmes11 nor Sundal09 report lake size consistently within 1 standard deviation of values reported in the manually delineated sample (Figure 4.8). When compared with ASTER data, the size of manually delineated lakes were found to have an RMSD of 0.24 km^2. By comparison, the area of lakes reported by Sundal09 and Johansson13 was found to have an RMSD of 0.39 km^2 and 1.47 km^2. No observations of SGLs, contemporaneous with the ASTER data, were available using the Selmes11 method, and so an assessment of this algorithm's performance against ASTER was not possible. A possible explanation for the Johansson13 dataset over-estimating the area of lakes is the fact that their procedure employs optical data acquired in the wavelength range 545-565 nm (band 4), which is known to be overly sensitive to shallow water (Sneed and Hamilton, 2007).
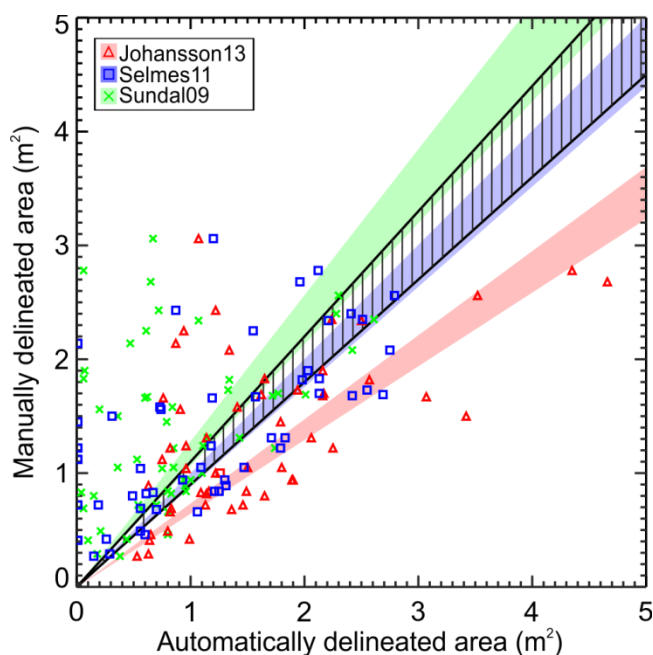
Figure 4.8: Comparison between automatically derived area and manually delineated area of 60 separate lake images. Shaded regions relate to a linear fit +/- 1 σ. Hatched region indicates a one-to-one fit, +/- the 1 σ uncertainty in the manually delineated sample.

To assess the relative performance of each dataset, an overall performance score was calculated based on the linear sum of the relative performance of each dataset in terms of describing lake area and lake frequency, when compared to manually delineated data. Based

upon this analysis, the relative performance of the Selmes11, Sundal09 and Johannson13 datasets was found to be 0.75, 0.72 and 0.53, respectively, where a higher score indicates a better performance (Table 4.4).

Table 4.4: Inter-comparison of automatically derived SGLs with a manually delineated sample of SGL area. RMSD values are transformed into a relative performance score, P, with respect to each parameter. A total performance score is calculated for each dataset by the linear sum of weights for reported lake area and daily number of lakes.

	Johansson13		Sundal09		Selmes11	
	RMSD	P	RMSD	P	RMSD	P
Area (km^2)	0.95	0.24	0.78	0.29	0.48	0.47
Daily number of lakes	60.53	0.29	40.23	0.44	64.03	0.27
SCORE		0.53		0.72		0.75

4.5 A combined dataset of supraglacial lake evolution

Combining the three automatically-derived SGL datasets leads to an increase in the number of lakes reported. On average, 67% more lakes are reported on each day than are reported by the least populous (Selmes11) dataset alone (Figure 4.9). As a consequence, estimates of spatially integrated SGL characteristics, for example daily lake covered area, using the combined (optimised) dataset, may be considered more robust than those made using a single dataset. The combined dataset also increases the temporal sampling of the most infrequently sampled datasets (Sundal09 and Johansson13). For example, in 2005, 2006, and 2007, the combined dataset includes 15, 19 and 17 days, as compared to 12, 12, and 12 days in the least sampled dataset. This offers a potential reduction in uncertainty due to sample size (Figure 4.6), for example, onset day is delayed half as much on average, when a sample size of 19 is used compared to a sample size of 12, i.e. 2 days and 4 days respectively. Also, the mean underestimate of maximum altitudinal extent is reduced from 3 m a.s.l (which encompasses an area of 30.42 km^2), when a sample size of 12 is used, to 0.5 m a.s.l. (4.95 km^2), with a sample size of 19. Likewise, maximum lake covered area is underestimated by 16% and 5% on average, and number of lake appearances is underestimated by 23% and 15% on average, when sample sizes of 12 and 19 are used, respectively.

Inter-annual variability is considerable in both the combined and individual SGL datasets over the three years under consideration (Figure 4.10, Figure 4.9). For example, in 2007 - a relatively high runoff year - lake onset at high elevations occurs earlier than in either 2005 or

2006 (Figure 4.10). Johansson et al. (2013) calculate that a threshold value of melting has to be exceeded for lakes to form, and it is likely that this threshold is exceeded sooner in high runoff years, as is evidenced here. Also, in 2007 the rate of lake covered area increase was faster, and the widespread disappearance of lakes occurred sooner than in the low and moderate runoff years of 2005 and 2006, respectively (Figure 4.9). This behaviour is consistent with a noted correlation between the intensity of melting and the onset of lake drainage (Liang et al., 2012). Each of the automatically derived datasets, and the combined dataset, report the inland progression of SGLs throughout as the melt season progresses, with similar timing (Figure 4.10).
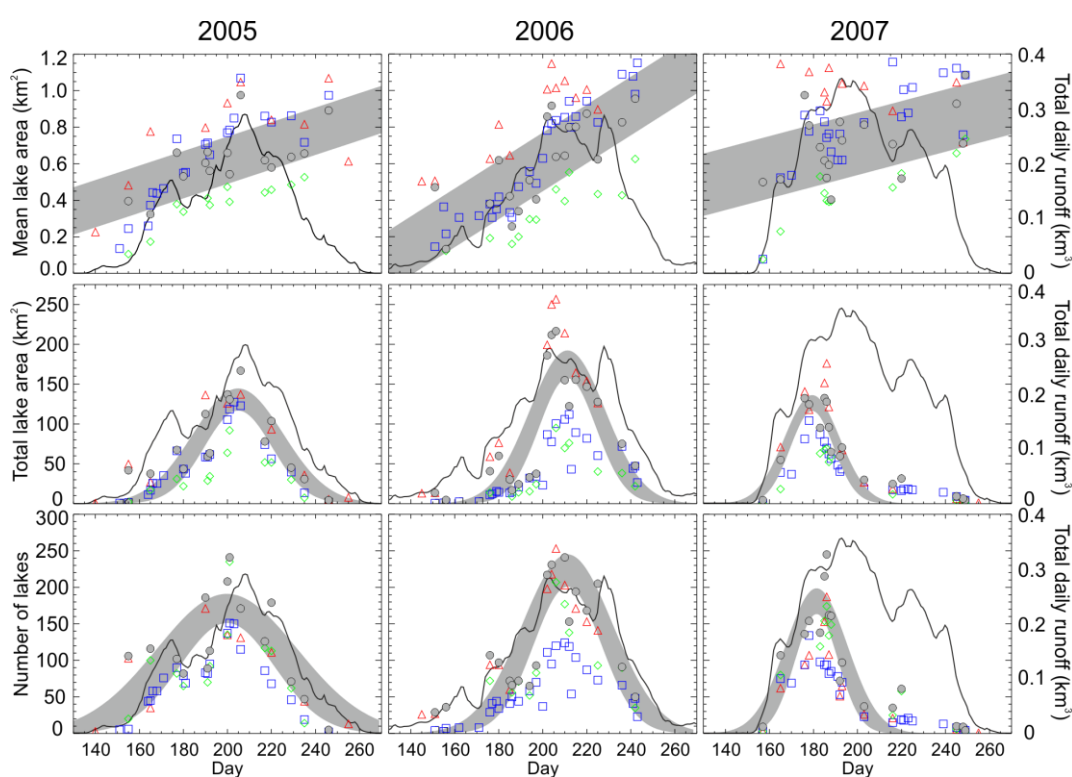
Figure 4.9: Inter-annual variability of SGL evolution using the new, combined SGL dataset. Rows are time series of mean lake area, total lake covered area and number of lakes, for 2005, 2006 and 2007. Diamonds indicate Sundal09, squares indicate Selmes11, triangles indicate Johansson13 and filled circles indicate the combined dataset. Shading delineates a linear (mean area) or Gaussian (total area and number of lakes) fit to the combined dataset, including the 1 σ uncertainty on this fit. Also shown (black line) is the daily runoff (km^{3}d^{-1}) integrated over the study region, as simulated using the MAR model (Fettweis, 2007).

This new, combined dataset was used to investigate differences in patterns of SGL evolution between 2005, 2006 and 2007. The lowest peak in maximum lake covered area occurs in 2007 (Figure 4.9). This finding is surprising, because Sundal et al. (2009) observe a general correlation between maximum lake-covered area and total annual runoff. In the combined

dataset, lake covered area remains small following drainage, despite continued abundance of runoff production. A possible explanation for this behaviour lies in the process of hydrofracture beneath SGLs, which is believed to establish conduits linking the ice sheet surface and base (e.g. Krawczynski et al., 2009). These conduits can then remain open for the remainder of the melt season (e.g. Das et al., 2008, Doyle et al., 2013), thereby inhibiting further lake formation and growth. Such behaviour is less apparent in 2005 and 2006; however, in 2007 a higher proportion of lakes are known to have disappeared through rapid drainage (Selmes et al., 2013). Finally, the rate of lake covered area growth in all three years follows the rate of change of runoff production (Figure 4.9). For example, in 2007, runoff production accelerates quickly and there is a corresponding rapid growth of number of lakes and total lake covered area. This suggests that total annual runoff amount is not the only control on SGL evolution.
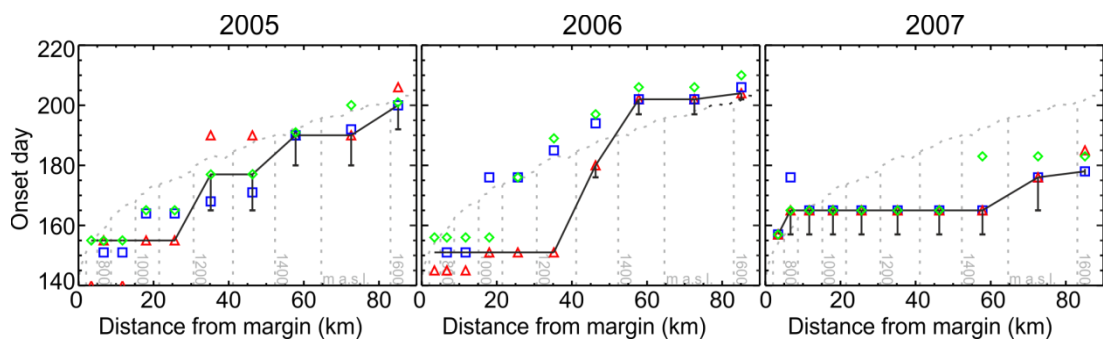
Figure 4.10: Variation of regional SGL onset day with distance from margin in 2005, 2006 and 2007. Symbols indicate dataset; Sundal09 is indicated by diamonds, Selmes11 with squares and Johansson13 with triangles. The combined dataset is given by a solid line. Here, error bars indicate uncertainty due to temporal sampling.

4.6 Summary

Uncertainty within observational datasets of SGL evolution, derived using automated methods, has been investigated. The results presented here reveal a strong dependence between the frequency of the satellite imagery and the maximum lake covered area, the lake onset date, the maximum lake extent and the number of lake appearances reported in the automated datasets. For example, using a sample size of 10 days, lake onset is delayed by 4 days on average, and the maximum lake covered area is underestimated by 16% on average, compared to values reported using a 28 day sample. It is recommend that a minimum of 20 images per year of observations is required, preferably uniformly distributed in time, in order to minimise uncertainties associated with poor temporal sampling. However, given

the scarcity of entirely cloud free MODIS images, particularly prior to 2008, it may be more appropriate to use a model, in conjunction with temporally sparse observations to investigate problems requiring a high degree of accuracy. The model described in this thesis, would be a useful tool for this purpose.

The performance of three independent SGL datasets derived using different automated methods, each based on MODIS satellite imagery, was assessed in terms of their ability to describe the area and number of lakes when compared to manually delineated data. The observations of Selmes et al. (2011) were found to report *the area of lakes* most accurately (RMSD = 0.48 km^2), whereas the observations of Sundal et al. (2009) were found to report the *number of lakes on each day* most accurately (RMSD = 40 lakes). Each of the three automatically-derived datasets are also shown to include false positives, ranging from 5% to 33% for Selmes11 and Johansson13, respectively. Using an objective assessment, the observations of Selmes et al. (2011) are judged to perform best overall, and the observations of Johansson and Brown (2013) are judged to perform least well overall. However, the spread of performance estimates is narrow (0.53-0.75), and all three datasets are in agreement when describing temporal patterns of SGL evolution at the seasonal and inter-annual timescales.

Each dataset exhibits different strengths and weaknesses, and it is advantageous to combine them into a single optimised product, in order to provide more data points which may be used for model evaluation. This combined dataset reports more lakes each day, which are identified manually, than a single dataset and offers a significant reduction in uncertainty due to improved sample size. In 2007, a particularly high runoff year, lakes begin to disappear through drainage much sooner than in the years where less runoff is produced. Following drainage, lake covered area remains low, despite the continued production of runoff. This may be attributed to the creation of conduits linking the ice sheet surface and base, presumably through hydrofracture of SGLs. In these three years of data, there is no apparent correlation between total annual runoff and maximum lake covered area. However, the rate of lake covered area growth is found to be correlated with the rate of runoff production. Therefore, these results suggest that total annual runoff is not the only control on SGL evolution. However, these findings are based on just three years of satellite data, and a more extensive and densely sampled record would lead to improved confidence in assessments of inter-annual variations in SGL evolution.

Chapter 5

Inter-annual and longer-term variability in supraglacial lake evolution from observations and modelling

5.1 Introduction

The spatial and temporal evolution of supraglacial lakes (SGLs) is known to exhibit inter-annual variability (e.g. Sneed and Hamilton, 2007a, Selmes et al., 2011). Observational studies suggest that this inter-annual variability is driven by meltwater supply (e.g. Sundal et al., 2009, Liang et al., 2012). The date of lake formation (onset) has been found to vary by up to 1 month inter-annually (Sundal et al., 2009), and this has been shown to be driven by total melt as lake initiation begins once a threshold of melting has been exceeded (Johansson et al., 2013). In Chapter 4, a direct link was proposed between lake filling rate and rate of change of runoff production, based on three years of observations. A relationship between the intensity of melting and lake drainage has also been observed, and it has been found that lakes drain earlier and more frequently in years of higher melting (Liang et al., 2012). The area of the ice sheet covered by SGLs varies from year-to-year (e.g. Sundal et al., 2009, Sneed and Hamilton, 2007a, Selmes et al., 2011). This variability has been shown to be positively correlated with modelled runoff amount (Sundal et al., 2009). A corresponding relationship between the intensity of melting and the maximum elevation at which lakes may be found has also been documented (Liang et al., 2012). This has been borne out by the inland migration of SGLs over the past 40 years as the climate of the Arctic region has warmed (Howat et al., 2013). These relationships suggest that the spatial and temporal distribution of SGLs is responsive to long-term changes in climate. It has been suggested that SGLs can affect seasonal and shorter-term ice sheet velocity changes when they drain (e.g. Shepherd et al., 2009, Palmer et al., 2011, Bartholomew et al., 2012), and that peak seasonal speed-up occurs shortly after maximum lake covered area has been reached (Shepherd et al., 2009), presumably as this marks the onset of widespread drainage. As such, their response to a changing climate may have implications for ice sheet dynamics. However, an assessment of inter-annual variability and long term changes in the spatial and temporal evolution of SGLs is lacking.

In Chapters 2 and 3, a model of SGL initiation and growth (the SLInG model) was described and evaluated against one year (2003) of temporally dense observations derived using an automated classification of satellite data. According to the MAR (Modèle Atmosphérique Régional) regional climate model (RCM) (Fettweis, 2007), 2003 is characterised as having abundant melting, leading to runoff 26% greater than the decadal (2001-2010) mean. Preliminary investigations were also made as to the efficacy of the model in reproducing SGL evolution for the period 2005-2007. However, it was concluded in Chapter 3 that more observational data was required in order to perform a robust evaluation of model performance in different years. In Chapter 4, three independent datasets of daily SGL distribution, derived from Moderate Resolution Imaging Spectroradiometer (MODIS) imagery using a variety of automated classification methods, were compared, evaluated and combined into a new consolidated dataset covering the period 2005-2007 (hereafter, 'Leeson13'). This period encompasses years when runoff was higher (2007), lower (2005), and close to (2006), the decadal mean (118%, 81%, and 91%, respectively). Using Leeson13, it was concluded in Chapter 4 that, within the three years under consideration, there was no correlation between total annual runoff and maximum SGL covered area. However, a relationship between the rate of increase in runoff and the growth rate of SGL area was identified. In addition, during a year of high melting (2007), SGLs were observed to drain quicker and thereafter remain empty, despite continued production of runoff.

In this chapter, inter-annual and longer-term variability in SGL evolution is investigated using Leeson13 and the SLInG model. As the SLInG model does not simulate lake end-of-life processes, such as refreezing and drainage, this study focuses on pre-drainage parameters (such as onset day) and drainage-independent parameters (such as maximum elevation). In Section 5.2, inter-annual variability in runoff is discussed. In Section 0, modes of inter-annual variability in SGL evolution are investigated. This includes an evaluation of the performance of SLInG at the inter-annual timescale, against the new, robust, combined dataset Leeson13. In Section 5.5, linear relationships between SGL characteristics and runoff are investigated for the 2001-2010 period using SLInG. In Section 5.6, the impacts of recent climate change on SGL evolution are investigated using SLInG for the period 1971-2010. Finally, in Section 5.7 a summary of this chapter's work is provided.

5.2 Inter-annual and longer-term variability in climate and runoff data

Runoff is calculated as the sum of meltwater and wet precipitation, minus any water that is retained in the snowpack or refrozen. The principle atmospheric controls on runoff

production are temperature and precipitation, which means that patterns of runoff availability are highly responsive to climate forcing.

Runoff in any given year can be characterised by three gross parameters, 1) the total annual amount produced, 2) the length of the melt season and 3) how quickly runoff production accelerates from zero to the peak annual rate (Runoff$_{max}$). Runoff production for the 2001-2010 period, as simulated by MAR, is given in Figure 5.1 (Fettweis, 2007). The years 2003, 2007 and 2010 set successive records for extreme climate. For example, the summer of 2003 was found to be the warmest since 1958 (Hanna et al., 2008b). The year 2007 was characterised by unusually warm conditions and low accumulation leading to an extreme surface melt event (Mote, 2007, Tedesco, 2007); simulations suggest that 2007 had the second highest runoff amount in the previous 50 years, after 1998 (Hanna et al., 2008b). In addition to total amount of melt produced, 2007 saw a new record in melt extent. MAR simulates an equilibrium line in 2007 which is considerably higher than the 1988-2006 mean, with melt simulated up to about 2500 m a.s.l. in the Russell Glacier area (Tedesco et al., 2008). Similarly, in 2010, total runoff amount and total melt extent reached new record levels, over those observed in 2007, which was attributed to the exceptionally early onset of the melt season, leading to 50 days more melt than the 1979–2009 average (Tedesco et al., 2011a). Although runoff produced in 2007 reached a record high, the melt season was relatively short at only 118 days. The years with the longest melt season were 2003, 2002, 2006 and 2010 with 167, 151, 151 and 163 days, respectively.

The climate during the 1971-2010 period was characterised by little/no temperature change during 1971-1990 followed by large temperature increases during 1991-2000 and 2001-2011 (e.g. Hanna et al., 2012, Box et al., 2009, van den Broeke et al., 2009). These changes are particularly obvious on the west coast of Greenland; in south-west Greenland, mean summer air temperature for 2001-2011 was 2.2^{o}C warmer than the 1971-2000 mean (Hanna et al., 2012). The GrIS surface has warmed up to +2.4^{o}C since 1979 and this has been attributed to anthropogenically induced atmospheric warming (Fettweis, 2007). This surface warming has had a corresponding impact on surface mass balance and runoff production; modelling studies suggest that runoff has increased from ~170 Gt in 1990 to ~260 Gt in 2010 (Vernon et al., 2013). This increase in runoff production has led to the inland expansion of the region of the ice sheet where melt occurs. In 2012, 98.6% of the GrIS experienced melting; the largest melt extent on record (Nghiem et al., 2012).
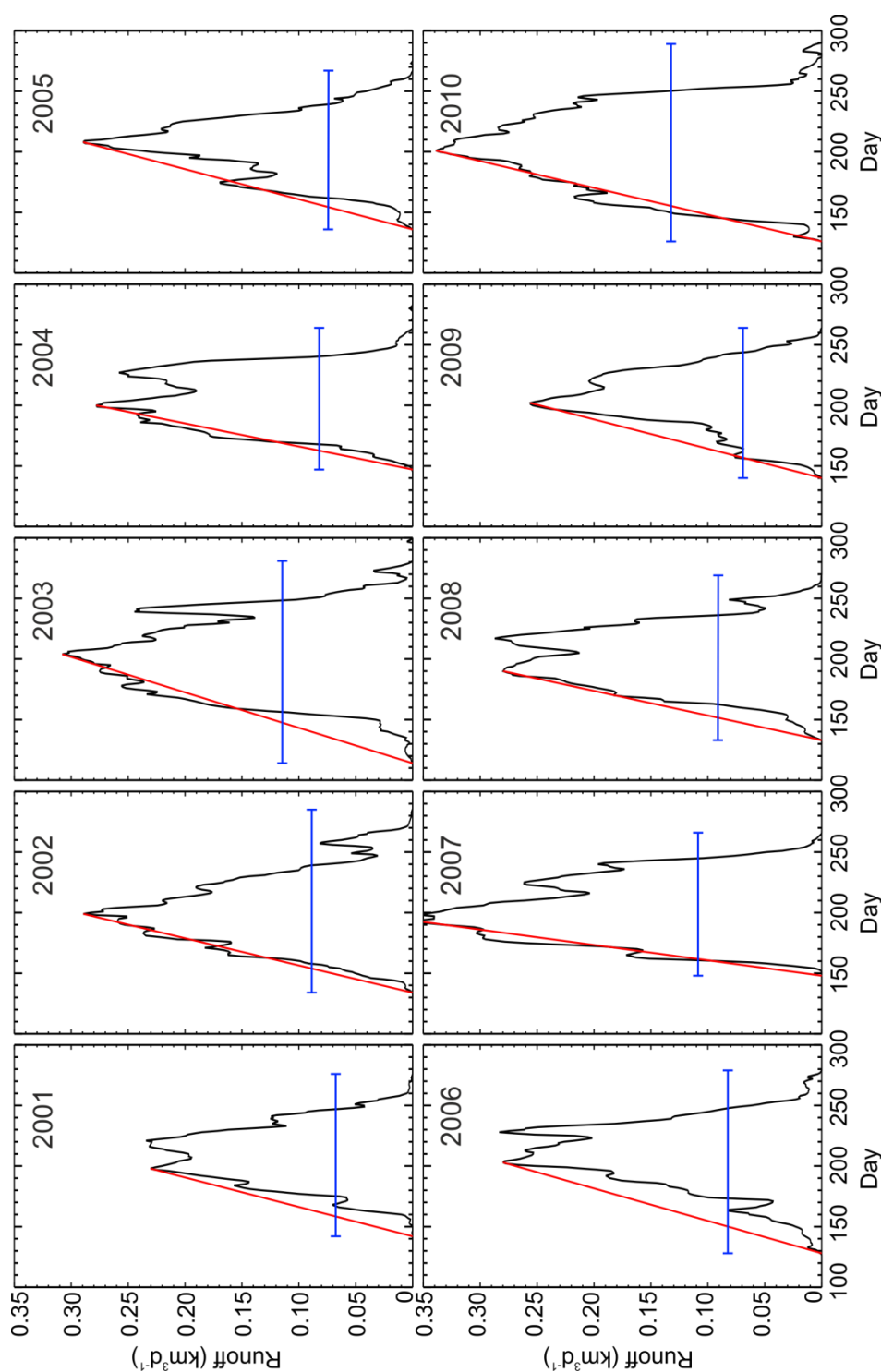
Figure 5.1: Runoff availability during 2001-2010 as simulated by the MAR RCM in the Russell Glacier region of the GrIS (Fettweis, 2007). Total daily runoff is given in black. Blue lines indicate the length of the melt season (length) and the mean daily runoff amount (y position). Red lines indicate an approximation of the derivative of the daily runoff curve, from 0 mm per day to the first maxima.

In the longer-term climatic context, studies using over 100 years of meteorological observations have shown that the Atlantic Multidecadal Oscillation (AMO), a key driver of multi-decadal variability in sea surface temperature in the North Atlantic, has historically had a strong influence on the multi-decadal summer climate of southern Greenland

(Arguez et al., 2009). In addition, a negative correlation between the North Atlantic Oscillation index (NAOI) and Greenland air temperature has been proposed (Hanna et al., 2009). In recent years however, the strength of this correlation has become weaker, since the effect of global warming on Arctic climate has become more significant (Hanna et al., 2008a, Simmonds et al., 2008). In fact, during the period 1958 and 2010, no statistically significant correlation can be seen between weather-station based observations of temperature or runoff and the NAOI (Hanna et al., 2013). A third influential mode of atmospheric variability, specific to Greenland, has also been proposed; the Greenland Blocking Index (GBI). The GBI uses the mean 500 hPa geopotential height over Greenland to characterise regional patterns of airflow (Fang et al., 2004). Both runoff and air temperature have been significantly correlated with the GBI (r=0.60), and also with the AMO (r=0.44), between 1958 and 2010 (Hanna et al., 2013). Since the AMO is associated with timescales of around 50 years and the NAO is associated with timescales of around 12 years (Arguez et al., 2009), it is unlikely that the observations of SGL evolution currently available are able to capture any influence these large scale atmospheric circulation indices may have on runoff, and consequently SGL behaviour.

5.3 Data and methods

In the remainder of this chapter, years will be discussed in terms of total annual runoff, the length of the melt season, and the rate of runoff increase to peak production. Total annual runoff is calculated as the sum of daily runoff, produced in a 1 year period. The length of a melt season is typically defined as the duration of time for which positive runoff is produced at the ice sheet surface. Because, in practise, small amounts of runoff are produced every day (for example, through rainfall at low elevations), here the melt season is approximated as the amount of days on which runoff exceeds 0.1% of the maximum value for that year. Calculated melt season lengths for 2001-2010 are shown in Figure 5.1. The rate of runoff increase is approximated as the gradient of runoff production between the dates on which runoff rises from 0.1% of the maximum value to the maximum value (e.g. Figure 5.1).

The combined SGL record, Leeson13, is used in order to evaluate the performance of SLInG for the period 2005-2007 in terms of locating SGLs and reproducing their spatial and temporal evolution. This improves upon the evaluation of the model described in Chapter 3 which used data from Sundal et al. (2009) (hereafter, 'Sundal09') only, to assess model performance in 2003 and over the 2005-2007 period. Leeson13 offers a reduction in

uncertainty compared to the observations of Sundal09 in isolation, for the 2005-2007 period, and as a consequence can be considered a better dataset despite a higher proportion of false positives. Sundal09 has 9% false positives whereas Leeson13 has 33% false positives. Leeson13 reports 54% more of lakes that can be manually identified in satellite imagery than Sundal09. In addition, because of the small sample size in these data (12 images), Sundal09 underestimates maximum lake covered area by up to 59% (~8% on average) (see Chapter 4). In Leeson13, this value is reduced to 31% (~1% on average). Likewise, Sundal09 may overestimate the start of the period where lakes are present on the GrIS by up to 37 days (~5 days on average), and underestimate the maximum elevation at which lakes may be found by 126 m a.s.l. (~5 m a.s.l. on average). In Leeson13, this is reduced to 18 days (~1 day) and 48 m a.s.l. (0 m a.s.l.). Thus, the combined observational record (Leeson13) is the most robust for evaluating the performance of SLInG.

Several parameters are used to assess model performance, including lake location, lake distribution, lake onset day and the temporal evolution of lake number, mean lake area and total lake covered area. The performance of SLInG in reproducing lake location is expressed in terms of percentage of observed lakes that are co-located by the model. Lake distribution in the model and observations is compared by examining the maximum elevation at which lakes may be found. Since, in recent years, lakes have been observed beyond the limits of the DEM used in SLInG (up to ~1900 m a.s.l.) (Howat et al., 2013), SLInG is not able to simulate the absolute maximum altitudinal extent. Because of this, the elevation of the 90th percentile of total lake area is used to represent the maximum lake elevation, following the method of Liang et al. (2012). SLInG simulated maximum elevation and simulated elevation of 90th percentile were found to be strongly correlated (r=0.69) for the years 1971-1981, during which period maximum lake elevation in this region did not extend beyond the bounds of the DEM (Howat et al., 2013). The mean difference between the 90th percentile of lake elevation and maximum lake elevation was found to be ~207 m a.s.l. for this period.

Lake onset can either be defined at the regional scale, i.e. day of first appearance of any lake in a given region, or at the individual scale, i.e. day of first appearance of a specific lake. Model performance in reproducing the onset day of individual lakes was assessed using the Pearson correlation coefficient (PCC) between simulated and observed onset days of all co-located lakes. The ability of SLInG to reproduce the spatial distribution of onset day, i.e. the

day of first appearance of any lake in successive elevation bands is assessed using the root-mean-square deviation (RMSD). Model performance in terms of temporal evolution of lake number, mean lake area and total lake covered area is assessed using the RMSD between modelled and observed time series. In order to assess the performance of SLInG across the whole seasonal cycle, a cumulative time series of observed lake distribution is also created using Leeson13 and the method outlined in Section 3.2.1.1. This renders all observed lakes available for comparison with their simulated counterparts that do not drain, from the point at which they are first observed until the end of the melt season. Finally, a single score is assembled for each year, based on the linear sum of performance metric, normalised to indicate relative performance between years (Equation 5.1). Where decreasing values of performance metric indicate greater skill (e.g. RMSD), values are first adjusted by taking the reciprocal (Equation 5.2).

$$N_j = \frac{P_j}{\sum\limits_{j=1}^{n} P_j}$$

<div style="text-align: right">5.1</div>

$$N_j = \frac{P_j^{-1}}{\sum\limits_{j=1}^{n} P_j^{-1}}$$

<div style="text-align: right">5.2</div>

The strength and direction of relationships between runoff parameters and SGL characteristics for the ten-year period 2001-2010 are determined using the PCC. Runoff parameters include total runoff amount, length of melt season and rate of increase of runoff. These runoff parameters are calculated from MAR output (Figure 5.1). SGL characteristics are: mean lake onset day, lake filling rate, maximum lake covered area, the timing of maximum area and maximum elevation at which lakes may be found. The mean lake onset day in each year is calculated using the simulated onset day of each reported lake. Lake filling rate is approximated by the total lake covered area growth rate, $\dot{A}$ (here, dot notation is used to denote the time derivative), and the timing of maximum area is the day on which maximum lake covered area is simulated. SGL characteristics are as simulated by SLInG.

5.3.1   *Model set-up and experiment design*

Simulations were performed for the 1971-2010 period using the SLInG model in order to

investigate inter-annual variability in SGL evolution. Model setup follows that detailed in Chapter 2; a short summary is provided here. The model was again run with a resolution of 100 m x 100 m in a 6,753 km^2 region of western Greenland ranging from 1100 m a.s.l. to 1752 m a.s.l., in the vicinity of the Russell Glacier (Figure 5.2). Simulations were forced by runoff, snow depth and snow density, generated by the MAR RCM run at 25 km resolution over Greenland. The MAR model features a comprehensive snow and ice component which is based on the CEN (Centre d'Etudes de la Neige) snow model CROCUS (Brun et al., 1992). This component of MAR determines the energy fluxes between the atmosphere and the ice sheet surface and calculates runoff accordingly, accounting for snow thermodynamics, snow metamorphism, retention and refreezing. MAR is forced at the boundaries by the European Centre for Medium Range Weather Forecast (ECMWF) ERA-Interim reanalysis for the period 1988-2010. MAR is forced by the ECMWF ERA-40 reanalysis for the period 1971-1987.

SLInG is run with a 90 second time step, and lake distribution is reported every model day for days 100 to 300 on each year (a period that encompasses the full duration of the melt season). All of the SGL observations used in this chapter are derived from MODIS imagery, which has a resolution of 250 m, and so lakes smaller than 0.0625 km^2 (250 m x 250 m) are masked out of daily distributions simulated by SLInG. A high resolution digital elevation model (DEM) created from Interferometric Synthetic Aperture Radar (InSAR) data acquired in 1996 by the European Remote Sensing satellites (Palmer et al., 2011) forms the surface of the ice sheet in all simulations referred to in this chapter. Since end of life processes such as drainage and re-freezing are not represented within the model, water is not allowed to overwinter in lakes, and it is assumed that all water stored in lakes drains away completely. The initial condition of an 'empty' ice sheet surface at the start of each model year is imposed and therefore each year of simulations can be considered to represent a separate time-slice. It is assumed that there are no inter-annual topographic fluctuations, and so the DEM surface is not evolved. Surface topography is largely controlled by the transmission of basal conditions through the ice sheet (Gudmundsson, 2003). This influence has been shown to hold for topographic undulations of wavelengths conducive to the formation of lakes (Lampkin and VanderBerg, 2011). In addition, observational studies of SGLs have shown that they appear in the same locations annually (Selmes et al., 2011, Echelmeyer et al., 1991).
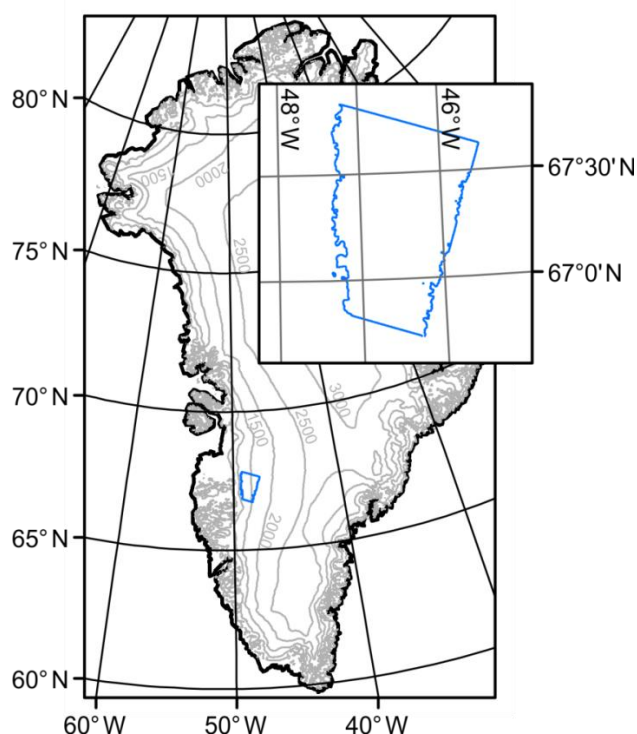
Figure 5.2: Map of Greenland showing study area (bounded in blue) considered in this chapter. Also shown are elevation contours, from Bamber et al. (2001), at 500 m intervals from 500 m a.s.l..

5.4 An evaluation of SLInG at inter-annual timescales

SLInG has been shown to reproduce 66% of lakes of area greater than 0.125 km^2 that were observed to form during the 2003 melt season in the Sundal09 dataset (see Chapter 3). Here, the proportion of lakes observed in the Leeson13 combined dataset, which are successfully simulated by SLInG, is calculated to be 54%, 48% and 72% in 2005, 2006 and 2007. However, because Leeson13 is likely to include 29%, 36% and 31% false positives in 2005, 2006 and 2007 (see Chapter 4); this can be considered a lower bound.

In 2005, 2006 and 2007, SLInG estimates the elevation of the 90th percentile of total lake area to be 1441 m a.s.l., 1514 m a.s.l. and 1548 m a.s.l.. In the same years, Leeson13 estimates the elevation of the 90th percentile of total lake area to be 1570 m a.s.l., 1583 m a.s.l. and 1599 m a.s.l. SLInG underestimates the elevation of the 90th percentile of total lake area by 83 m a.s.l. on average, compared to the observations. This is to be expected because in SLInG, lakes form from runoff produced within the bounds of the DEM only. In reality, any water produced upstream of the DEM boundary would also contribute to lake growth at upper elevations. Despite not reproducing the absolute values, SLInG reproduces

the inter-annual variability of maximum lake elevation well. In both Leeson13 and the simulation, maximum elevation is highest in 2007, next highest in 2006 and lowest in 2005. Since the impact of SGLs on ice dynamics is thought to be more important at higher elevations (Howat et al., 2013), it is particularly useful to be able to simulate the distribution and maximum elevation of lakes.
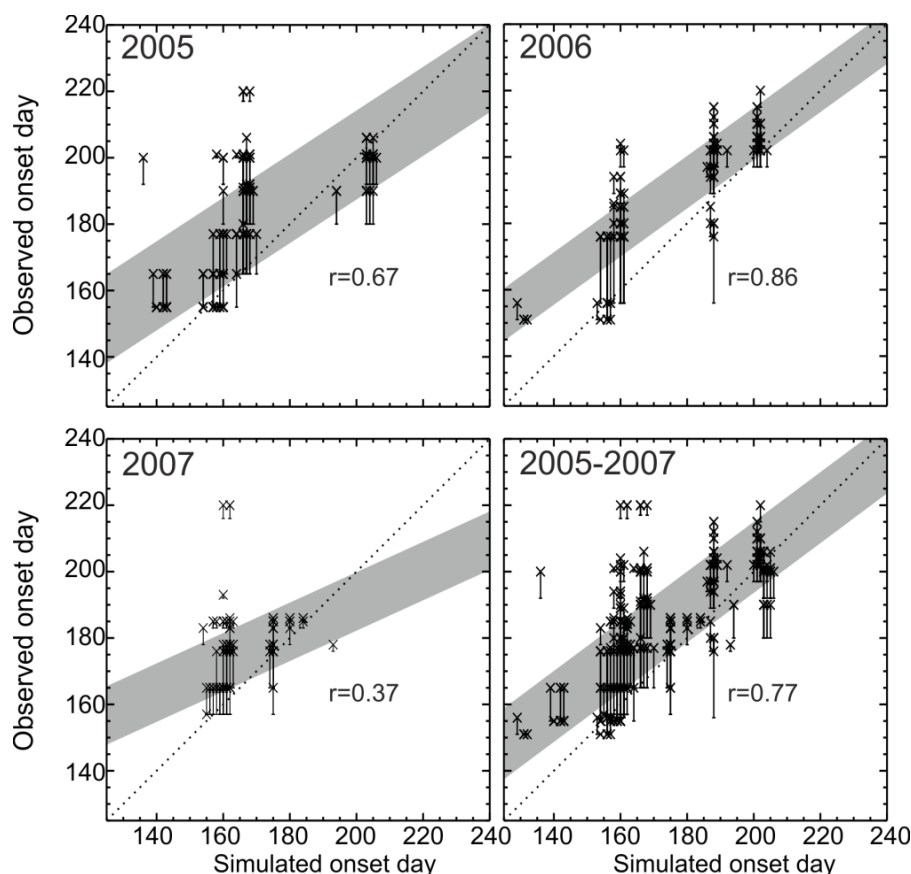
Figure 5.3: Comparison of simulated (using SLInG) and observed (Leeson13) onset day for co-located lakes over a three year period. Error bars indicate uncertainty due to temporal sampling. Shaded regions indicate a linear fit through the data, +/- the 1 σ uncertainty in the fit. A one-to-one fit is given with a black dashed line.

For the 2005-2007 period, SLInG was found to reproduce the onset day of lakes which are both simulated and observed with a PCC of 0.77 (Figure 5.3). SLInG tends to underestimate onset day in the early part of the melt season but from around day 160, model and observations are in agreement. Performance is variable across the three year period, with calculated PCCs of 0.67, 0.86 and 0.37 for 2005, 2006 and 2007 respectively. The weakest correlation is exhibited in 2007, in which year lake onset is clustered around the early part of the melt season; most lakes have appeared by day 200. In both 2005 and 2006, lakes

continue to appear after this time with lake appearances up to approximately day 220. This pattern can be seen in both the observations and the model.

Here, the ability of SLInG to reproduce the seasonal progression of SGLs at the inter-annual timescale is investigated (Figure 5.4). Simulated lakes begin to form at low elevations at the start of the melt season, and then progress inland/higher up as melting becomes more abundant. This is in agreement with Sundal et al. (2009). The RMSD between simulated and observed elevation dependent onset, for elevation bands indicated in Figure 5.4, is 14, 13 and 8 days for 2005, 2006 and 2007, respectively. Simulated lakes appear ~1 week earlier than observed lakes; the mean bias between model and observations is -10.9, -7.3, -7.1 days for 2005, 2006 and 2007. Observational studies have suggested that for lake reporting to begin, a threshold value of total melt needs to have been achieved (Johansson et al., 2013). This water is needed to saturate the snow pack, fill existing cracks and crevasses and pool sufficiently in order to be visible in satellite imagery. This process is not currently included in SLInG. In 2007, the progression of lakes inland/higher up is less obvious; there is simultaneous widespread initiation of lake growth across multiple elevation bands in both the model and observations. This may be attributed to the pattern of runoff production in 2007. Large quantities of runoff are produced over a short time period, rather than a more gentle increase in the rate of runoff production as seen in 2005-2006 (Figure 5.1).
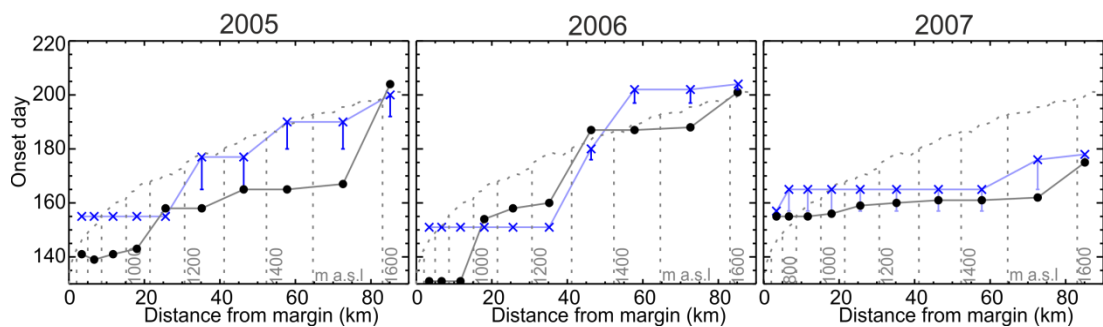
Figure 5.4: Inter-annual variability in elevation-dependent onset of lake growth. Symbols indicate day on which any lake is first observed in Leeson13 (blue) or simulated using SLInG (black) in that elevation band. Points are connected by linear interpolation for information only; lines do not indicate continuous reported values. Error bars on the observations from the combined dataset refer to uncertainty due to sampling frequency.

By comparison with observational estimates, SLInG reproduces the temporal evolution of mean lake area, total lake covered area and number of lakes, up to the point of drainage, fairly well (Figure 5.5). SLInG also captures inter-annual variability in all SGL

characteristics but the maximum lake covered area. In the observations, lake covered area grows as the melt season progresses, and then begins to shrink as area loss from drainage begins to outweigh area gained from new lakes and lake growth. Since SLInG does not include drainage at this time, lake covered area continues to grow until lakes reach their topographic limit, or runoff ceases to be produced. The year in which maximum peak lake covered area is simulated using SLInG is 2007 (a high runoff year), and the year in which maximum peak lake covered area is observed is 2006 (a moderate runoff year). Differences between the simulation and observations are certainly due to the absence of drainage in the model. In years with high runoff, drainage begins sooner (Liang et al., 2012). In these years, drainage may begin prior to the maximum lake covered area being achieved, thus acting to mitigate any effect of increased runoff that may otherwise be observed. Despite this, inter-annual variability in the timing of maximum lake covered area is reproduced well by SLInG; maximum lake covered area is reached earliest in 2007, then in 2005 and latest in 2006 in both the model and observations, although the model lags the observations by ~23 days on average.
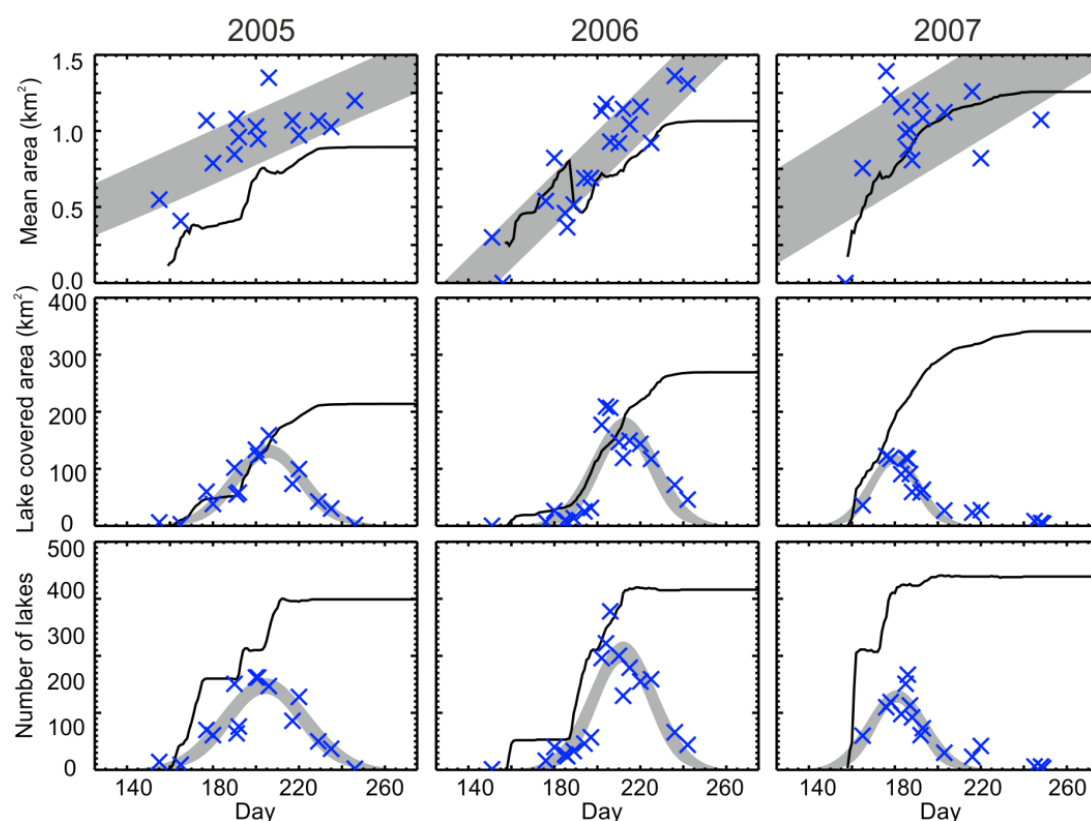
Figure 5.5: Comparison between simulated (SLInG -black) and observed (Leeson13 -blue) time series of mean area, lake covered area and number of lakes for 2005-2007. Shaded regions indicate a linear/Gaussian fit to the observed values, +/- 1 σ uncertainty.

In all three years under consideration here, lake filling rate (growth of lake covered area), up to the observed time of lake drainage, is reproduced well using SLInG. Up to the observed time of drainage, lake covered area grows at a rate of 6, 5 and 10 km^2d^{-1}, in 2005, 2006 and 2007 in the Leeson13 dataset, and at a rate of 5, 6 and 14 km^2d^{-1} in the SLInG simulation. The model captures the temporal evolution of mean lake area in 2006 and 2007, within uncertainty ranges. However, in 2005 the model systematically underestimates mean lake covered area with a mean bias of -0.3 km^2. The model overestimates the number of lakes in all three years with a mean bias of 60, 41 and 125 lakes. Discrepancies between the model and observations are likely due to a combination of uncertainty in the observations and lake drainage, i.e. lakes reported in the observations may drain slowly through the incision of lateral channels into the ice by increased flux of runoff (Selmes et al., 2013, Tedesco et al., 2011b), or rapidly through hydrofracture before the peak in area is reached (e.g. Krawczynski et al., 2009, Das et al., 2008). Drainage through channel incision is not included in SLInG at this time since meltwater channels are a sub-grid scale feature. SLInG also omits rapid drainage through hydrofracture, because this process is not well understood at present.

In all three years, the cumulative mean lake covered area is larger in the observations than in the simulation (Figure 5.6); a mean bias between the model and observations of -0.38 km^2, -0.27 km^2 and -0.29 km^2 can be calculated in 2005, 2006 and 2007, respectively. This is to be expected because small lakes are hard to identify in MODIS images (Johansson and Brown, 2013). Although lakes that are smaller than the resolution of the MODIS instrument are masked out of simulated SGL distributions when making this comparison, this does not account for lakes that are resolved by MODIS but not identified by the automated lake delineation methods. As a corollary, it may be expected that SLInG would identify a higher number of lakes than the observations and, although this is true in 2007, in 2005 and 2006 an average of 17 and 61 more lakes are reported in Leeson13 than in the SLInG simulation. In Chapter 3, it was suggested that SLInG reproduced cumulative observed lake filling rate poorly in 2003, because supraglacial channels are not included in the model. Here, it can be seen that cumulative observed filling rate is not well reproduced in 2005 and 2006 also. However, non-cumulative filling rate is reproduced very well by the model (Figure 5.5), in all three years considered here, up to the observed onset of widespread drainage. These results suggest that disagreement between SLInG simulations and cumulative observations may, in fact, be an artefact of uncertainty in the observations rather than a result of missing processes in the model. For example, Leeson13 is known to include false positives, potentially 36% per day in 2006, and the number of false positives in the observations is

compounded at each new cumulative time step. More robust observations, which are not currently available, are required in order to characterise this disagreement between the model and cumulative observations effectively.
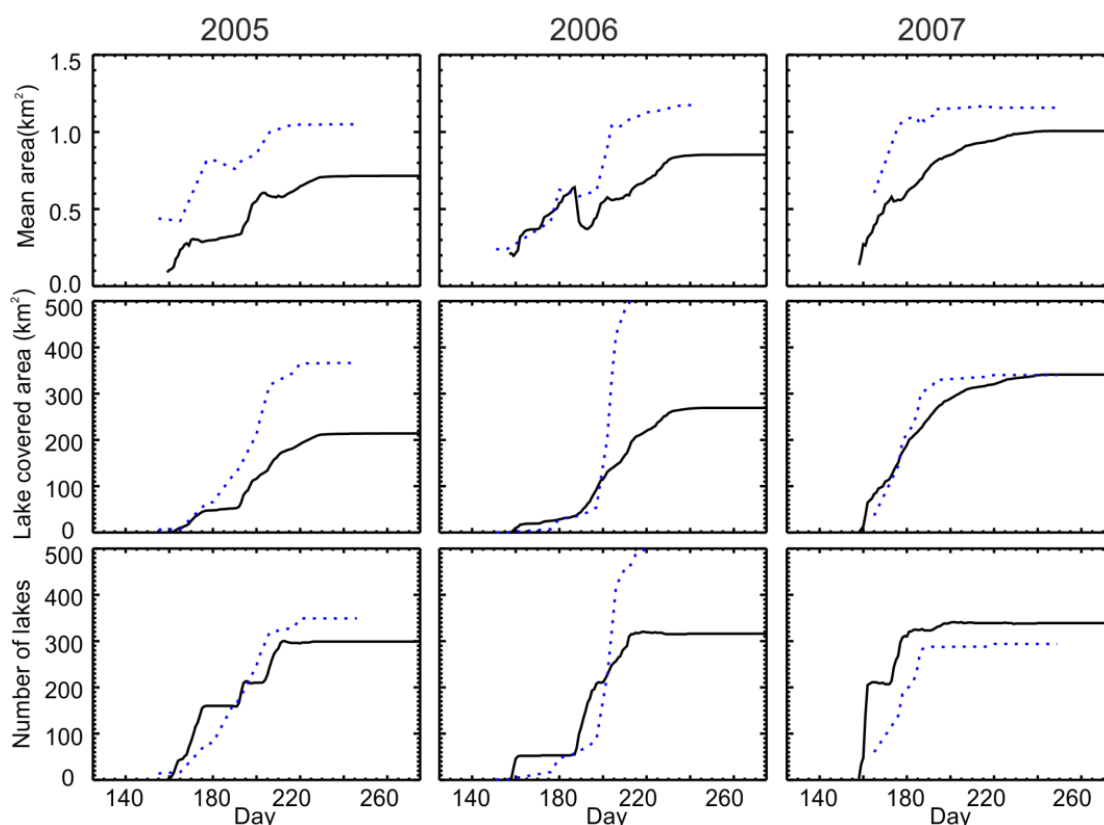
Figure 5.6: Comparison between simulated and observed values of mean area, lake covered area and number of lakes using cumulative observations of lake distribution. SLInG simulated values are given by a solid black line and Leeson13 is given by a blue dashed line.

Table 5.1 summarises model skill in reproducing SGL characteristics across the three year period, 2005-2007. Differences can be seen between years in different metrics of model skill, e.g. SLInG performs 100% better in reproducing the total observed lake covered area, up to the point of drainage, in 2005 than in 2006 and 2007. Also in simulations of lake evolution for 2007, the model performs nearly 50% better in reproducing the number of observed lakes than for 2005 and 2006. The total performance scores for each year are similar, at 3.26, 3.11 and 3.63 for 2005, 2006 and 2007 respectively. This suggests that there is no general performance bias between high (2007) and low (2005) runoff years in SLInG.

Table 5.1: Summary of model skill in simulating SGL evolution in 2005-2007. Values refer to performance metric (P) as indicated, and performance metric normalised to indicate relative performance between years (N), where descending values of performance metric indicate greater skill, values are first adjusted by taking the reciprocal. For mean area, total area and number of lakes located, value refers to time period prior to the onset of widespread drainage. Total score for each year is calculated as the linear sum of the normalised performance metric.

	2005		2006		2007		2005-2007
	P	N	P	N	P	N	P
Coincident lakes (%)	54	0.31	48	0.28	72	0.41	58
Underestimate of maximum elevation (m a.s.l.)	129	0.19	69	0.35	51	0.47	83
Onset day (r)	0.67	0.35	0.86	0.45	0.37	0.19	0.77
Overestimate of regional onset (RMSD-days)	14	0.26	13	0.28	8	0.46	12
Mean area ($\overline{A}$) (RMSD -km^2)	0.34	0.26	0.22	0.4	0.25	0.35	0.27
Total area (A_{tot}) (RMSD -km^2)	18.47	0.51	38.42	0.25	39.32	0.24	32.65
Number of lakes (RMSD)	71	0.38	64	0.43	144	0.19	100
Cumulative $\overline{A}$ (RMSD -km^2)	0.4	0.29	0.32	0.36	0.32	0.36	0.35
Cumulative A_{tot} (RMSD -km^2)	119.53	0.23	213.15	0.13	42.58	0.64	146.47
Cumulative number of lakes (RMSD)	50	0.48	120	0.2	75	0.32	89
Total score		3.26		3.11		3.63	

5.5 The role of runoff in inter-annual variation in SGL evolution

SLInG simulates differences in SGL characteristics between years during the 2001-2010 period, in terms of both temporal and spatial evolution (Table 5.2). Mean lake onset day ranges by up to 1 month, from 6th June (2003), to 7th July (2001). This is in agreement with the observations of Sundal et al. (2009). The day on which maximum lake covered area is achieved also varies, although within a slightly narrower range (~25 days). Lake covered area growth rate (lake filling rate) shows dramatic variability, being three times faster in 2007 (14 km^2 d^{-1}) than in 2009 and 2006 (5 km^2 d^{-1}). The maximum elevation of the 90th percentile of total lake area ranges by 118 m a.s.l. (from 1441 m a.s.l. in 2005 to 1559 m

a.s.l. in 2010). This is in agreement with the findings of Liang et al. (2012), who found a maximum range of 105 m a.s.l. in the elevation of the 50th percentile of total lake area during this period. This difference in simulated 90th percentile of total lake area equates to an additional 1779 km^2 (26%) of the study region over which lakes are present in 2010 compared to 2005. The year with the largest total lake covered area was 2010 (472 km^2 – 7%) and the year with the smallest lake covered area was 2005 (321 km^2 – 5%).

As previously noted, simulated inter-annual variability in values of most SGL characteristics is in good agreement with that observed, although the model exhibits biases in representing the absolute values. However, when compared to observations, the model performs poorly in reproducing both the absolute value of, and inter-annual variability in, maximum lake covered area. This is certainly due to missing drainage in the model. Three years which set successive records for extreme climate (2003, 2007, 2010) exhibit earlier/larger than average values for most SGL characteristics.

Table 5.2: Simulated SGL characteristics for the 2001-2010 period using the SLInG model. Brackets indicate observed values in the Leeson13 observational dataset. Grey shading indicates the years which show earlier/greater than average values (as appropriate).

Year	Mean onset day	$\dot{A}$ (km^2 d^{-1})	A_{max} (km^2)	Day of A_{max}	Max elevation (m a.s.l.)
2001	188	6	339	215	1494
2002	166	7	371	195	1520
2003	157	6	437	194	1558
2004	176	9	394	200	1523
2005	177 (186)	6 (6)	321 (166)	206 (181)	1441 (1570)
2006	179 (196)	5 (5)	376 (214)	212 (189)	1514 (1583)
2007	166 (178)	14 (10)	449 (132)	190 (170)	1548 (1599)
2008	171	7	405	194	1544
2009	183	5	360	213	1510
2010	156	7	472	196	1559
2005-2007	174 (187)	8 (7)	382 (171)	201 (180)	1501 (1584)
2001-2010	172	7	392	202	1521

Inter-annual variability in SGL characteristics has been attributed to total annual runoff amount. Linear relationships have been previously proposed in observational studies between SGL onset day and total annual runoff (Johansson et al., 2013), onset of drainage and total annual runoff (Liang et al., 2012), maximum elevation of total lake area and total annual runoff (Liang et al., 2012), and lake filling rate and rate of runoff production (Chapter 4 of this thesis). Here, SLInG simulations for the period 2001-2010 and MAR simulated total annual runoff are used to corroborate these findings (Table 5.3, Figure 5.7).

Table 5.3: Pearson correlation co-efficient calculated between simulated SGL parameters and runoff parameters. Correlations can be considered strong if their absolute value exceeds 0.68 (Bluman, 2004).

Runoff parameter	Simulated SGL characteristics			
	Mean onset day	$\dot{A}$	Day of A_{max}	Maximum elevation
Annual total	-0.93	0.38	-0.74	0.77
Melt season	-0.59	-0.45	-0.18	0.36
Rate of change	-0.17	0.96	-0.52	0.26

Total annual runoff and mean onset day are found to have a strong (> 0.68) (Bluman, 2004) negative correlation (Table 5.3) which suggests that in high runoff years, lakes appear sooner. This is in agreement with the findings of Johansson et al. (2013). A weak correlation (< 0.68) is also simulated between mean onset day and length of melt season. This may be because in years with a longer melt season, melting begins earlier and so lakes appear sooner; MAR simulated length of melt season and first day of melting are strongly negatively correlated (r=-0.89). Onset day can be used in order to constrain the earliest possible day on which drainage may begin; lakes have been estimated to have a minimum lifetime of 4 days and a mean lifetime of 24 days (Johansson et al., 2013).

Total annual runoff amount and SLInG simulated timing of maximum lake covered area are also found to exhibit a negative linear relationship (Table 5.3, Figure 5.7). This suggests that in high runoff years, maximum lake covered area will be reached sooner and, as a corollary, drainage of SGLs will occur earlier in the year (Shepherd et al., 2009). This is in agreement with the findings of Liang et al. (2012). It ought to be noted here that SLInG exhibits a ~+23 day bias in simulated timing of maximum lake covered area (Section 5.4, Figure 5.7). The timing of maximum lake covered area in the simulation is a direct response

to the amount of runoff produced (because simulated lakes do not drain), whereas in the observations, it can be expected to be a more complex mixture of the onset day-runoff relationship and the cessation day-runoff relationship. In a high runoff year, lake drainage begins sooner; this can be expected to bring the day on which drainage begins to outweigh lake growth (i.e. day of maximum lake covered area) forward in time.
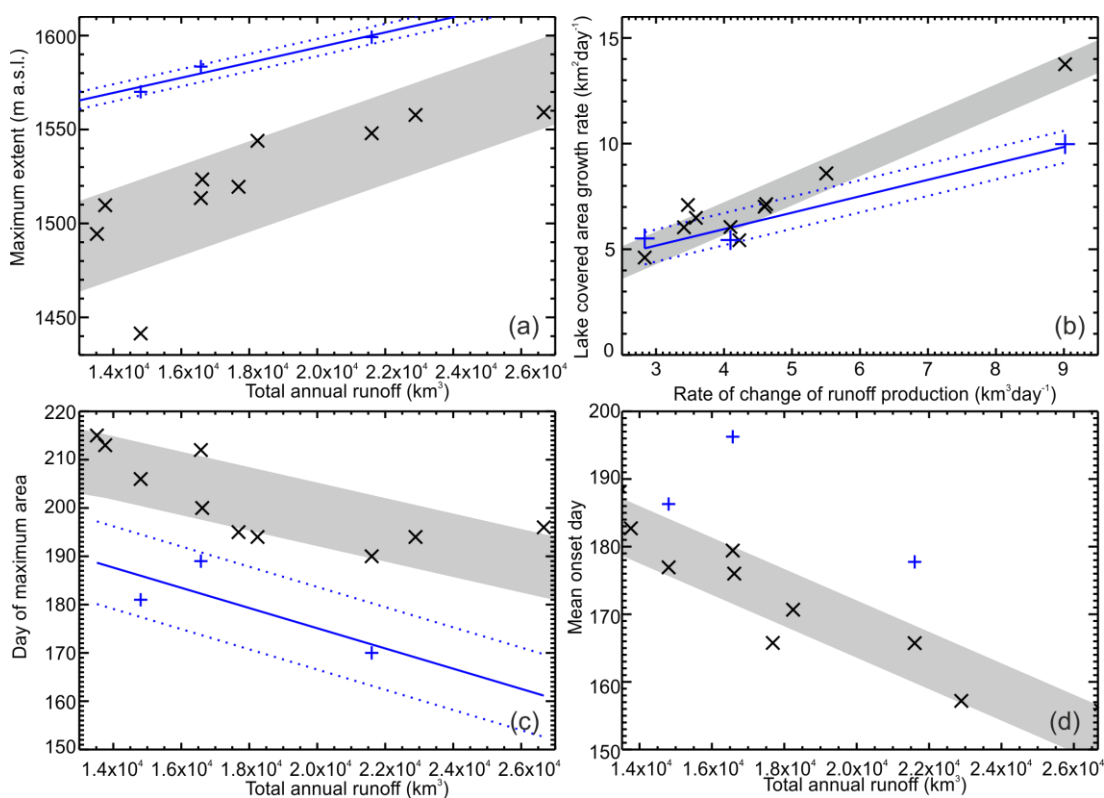
Figure 5.7: Linear relationships between SGL characteristics and MAR simulated runoff. Shown is (a) Maximum extent vs. total annual runoff, (b) lake covered area growth rate vs. rate of change of runoff production, (c) day of maximum lake covered area vs. total annual runoff and (d) mean onset day vs. total annual runoff. SLInG simulated values are indicated in black, shaded region indicates a linear fit to these data +/- the 1 σ uncertainty on this fit. Blue crosses indicate values reported in Leeson13; where a statistically significant correlation exists, solid lines indicate a linear fit to these data. Dashed lines indicate the +/- 1 σ uncertainty on this fit.

Also in agreement with the findings of Liang et al. (2012), total annual runoff is found to be directly correlated with the 90th percentile of total lake area in the SLInG simulation, i.e. as runoff amount increases, SGLs form higher up on the ice sheet/further inland. This is important because Artic temperatures are predicted to increase by 4-8 ^{o}C by 2100 (Meehl, 2007), and meltwater production is correlated with temperature (e.g. Reeh, 1991, Braithwaite and Olesen, 1984). SGLs are known to have already migrated ~250 m a.s.l. further up/inland on the GrIS over the past 40 years (Howat et al., 2013).

A strong linear relationship between rate of growth of lake covered area, $\dot{A}$, and rate of change of runoff production $\dot{R}$, was also calculated (Table 5.3) This substantiates the suggestion made in Chapter 4, that the faster runoff production increases, the faster lakes fill and lake covered area grows. Runoff is supplied to SGLs in SLInG via open channel flow and flow through firn/snow. SGLs in reality are supplied with runoff via overland flow and supraglacial streams. Both the rate of flow overland and the rate of flow in supraglacial streams are forced by changes in runoff production, since supraglacial streams are fed by runoff routed by overland flow. However, flow in supraglacial channels is typically much faster than overland flow (Jarosch and Gudmundsson, 2012). This result suggests that this dynamic routing through the supraglacial hydrological network does not attenuate the runoff production signal; i.e. runoff is supplied to the lake in direct proportion to the rate at which it is produced.

5.6 Changes to the spatial and temporal distribution of supraglacial lakes on the Greenland ice sheet between 1971-2010.

Due to their correlation with runoff production, the mean onset day, filling rate (growth of lake covered area, $\dot{A}$), timing of maximum area and maximum altitudinal extent (elevation of 90th percentile) of SGLs, are all characteristics which may respond to changes in climate, and that are reproduced well by SLInG. Here, changes to these SGL characteristics over the period 1971-2010 are explored using the model.

Over the past 40 years, mean onset day has steadily decreased; lakes are appearing earlier each year at a rate of approximately half a day per year, in an anti-correlation with MAR simulated total annual runoff (Figure 5.8). This is presumably in response to climate change; south west Greenland has exhibited 2.2^{o}C of atmospheric warming since 1971 (Hanna et al., 2012). $\dot{A}$ increased by approximately 25% between 1971 (5.8 km^{2}d^{-1}) and 2010 (7.3 km^{2}d^{-1}), again at a steady rate (Figure 5.8). $\dot{A}$ has increased at a slower rate than total annual runoff, this is because total annual runoff is not the main driver of lake filling rate, rather, rate of change of runoff production, $\dot{R}$, is (Section 5.5). This suggests that $\dot{R}$ has also increased over the 40 year period, though this change has not been as rapid as the increase in total annual runoff. Simulations suggest that there has been no overall change in the timing of maximum lake covered area, despite the steady decrease in mean lake onset. As a corollary, it can be assumed that there has been no corresponding change in the timing of peak supraglacial forcing of ice dynamics as a result of changing climate. However, in
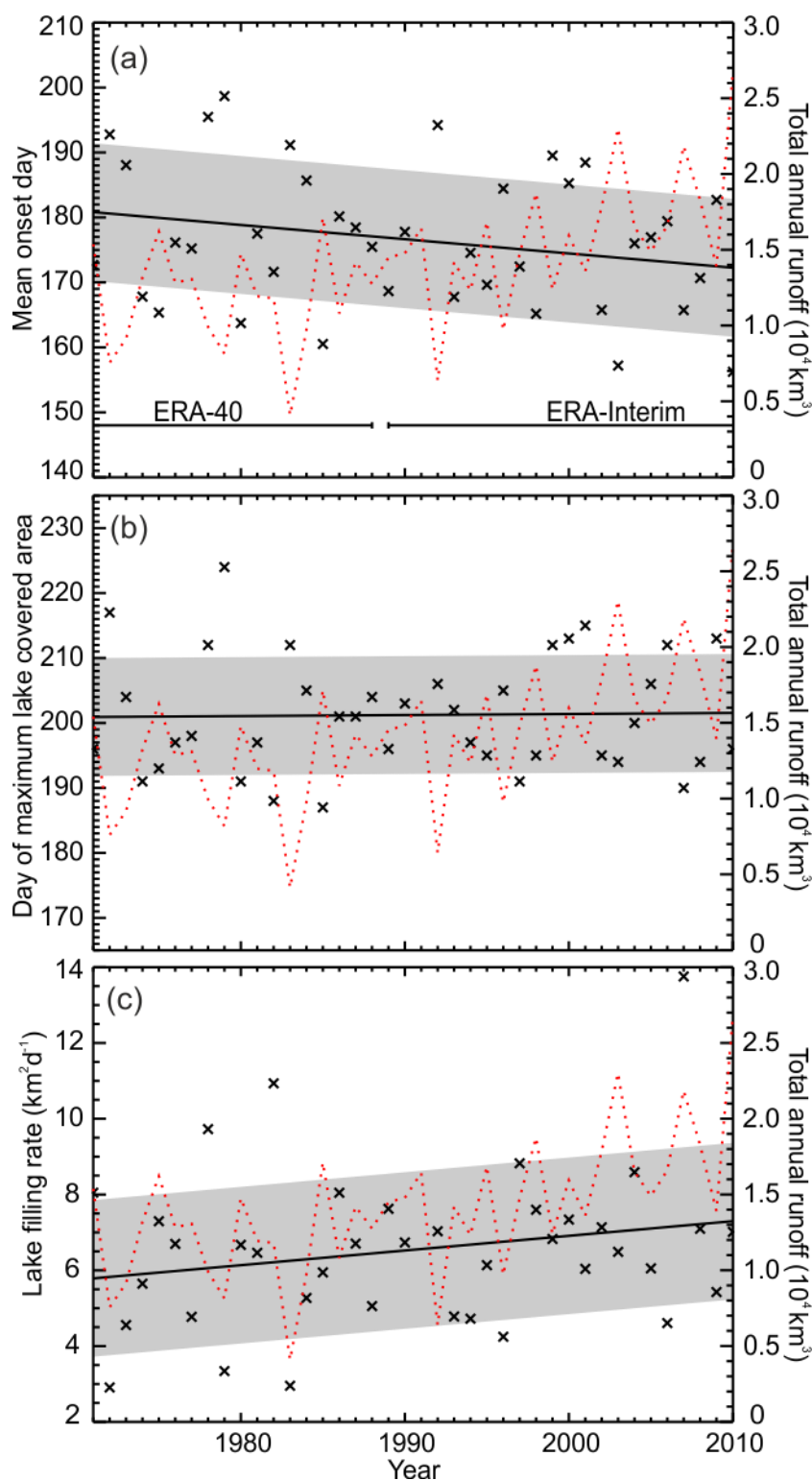
Figure 5.8: Forty years (1971-2010) of SGL characteristics simulated using the SLInG model. (a) Mean onset day, (b) day of maximum lake covered area, (c) lake filling rate. Solid black line indicates a linear fit to the data. Shaded region indicates the +/- 1 σ uncertainty on this fit. SLInG was forced by runoff data produced by the MAR RCM, in turn forced by the ECMWF ERA-40 and ERA-Interim re-analyses, as indicated. Also shown (dashed red) is MAR simulated total annual runoff, integrated over the study region, for 1971-2010 period.

time series of onset day, rate of growth of lake covered area and timing of maximum lake covered area, variability is large and it is difficult to infer a meaningful trend from these data. SLInG is forced by runoff simulated by the MAR RCM, which is in turn forced, during this 40 year period, by the ECMWF ERA-40 (1971-1988) and ECMWF ERA-Interim (1989-2010) reanalyses. The switch between forcing datasets has had no apparent impact on any of the parameters investigated here.

The elevation of the 90th percentile of total lake area (again used to characterise maximum elevation at which lakes form), as simulated by SLInG, has also increased over the past 40 years, from 1447 m a.s.l. in 1971 to 1559 m a.s.l. in 2010. However, this increase has not been uniform throughout the period (Figure 5.9). SLInG simulated values of daily distribution suggest that maximum lake elevation underwent little/no change from 1971 to ~1995, but that from ~1996 to 2010 the area of the ice sheet covered by lakes underwent rapid expansion inland. In fact, the mean decadal lake distribution (Figure 5.10) shows that while lakes were distributed over ~50% to 75% of the study area during 1971-2000; SGLs
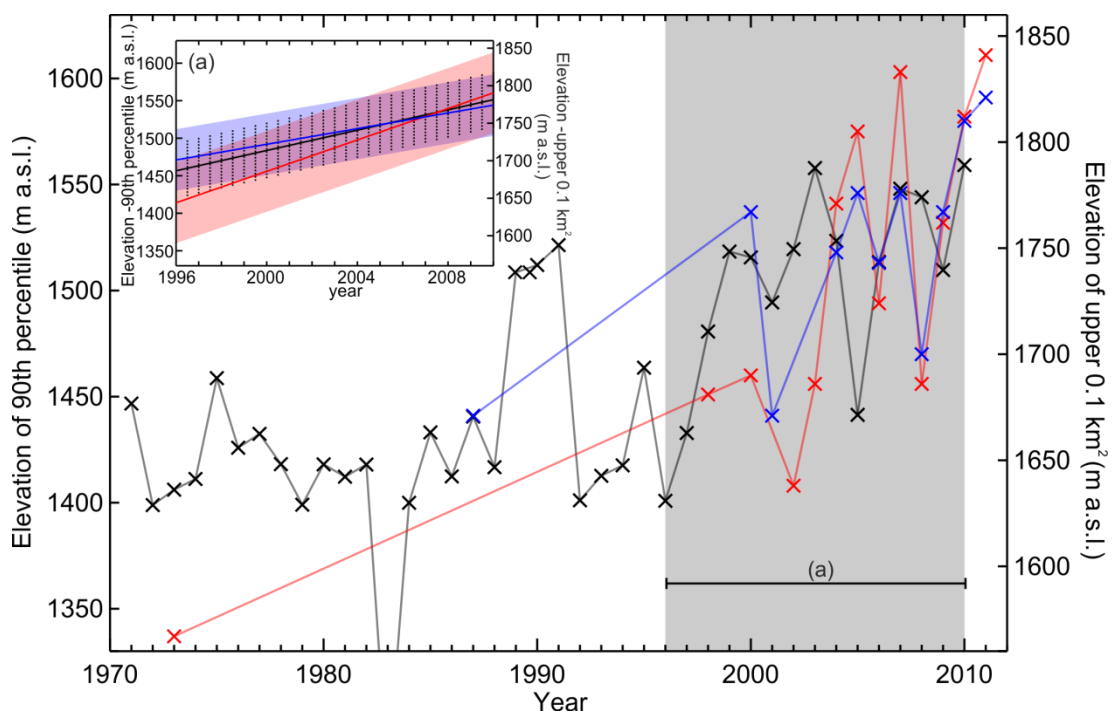
Figure 5.9: Changes to the maximum elevation at which SGLs may be found, in the vicinity of Russell Glacier on the GrIS from 1971-2011. Maximum extent is characterised by the elevation of the 90th percentile of lake area simulated by the SLInG model (black) and the upper 0.1 km² of lake area as observed in satellite imagery (red and blue, Howat et al. 2013). Point data is connected by linear interpolation to aid visual interpretation only; solid lines do not denote continuous values. Simulation results and observations indicated in blue, are spatially coincident. The observations indicated in red were obtained slightly to the north of the region considered in the simulation. Inset: a linear fit through each time series. Colours as before, shaded/hatched regions delineate +/- 1 σ uncertainty on this fit.

formed over the full extent of the region in 2001-2010. This rapid recent expansion of the extent of SGL covered area follows the trend in surface air temperature (Hanna et al., 2012). These data confirm the findings of Howat et al. (2013) who used forty years of maximum lake elevation derived from satellite data to conclude that the area of the ice sheet on which lakes form has expanded inland/higher up over the past 40 years. However, SLInG simulated values are systematically ~175 m lower than the observations of Howat et al. (2013). This can be attributed to the use of the elevation of 90th percentile of lake area, within the bounds of the DEM, to represent the trend in maximum lake elevation in the simulation, and the use of the uppermost 0.1 km^2 of lake area to represent maximum lake elevation in the observations. The elevation of the 90th percentile of simulated lake area has been shown to lie ~ 207 m a.s.l. below the maximum elevation at which simulated lakes are found. In general, the SLInG simulated trend and that reported by Howat et al. (2013) show good agreement (Figure 5.9).
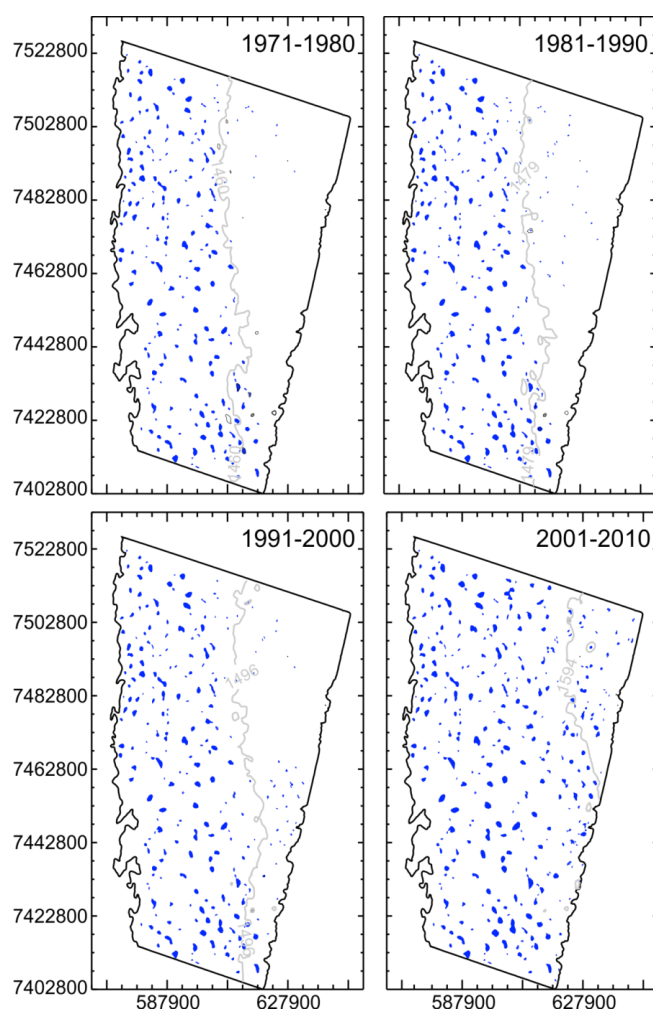
Figure 5.10: Maps of decadal mean lake distribution for the forty year period 1971-2010 as simulated by SLInG. Simulated lakes that are reported in at least 5 years are indicated in blue. The elevation of the 90th percentile of lake elevation is contoured in grey.

Observations and model results for the 1996-2000 period suggest that the expansion of SGLs is on an upward trajectory in response to observed warming (Figure 5.9). Since climate warming over Greenland is expected to continue (Meehl, 2007), it may be expected that this upward/inland trend in maximum SGL elevation will respond accordingly. Although this thesis has confirmed a reported correlation between maximum elevation of SGLs and runoff amount (Liang et al., 2012) it is uncertain whether the ice topography will allow further inland expansion of lake covered area. Although the depressions in which SGLs form are largely intransient (Echelmeyer et al., 1991, Selmes et al., 2011), the transmission of basal topography through the ice to the surface becomes more muted as ice thickness increases (Gudmundsson, 2003). This leads to the question of whether the surface at the summit of the GrIS, for example, contains sufficient undulations to form lakes, should melting provide sufficient runoff. Further work, beyond the scope of this thesis, is needed in order to provide the answer to this question.

5.7 Summary

In this chapter, the inter-annual variability in SGL evolution in the region of the Russell Glacier in west Greenland was investigated using the SLInG model and satellite derived observations. The new Leeson13 observational dataset was used to assess the performance of SLInG at the inter-annual timescale. It was concluded that SLInG is able to reproduce inter-annual variability of pre-drainage and drainage independent characteristics of SGL evolution very well, particularly the spatial evolution of SGLs. However, both maximum lake covered area and the timing of maximum lake covered area were found to exhibit a greater dependence on lake drainage behaviour than expected. Systematic biases were discovered between the model and the observations in terms of onset day, timing of maximum lake covered area and maximum altitudinal extent. Lakes appear ~2 weeks earlier on average in SLInG than in the observations. In addition, regional onset, in ten 100 m elevation bands between 700 m a.s.l. and 1600 m a.s.l., occurs ~1 week earlier in SLInG than in the observations. This underestimate can be attributed to the absence of a filling period (of existing cracks and crevasses, and allowing lakes to reach observable size) in the model, which is evident in the observations. 90th percentile of lake elevation is consistently underestimated by SLInG by 83 m a.s.l., this is because lakes in SLInG are formed from runoff produced within the bounds of the DEM only; in actuality runoff produced further upstream also contributes to lake growth. SLInG overestimates the day of maximum lake covered area by ~20 days, because of the lack of drainage in the model at present. Modes of inter-annual variability in selected characteristics of SGL evolution were investigated with

respect to runoff using SLInG. The timing of maximum lake covered area is correlated with total annual runoff (r=-0.74), despite the lack of drainage in the model, presumably because the onset of lake drainage is correlated with melt intensity (Liang et al., 2012). Previously proposed correlations between total annual runoff amount and SGL onset day and maximum elevation were corroborated using SLInG (r=-0.93 and r=0.77). Lake covered area growth rate was also found to be strongly correlated with the rate of increase of runoff production (r=0.96).

In Section 5.6, SLInG was used to investigate recent changes in SGL characteristics that are correlated with runoff and presumably therefore responsive to changes in climate. Lake onset day and filling rate were both found to have responded to observed changes in climate with increases in both cases, over the 1971-2010 period. No change was simulated in timing of maximum lake covered area. The maximum elevation at which SGLs form has undergone major changes in the past 15-20 years particularly, with the 90th percentile of simulated total lake area within the study area shifting approximately 100 m a.s.l. higher between 1996 and 2010. This is the first model assessment of this trend and is in agreement with recent findings from observational studies. These results suggest that under projected climate change scenarios, lakes may be expected to form further inland/higher up on the ice sheet, which could have serious implications for ice sheet dynamics. For example, if SGLs were to form and drain in regions of frozen bed, drainage through hydrofracture may encourage decoupling of the ice-bed interface and subsequent basal sliding (Howat et al., 2013). In addition, the passage of meltwater from surface to bed may cause a warming effect, reducing the effective viscosity of the ice and increasing flow through internal deformation (Phillips et al., 2010). Although runoff projections suggest an increase in the region of the ice sheet regularly experiencing melt in future years (Rae et al., 2012), it remains to be seen whether the surface topography will allow the formation of lakes at higher elevations. This could be investigated using the SLInG model; however, it would require a more extensive high resolution DEM. Although the application of SLInG over a larger area is beyond the scope of this thesis, such a study would clearly be of use and will form the focus of future work.

Chapter 6

Summary and conclusions

6.1 Introduction

Supraglacial lakes (SGLs) potentially have three important impacts on the mass balance of the Greenland ice sheet (GrIS). Firstly, they have a much lower albedo that the surrounding ice (e.g. Greuell et al., 2002) which acts to reduce the area-averaged albedo in lake-covered regions. Secondly, SGLs have been observed to perturb local ice sheet dynamics when they drain (Das et al., 2008, Doyle et al., 2013). Currently, net ice sheet flow speed, integrated over the entire year, is not faster in high runoff years (e.g. Sundal et al., 2011, Podrasky et al., 2012). However, it has been suggested that as SGLs form further inland (Howat et al., 2013), their rapid drainage may contribute to a net speed-up of the ice sheet through, instigating temporary spikes in subglacial water pressure (Schoof, 2010, Bartholomew et al., 2011a), de-coupling of the ice and bedrock in regions of currently frozen bed (Howat et al., 2013), and cryo-hydrologic warming leading to an increase in flow due to internal deformation (Phillips et al., 2010). A net speed-up of the ice sheet may lead to a third mechanism by which SGLs may impact ice sheet mass balance; enhanced ablation through modified hypsometry, i.e. a thinning and flattening of the ice sheet would effectively move the equilibrium line further inland/higher up (Parizek and Alley, 2004).

Because of their potential importance for ice sheet mass balance, a thorough understanding of past changes in SGL evolution is vital for constraining the response of the ice sheet to future changes in climate. Observations of SGLs are either made in-situ, where detailed studies of a small number of lakes are conducted over a short-time period (e.g. Doyle et al., 2013, Das et al., 2008), or remotely using satellite data (e.g. McMillan et al., 2007, Johansson et al., 2013). Observations derived from satellite data are typically sparse in time and are limited in their temporal coverage by the operational period of the satellite (e.g. Sundal et al., 2009, Liang et al., 2012). As such, no long-term continuous record of SGL evolution is available. This thesis aims to improve our scientific understanding as to the behaviour of SGLs with the aid of observations and model simulations of their temporal evolution. In order to achieve this aim, four objectives were identified. These objectives are 1) to create a new model of SGL initiation and growth, 2) to inter-compare

satellite derived observations of SGL evolution and assemble a combined (optimised) dataset, 3) to evaluate the model with the aid of satellite-derived observations and 4) to examine inter-annual and longer-term variability in SGL evolution using the new model and combined observational dataset. The following section will summarise how these objectives have been addressed in this thesis and highlight the major findings of this work.

6.2 Summary

In Chapter 2, a novel method of modelling SGL initiation and growth (the SLInG model), was described. SLInG is a new 2-D transient hydrology model, which uses high-resolution digital elevation data to simulate the routing of runoff over the GrIS surface. SLInG is optimised for forcing by regional climate model (RCM) output, and simulations described in this thesis are forced by runoff, snow depth and snow density values simulated by the MAR (Modèle Atmosphérique Régional) RCM (Lefebre et al., 2005). This method improves on previously published SGL evolution models by enabling a more detailed treatment of runoff production and allowing the model to be used for prognostic purposes. In addition, SLInG employs a more sophisticated transient flow routing scheme than previously published SGL models which enables the complete flow path of runoff to be traced, from point of production overland to destination (e.g. into an SGL or off the ice sheet). Because of missing end-of-life processes in the model, SLInG is unable to simulate SGL drainage and refreezing at present.

In Chapter 4, the evolution of SGLs as reported in three datasets, each based on automated classification of satellite imagery, was investigated. The observed SGL datasets span the period 2001 to 2010, though there are differences in temporal sampling, and only the years 2005 to 2007 are common. All three automated datasets omit a sizeable (48, 41, and 29%) fraction of lakes identified through manual classification of satellite imagery. It was estimated that the three SGL datasets document the average size of the lakes they report to within 0.98, 0.89, and 0.60 km^2. The SGL datasets were combined using an hierarchical scheme to produce a single dataset of lake distribution. This combined and optimised SGL dataset led to an increase of 67% in the number of lakes reported. Using this dataset, it was found that during 2005 to 2007, maximum lake covered area ranged from 133 to 217 km^2, and the date of peak area ranged from mid-July to mid-August. Although the rate of SGL growth tends to follow the rate at which runoff increases on each year, inter-annual variations in peak lake covered area and runoff are not well correlated. In 2007, when the rate of runoff increases rapidly, lakes drain earlier and remain absent, despite continued

runoff. This suggests the continuance of lakes as open surface-bed conduits after drainage.
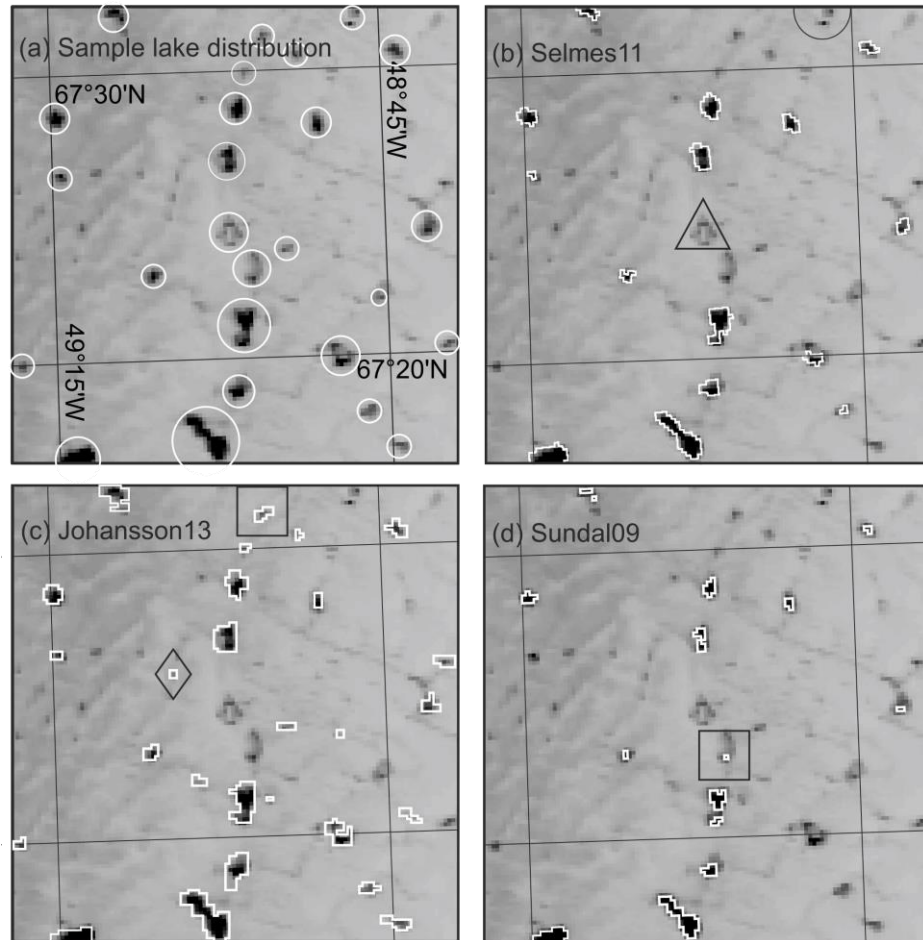
Figure 6.1: Comparison of manually and automatically derived lake distributions on 14th June 2005 (day 165). Background is the original MODIS image. In a) circles surround SGLs identified manually. In b) the triangle indicates an ice covered lake, and the semicircle indicates an ice-free lake, not reported in any of the automatically derived lake distributions. Squares in (b) and (d) illustrate lakes reported in a single dataset. Diamond in (c) indicates a reported lake that has been identified as a false positive. Observations are taken from (b) Selmes et al. (2011), (c) Johansson and Brown (2013) and (d) Sundal et al. (2009). Figure featured in Chapter 4.

Major finding 1: Different methods of automatically deriving SGL distribution from the same satellite data report markedly different lake size and distribution. Temporal sampling is also a significant source of uncertainty in observational estimates of SGL characteristics. Because of this uncertainty, observational estimates of, for example, maximum lake covered area, and date of lake onset and cessation, should be used with care. Some of the uncertainty in observational estimates of SGL evolution can be minimised by combining several datasets, and the use of a model (e.g. SLInG) in conjunction with observations is recommended in order to contextualise this uncertainty.

In Chapters 3 and 5, the performance of the SLInG model was evaluated at the seasonal and inter-annual timescales using observations of lake evolution derived from MODIS imagery acquired during the 2003 and 2005-2007 melt seasons, respectively. The model was found to perform well in reproducing pre-drainage and drainage independent SGL characteristics in all four years. Using temporally dense observations of SGL evolution in 2003, the SLInG model is demonstrated to be 19 times more likely to correctly predict the presence (or absence) of lakes than it is to make incorrect predictions, within an elevation range of 1100 to 1700 metres above sea level (m a.s.l.) (Figure 6.2). Of the 66% of observed lake locations which the model correctly reproduces in 2003, simulated lake onset day was found to be correlated with observed lake onset day with a Pearson correlation co-efficient (PCC) of 0.76. SLInG co-located 58% of observed lakes in 2005-2007 (83% if potential false positives in the observations are discounted) and a PCC of 0.77 was calculated between simulated and observed onset day for these lakes.
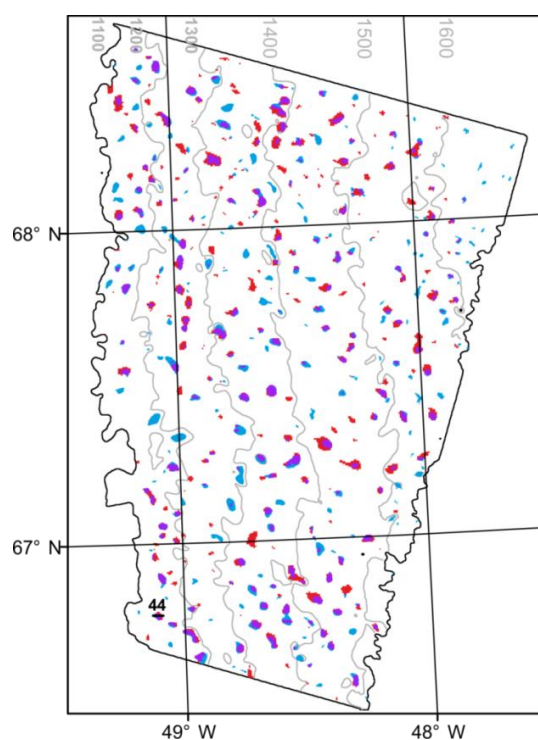
Figure 6.2: Simulated vs. observed lake distribution in the Russell Glacier region of the GrIS in 2003. Shown is MODIS observed lakes (red) (Sundal et al., 2009), lakes simulated using SLInG (blue), coincident lake area (purple). Figure featured in Chapter 3.

The model accurately simulates maximum cumulative lake covered area with only a 1.5% overestimate in 2003; however, it does not reproduce observed maximum daily lake covered area in any of the years considered. SLInG reproduces inter-annual variability well; the model and observations agree on the relative values between years (2005 to 2007) of

maximum altitudinal extent, patterns of regional onset day and rate of growth of lake covered area (Figure 6.3). Systematic biases were discovered between the model and the observations. Maximum altitudinal extent is consistently underestimated by SLInG by 83 m a.s.l., lakes appear ~1 week earlier than in the observations in 100 m elevation bands between 800 and 1700 m a.s.l. and the day of maximum lake covered area is systematically overestimated in SLInG simulations by ~20 days. No general performance bias between years was found, when a range of metrics was considered, though differences in performance with respect to specific SGL characteristics of up to 100% were found to exist.
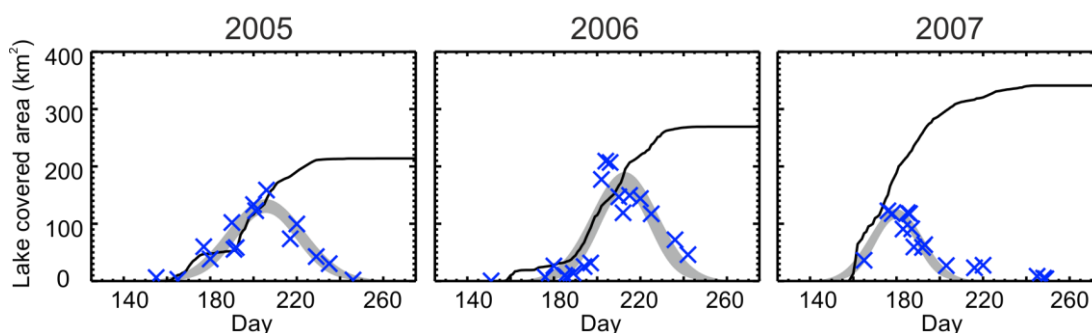
Figure 6.3: Comparison between simulated (SLInG - black) and combined observational data (Leeson13 -blue) time series o, lake covered area for the 2005-2007 period. Shaded regions indicate a Gaussian fit to the observed values, +/- the 1 σ uncertainty on the fit. Figure featured in Chapter 5.

Major finding 2: SLInG, a new model of SGL evolution, is able to successfully reproduce SGL initiation and growth at both the seasonal and inter-annual time scales. This means that SLInG simulations can be used with confidence to augment observational estimates of SGL evolution by providing continuous, long-term records of SGLs. In addition, SLInG can potentially be used to provide new estimates of SGL evolution where/when observations are not available, for example forward projections in time.

In Chapter 5, modes of inter-annual variability in selected characteristics of SGL evolution were investigated with respect to runoff availability. Previously proposed correlations between total annual runoff amount and onset day, and total annual runoff amount and maximum SGL elevation, were corroborated using SLInG (r=-0.93 and r=0.77). The timing of maximum lake covered area was found to be correlated with total annual runoff (r=-0.74) and lake covered area growth rate was found to be correlated with the rate of increase of runoff production (r=0.96). SLInG was also used to investigate recent changes in SGL behaviour. Observed changes in climate since 1971, particularly in the last 20 years (Hanna et al., 2012, Vernon et al., 2013), were found to have had little to no impact on the timing of

maximum area of SGLs. However, SGL mean onset day, filling rate and maximum altitudinal extent were found to have responded to observed changes in climate; onset day decreased steadily and lake filling rate increased steadily, over the 1971-2010 period. The maximum altitudinal extent of SGLs has undergone major changes in the past 15-20 years, with the 90th percentile of simulated total lake area within the bounds of the study area used here, shifting approximately 100 m a.s.l. higher between 1996 and 2010 (Figure 6.4). This is the first model assessment of this trend and is in good agreement with recent findings from observational studies.

Major finding 3: SLInG shows that SGLs are responsive to climate-driven changes in runoff. This suggests that under projected climate change scenarios, lakes may be expected to form earlier, fill quicker and extend to a higher elevation on the GrIS. Simulations performed using SLInG are able to provide a novel interpretation of this trend, as the model is able to provide the longest continuous record of SGL evolution to date.
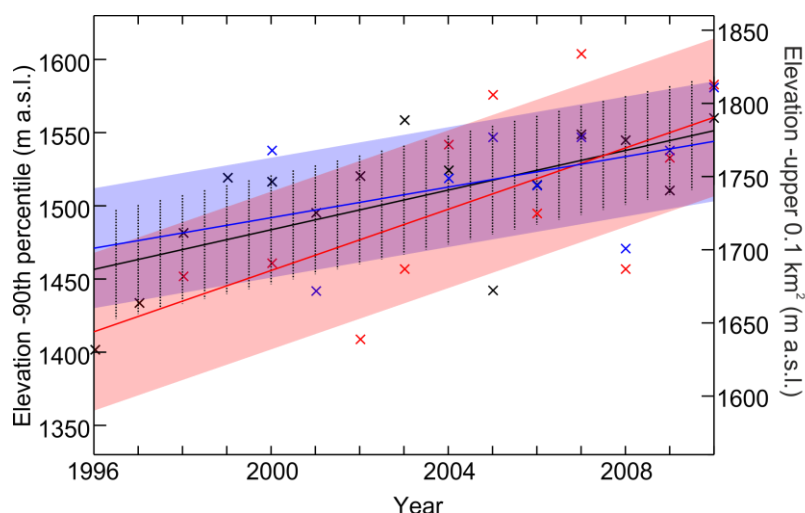
Figure 6.4: Changes to the maximum elevation at which SGLs may be found, in the vicinity of Russell Glacier on the Greenland ice sheet from 1996-2010. Maximum elevation is characterised by the 90th percentile of total lake area as simulated by the SLInG model (black) and the upper 0.1 km^2 of lake area as observed in satellite imagery (red and blue, Howat et al. 2013). Solid lines/shading denote a linear fit through each time series +/- 1 σ uncertainty Figure featured in Chapter 5.

6.3 Synthesis

The GrIS is losing mass as a consequence of climate change, contributing 8 (+/- 1.2) mm to global sea level rise since 1992 and ~1 mm yr^{-1} during the 2005-2010 period (Shepherd et al., 2012). If the 2005-2010 trend were to continue, the GrIS will have contributed 8 cm to global sea level rise by 2100. In addition, GrIS mass loss is projected to accelerate in a future, warmer climate (Gregory and Huybrechts, 2006) which could lead to an even larger

sea level contribution. This could have potentially severe implications to lives and livelihoods globally. For example, the number of people experiencing flooding can be expected to double, at the very least, given a sea level rise of 10 cm (Nicholls, 2002), global rice production can be expected to decrease by 1.1 million metric tons, given a sea level rise of 1 m (Chen et al., 2012), and an increase in incidences of mosquito-borne diseases is likely to be associated with the expansion of coastal wetlands due to sea level rise (Ramasamy and Surendran, 2012). It has been suggested that draining SGLs (SGLs) contribute to mass loss by enhancing the flow of the ice sheet, effectively speeding up discharge into the ocean. Current ice sheet models (ISMs) do not address key processes that could contribute to large rapid dynamical changes in the Antarctic and Greenland ice sheets, which could increase ice discharge, such as the growth and subsequent drainage of SGLs. This was outlined as a key uncertainty in the fourth assessment report of the Intergovernmental Panel on Climate Change (IPCC) (Lemke, 2007).

Satellite surveys of SGLs typically consist of short time series of data, with each year being sparsely sampled in time. For example, McMillan et al. (2007) used 12 images acquired in 2001 to study the seasonal evolution of SGLs in two regions of the GrIS, Lampkin and VanderBerg (2011) used 3 images acquired in 2007 to investigate the influence of topography on SGL location, and Georgiou et al. (2009) used 10 images acquired during the summers of 2002-2005 to investigate changes in SGL depth and volume. The results in this thesis have constrained the number of observations required per year in order to resolve the seasonal cycle in SGL evolution effectively. Future observational studies of SGLs should include at least 20 uniformly distributed days of observations in each year in order for meaningful interpretation of, for example, maximum lake covered area in a given year. Different methods of automatically delineating SGLs from MODIS imagery can result in large differences in reported lake size and distribution. Presumably, this is because the resolution of the MODIS instrument is low, with respect to the spatial scale at which lakes form. In order to minimise method-dependent uncertainty in delineation of lakes, lake distribution ought to be reported based on high resolution satellite imagery. However, in the absence of high resolution data, observations that have been automatically derived from MODIS imagery can be combined in order to provide a more robust product. Alternatively, observations can be interpreted with the help of a numerical model.

Previously developed models of SGLs have been somewhat empirical and omit key physical processes such as the transient routing of runoff (Clason et al., 2012, Luthje et al., 2006b), and the contribution of snow physics to estimates of runoff production (Banwell et al., 2012,

Clason et al., 2012, Luthje et al., 2006b). As the most physically based SGL evolution model to date, many of these processes are provided for in the SLInG model set-up. Given this advancement in SGL modelling, the processes in SLInG should be considered a benchmark for future SGL modelling work. At the very least, future SGL modelling work should use runoff generated by a state-of-the-art RCM featuring a comprehensive, physically based, snow model, which has been shown to give a significantly more realistic product over empirical and semi-empirical methods (e.g. Rae et al., 2012). To date there has been no attempt to explicitly model past changes in SGL evolution. SLInG provides the means by which observations can be augmented by a continuous long-term record of SGL initiation and growth. This enables robust conclusions to be drawn about the seasonal, inter-annual and long-term evolution of SGLs. Ultimately, this will lead to an improved understanding of SGL behaviour, and their potential impact of ice sheet mass balance.

Models of SGL evolution are particularly useful in order to interpret observations and to reproduce observed trends. Recent observations have suggested that SGLs have migrated upwards/further inland on the ice sheet, in response to climate forcing. Air temperature during 2001-2011 was 2.2°C warmer in south west Greenland than the 1971-2000 average (Hanna et al., 2012), this warming is likely the cause of a 53% increase in annual runoff production in 2010 compared to 1990. In addition to changes in the total annual amount of runoff, the annual melt extent (area of the ice sheet which experiences melting) has doubled since 1979 (Fettweis et al., 2011). To date, there has been no attempt to reproduce past trends in SGL evolution using a numerical model. In this thesis it has been shown that SLInG is able to reproduce the observed upward/inland migration with simulated lakes having migrated ~100 m a.s.l. during the 2001-2010 period. This is in good agreement with the observed trend and provides further evidence that SLInG is able to realistically simulate the complex behaviour of SGLs in this region. If this upward/inland migration were to continue, this could have serious implications for ice sheet dynamics, and subsequently mass balance. For example, if SGLs were to form and drain in regions of frozen bed, drainage through hydrofracture may encourage decoupling of the ice and bedrock with a subsequent expansion of the region of the ice bed experiencing sliding (Howat et al., 2013). In addition, the passage of meltwater through the ice may cause a warming effect, reducing the effective viscosity of the ice and increasing flow through internal deformation (Phillips et al., 2010). In this thesis, SLInG has been used to reproduce past SGL evolution. Given appropriate forcing data, for example forward projections of runoff and an appropriate DEM, SLInG could be used as a forecast tool in a predictive capacity, enabling SGL evolution to be projected forward in time. This will form the focus of future work, discussed in Section 6.5.

6.4 Limitations of this study

Limitations of the SLInG model were discussed in Chapter 2. A summary is provided here. The SLInG model does not include, or parameterise for, existing surface-englacial conduits such as crevasses and moulins. This means that the use of SLInG is limited to regions where moulins and crevasses are rare (i.e. at high elevations) (Phillips et al., 2011). This limitation can be considered insignificant because the impact of draining lakes is thought to be most important in these regions. Temporal variations in topography are also unaccounted for in SLInG simulations. This is because the surface topography is largely controlled by basal conditions (e.g. Gudmundsson, 2003), and SGLs have been shown to appear in the same locations year-on-year (e.g. Echelmeyer et al., 1991). Although not a limiting factor in simulations of the present-day/recent past, it is to be expected that the hypsometry of the ice sheet will evolve over long time periods in response to changes in climate. The DEM used to perform simulations using SLInG in this thesis is also likely to include re-frozen lakes in its representation of the ice sheet surface, as a consequence SLInG is likely to 'miss' true lakes in simulated lake distributions. This uncertainty is unquantifiable at present, due to a lack of observations contemporaneous with the data used to derive the DEM.

SLInG is the most physically based SGL evolution model to date, however some known processes that contribute to SGL evolution are not included in the model. For example, SLInG does not explicitly represent supraglacial channels as they are a sub-grid scale feature. This means that the removal of snow by the passage of water in these channels is also not represented. This may lead to uncertainty in calculated runoff velocity because Darcy-type flow (flow through snow) is assumed when in actuality Manning-type flow (open channel flow) ought to be calculated. SLInG also does not include lake growth by enhanced melting at the lake/ice interface. This means that SLInG potentially underestimates lake volume by 10%. The most obvious limitation of the SLInG model is that it does not incorporate rapid drainage or refreezing of SGLs at this time, because the conditions required for hydrofracture (and subsequent rapid drainage) to occur are not well understood. In addition, the proportion of lakes which drain and which refreeze has not been well enough constrained for a parameterisation to be developed. Because of the missing drainage and re-freezing (and also due to uncertainty in the DEM), SLInG can only be used in time-slice mode at present in order to examine drainage-independent and pre-drainage characteristics of SGL evolution. One of the major implications of this is that SLInG cannot be used to predict the time-varying area-averaged albedo change as a result of the formation, growth, and demise of lakes.

Although this study inter-compared all available SGL observations for the Russell Glacier region of the GrIS, other observational datasets of SGL evolution exist which focus on different geographical regions; for example the Swiss Camp/Jakobshavn Glacier region. One such dataset is the observations of Liang et al. (2012) who adopted a different method of automatically classifying MODIS images to those described in Chapter 4 and applied that method to ten years of MODIS imagery. The investigation into variability between observations of SGL evolution described here would be more robust if data using this method were to be included also. When the SGL observations automatically derived from MODIS imagery for the Russell Glacier region were investigated, they were evaluated against manually derived data, also from MODIS imagery. Although manual derivation was shown to out-perform automated derivation, an RMSD of 0.24 km^2 was calculated between the area of lakes manually delineated from MODIS imagery and the area of lakes manually delineated from ASTER imagery, which has a much higher spatial resolution (Figure 6.5). The independent evaluation of these datasets would be more robust if it was performed against a dataset which has been manually delineated from ASTER. However, no ASTER images on common days between all three datasets considered were available.
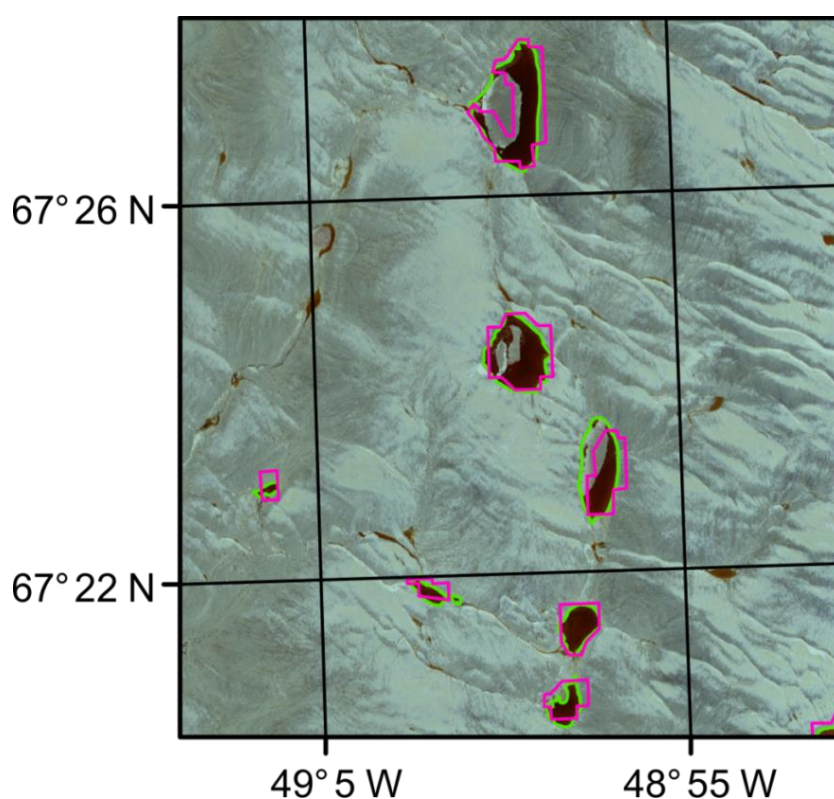
Figure 6.5: A selection of manually delineated MODIS lakes (pink) and manually delineated ASTER lakes (green) on 1st August 2001. Background is ASTER image from which lakes were delineated.

In this thesis, automated methods of delineating SGLs from MODIS imagery have been shown to exhibit significant method dependent biases with respect to reported lake size. In addition, the automated methods investigated here fail to report 29%-48% of lakes which can be identified manually. Observational records of SGLs also exhibit uncertainty due to sample size, however, inter-annual and seasonal variability of SGL evolution is consistently reported between datasets despite absolute values of, for example, total lake covered area, varying markedly. The evaluation of SLInG performed in this thesis is limited by this uncertainty in the evaluation data, although this uncertainty was minimised as much as possible by the construction of a combined dataset. This combined dataset was itself limited by its short time period of three years only. However, these three years encompassed a wide range of runoff scenarios. SLInG would benefit from further evaluation against more robust data, covering a longer time period. In addition, an area-averaged approach to investigating the evolution of SGLs is taken in this thesis, which excludes high resolution observations of individual lakes over a single melt season. Observations of this type have been made in the Russell Glacier region (Doyle et al., 2013). The evaluation of the SLInG model described in this thesis would be more robust if case study comparisons against one or more of these lakes were made.
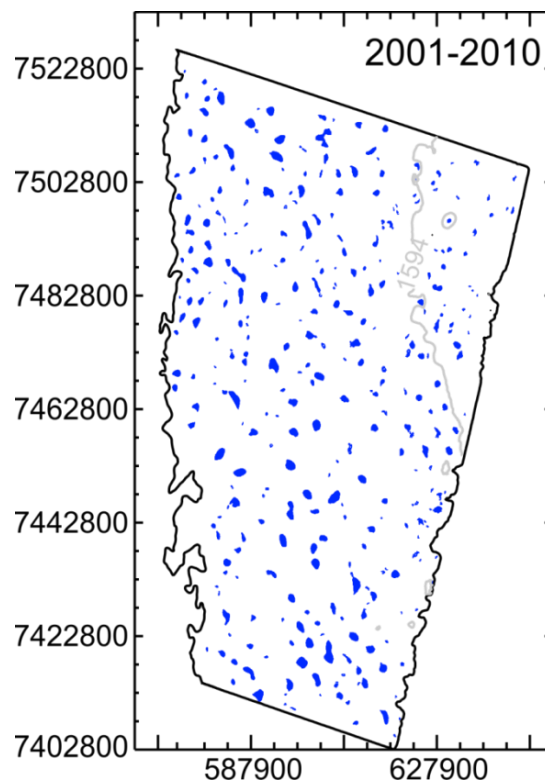
Figure 6.6: Decadal mean lake distribution for 2001-2010, as simulated by SLInG. Pixels included in this distribution were simulated to form part of a lake in 5 or more years during this period. Figure featured in Chapter 5.

While not strictly a limitation of the present work, this thesis has focused on the Russell Glacier region of the GrIS under present and past climates. In principle, a physically based model such as SLING should be able to route meltwater and form lakes on any given ice surface providing an appropriate DEM is available. However, as also noted previously, observations of SGLs are limited, which may make evaluation of the model challenging in some regions. Potential changes to future distribution of SGLs has been highlighted as a concern, particularly the possible inland migration of SGLs. This is something that SLInG can be utilised to address. However, in its present configuration, SLInG is limited by the extent of the DEM that is used for water routing; SGLs are already simulated across the whole extent of the study region imposed by the DEM (Figure 6.6).

6.5 Recommendations for future work

As a new model, many potential opportunities exist for the further development and testing of SLInG. For example, SLInG would benefit from an evaluation using more robust observations, for example, airborne data and it would also be interesting to compare differences in simulated SGL evolution when SLInG is forced by a different RCMs; e.g. RACMO (Regional Atmospheric Climate Model) (van Meijgaard, 2008). In addition, because the SLInG model architecture is designed to be portable and the processes that are included in the model are fairly generally applicable, myriad avenues of further work to which SLInG may be applied are open. For example a desirable next step would be to determine the applicability of the model to other regions of the GrIS or on other ice sheets; SGLs are known to form on floating ice shelves in Antarctica (LaBarbera and MacAyeal, 2011). Here, three specific pieces of further work are discussed in more detail.

6.5.1   *Model development – the inclusion of drainage and refreezing*

Different observational studies have proposed different fractions of the SGL population which drain away and which refreeze (Selmes et al., 2011, Johansson et al., 2013). However, recently a third mechanism (apart from rapid drainage and refreezing) by which lakes expire has been proposed, whereby lakes drain slowly via the incision of supraglacial channels intersecting the lake. By observing this phenomena, Selmes et al. (2013), were able to partition lake cessation into four distinct categories: rapid drainage through hydrofracture, slow drainage through channel incision, refreezing and unknown. While this still does not allow lake drainage to be modelled physically using SLInG, a crude parameterisation may now be developed. This could take the form of a random assignation

of lakes in these observed fractions to a randomly selected drainage day, once critical volume had been reached, and a fast or slow drainage rate applied as appropriate. The remaining lakes could be refrozen at a rate calculated as a function of surface temperature (e.g. Taylor and Feltham, 2004), a parameter which can easily be supplied by the MAR RCM. Although this would not enable the behaviour of specific lakes to be analysed, an area averaged assessment of SGL evolution post-drainage could be made. This would be a useful improvement to the current model configuration because drainage is a critical part of the SGL seasonal cycle.

Table 6.1: The fate of lakes on the GrIS for the 2005-2009 period. Values indicate a percentage of all lakes observed in those years. Shading indicates mean values across all years for the south-west region only. Modified from Selmes et al. (2013)

	2005	2006	2007	2008	2009	2005-2009 (south-west only)
Fast drainage	11.9	11.3	14.3	14.7	12.0	14
Slow drainage	35.1	24.5	37.6	38.6	34.2	37
Refreeze	46.5	58.0	38.1	44.9	48.1	40
Unknown	6.4	6.2	7.4	4.6	5.7	8.1
Total Frequency	2067	1996	2069	2127	1931	-

6.5.2   *Coupling with an Ice Sheet Model or a regional climate model*

It may be possible to parameterise the effect of SGL drainage in an ice sheet model, for example by modifying the rate of basal sliding (Greve et al., 2011, Seddik et al., 2012). However, by including or coupling with the SLInG model, specific foci for surface-induced perturbation of subglacial water pressure may be identified. In addition, the SLInG model may be used to constrain the earliest date that this drainage may begin (i.e. the onset day of the lake) and as a corollary, the earliest date that enhanced basal sliding as a result of surface-bed meltwater routing may occur.

The SLInG model has been proven to be an effective method of modelling SGL evolution, given the current resolution and forcing data. However, ISMs are typically run at much coarser spatial resolution than SLInG, for example SICOPOLIS (Simulation Code for Polythermal Ice Sheets) is typically run on a 10 km resolution grid (e.g. Greve et al., 2011)

and Elmer/Ice is run using an adaptive mesh which is initiated with a nominal resolution of 5 km (e.g. Seddik et al., 2012). Since the largest observed SGL has a diameter of 4.46 km (Box and Ski, 2007), SGLs are sub-grid scale with respect to these models. Next generation ice sheet models, which also typically use an adaptive mesh, have a much finer resolution. This can be of the order of ~1 km in the vicinity of outlet glaciers (e.g. Gillet-Chaulet et al., 2012, Larour et al., 2012). The DEM employed by SLInG is posted at the model resolution of 100 m, and sensitivity studies have shown that the coarsest operational resolution that yields acceptable results is 300 m. At 1000 m resolution, typically the finest resolution of an ISM, SLInG successfully locates only 16% of available lakes (Figure 6.7). However, all 43 lakes which are successfully simulated at a DEM posting of 1000 m, hold enough water volume to enable hydrofracture (Krawczynski et al., 2009). Simulated onset day for these lakes is correlated with observations with a PCC of 0.87. Although 1000 m resolution is not sufficient to capture the full range of supra-glacial lake behaviour in terms of water storage (area/volume) or impact on albedo (lake covered area), it could nonetheless be useful, provided that the SLInG architecture can be modified for use with an adaptive mesh, and that the differences in time-stepping are accounted for. This suggests that, with an extensive period of development and testing a useful coupling/integration may be achieved between SLInG and next generation ISMs.
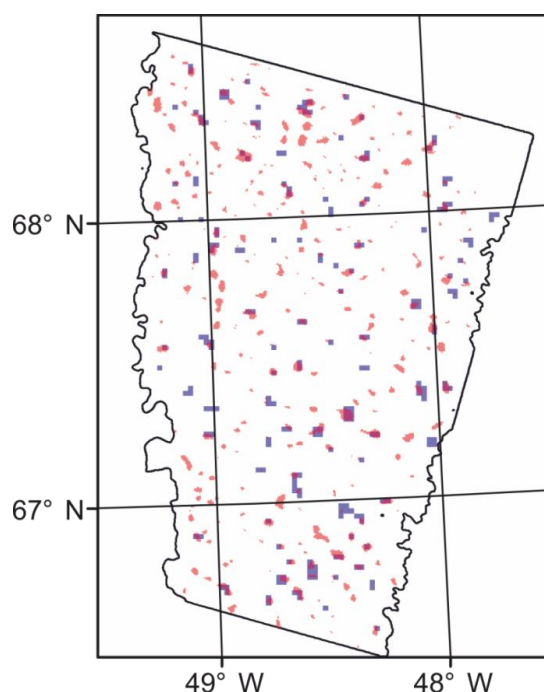
Figure 6.7: Observed (red) and SLInG simulated (blue) lake distribution in 2003. Observations are as reported in Sundal et al. (2009). SLInG simulation is performed using the DEM of Palmer et al. (2011); the nominal (100 m) resolution of the DEM is degraded to 1000 m using a neighbourhood averaging method. Figure featured in Chapter 2.

The MAR RCM uses a constant bare ice albedo (Lefebre et al., 2003), however SGLs have a lower albedo than the surrounding ice and have been shown to reduce the area averaged albedo of lake covered areas as a consequence (Greuell et al., 2002, Tedesco et al., 2012). As such, it would be a useful application of SLInG if it could be used to improve the representation of SGLs in RCMs. The operational resolution of RCMs prevents a direct coupling with SLInG; MAR typically operates at 25 km (Lefebre et al., 2005) and the finest resolution of the RACMO RCM is 11 km (van Meijgaard, 2008). However, it may be possible to provide for SGLs in RCMs through parameterisation of effects on surface albedo, in a similar manner to the parameterisation of melt ponds on sea ice (e.g. Pedersen et al., 2009, Koltzow, 2007). Because SLInG is not able to simulate time-varying albedo change due to the presence of lakes, the development of a suitable parameterisation for RCMs is, therefore, beyond the capabilities of SLInG at present. However, this would potentially be a very useful application of SLInG and if drainage and refreezing is successfully incorporated into the model, this ought to be revisited.

6.5.3 *Modelling future changes in SGL evolution*

Artic temperatures are projected to warm by 4-8°C by 2100 (Figure 6.8), and runoff is expected to increase in consequence (Rae et al., 2012). To date, no estimates of future changes to SGL evolution have been made. As a prognostic tool, SLInG provides the means by which such estimates may be made, given the availability of suitable forcing data. Runoff projections for the 2000-2100 period, simulated using the MAR model, are available. These are forced by a range of global circulation models for a range of climate change scenarios characterised by the representative concentration pathways (RCPs) developed for the fifth Assessment Report of the IPCC. However, using the DEM which currently represents the ice sheet surface (Palmer et al., 2011), SLInG is not able to capture any future changes to the altitudinal extent of lake covered area.

The commonly used Advanced Spaceborne Thermal Emission and Reflection Radiometer (ASTER) Global Digital Elevation Model (GDEM) is of sufficient resolution to resolve SGLs in a modelling environment such as SLInG, and has full ice sheet coverage. However the ASTER GDEM has been shown to be unsuitable for representing the GrIS ice sheet surface at high elevations (Meyer et al., 2011). A new product, the Greenland Mapping Project (GIMP) DEM has recently been made available, which uses SPOT-5 imagery and Advanced Very High Resolution Radiometer (AVHRR) photoclinometry to provide elevation data in regions where ASTER does not perform well (Howat I.M., in prep). The

GIMP DEM is posted at a resolution of 30 m and thus potentially may be used in SLInG to simulate future changes to the distribution of SGLs, although a period of development and testing would be required. In addition to addressing the limitation of the areal extent of the current model setup, the GIMP DEM has a resolution as fine as 40 m in parts, which would enable smaller lakes to be simulated. In addition, the GIMP DEM is formed from multiple years of data and as such, uncertainty due to the presence of refrozen lakes is minimised. A potential source of uncertainty in forward projections of SGL evolution using SLInG is that, in the model, the ice sheet surface is not currently evolved in time. Although this is valid over short-term simulations, or during periods of little or no mass loss, it is uncertain whether future climate change will have a corresponding impact on the hypsometry of the ice sheet. This will need to be considered in experiments that predict the future distribution of SGLs.
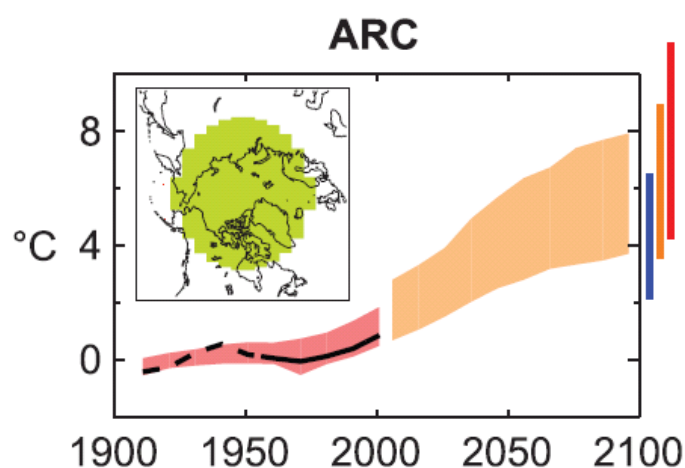
Figure 6.8: Past and Predicted Arctic temperature anomalies with respect to 1901 to 1950 (black line) as simulated (red envelope) incorporating known forcings; and projected for 2001 to 2100 for the A1B scenario (orange envelope). The bars represent the range of projected changes for the B1 scenario (blue), the A1B scenario (orange) and the A2 scenario (red). Modified from Meehl (2007).

References

ABDALATI, W. & STEFFEN, K. 2001. Greenland ice sheet melt extent: 1979-1999. *Journal of Geophysical Research-Atmospheres,* 106**,** 33983-33988.

ARGUEZ, A., O'BRIEN, J. J. & SMITH, S. R. 2009. Air temperature impacts over Eastern North America and Europe associated with low-frequency North Atlantic SST variability. *International Journal of Climatology,* 29**,** 1-10.

BAMBER, J. L., LAYBERRY, R. L. & GOGINENI, S. 2001. A new ice thickness and bed data set for the Greenland ice sheet 1. Measurement, data reduction, and errors. *Journal of Geophysical Research-Atmospheres,* 106**,** 33773-33780.

BANWELL, A. F., ARNOLD, N. S., WILLIS, I. C., TEDESCO, M. & AHLSTROM, A. P. 2012. Modeling supraglacial water routing and lake filling on the Greenland Ice Sheet. *Journal of Geophysical Research-Earth Surface,* 117.

BARTHOLOMEW, I., NIENOW, P., MAIR, D., HUBBARD, A., KING, M. A. & SOLE, A. 2010. Seasonal evolution of subglacial drainage and acceleration in a Greenland outlet glacier. *Nature Geoscience,* 3**,** 408-411.

BARTHOLOMEW, I., NIENOW, P., SOLE, A., MAIR, D., COWTON, T. & KING, M. A. 2012. Short-term variability in Greenland Ice Sheet motion forced by time-varying meltwater drainage: Implications for the relationship between subglacial drainage system behavior and ice velocity. *Journal of Geophysical Research-Earth Surface,* 117.

BARTHOLOMEW, I., NIENOW, P., SOLE, A., MAIR, D., COWTON, T., PALMER, S. & WADHAM, J. 2011a. Supraglacial forcing of subglacial drainage in the ablation zone of the Greenland ice sheet. *Geophysical Research Letters,* 38.

BARTHOLOMEW, I. D., NIENOW, P., SOLE, A., MAIR, D., COWTON, T., KING, M. A. & PALMER, S. 2011b. Seasonal variations in Greenland Ice Sheet motion: Inland extent and behaviour at higher elevations. *Earth and Planetary Science Letters,* 307**,** 271-278.

BATES, P. D. & DE ROO, A. P. J. 2000. A simple raster-based model for flood inundation simulation. *Journal of Hydrology,* 236**,** 54-77.

BLUMAN, A. G. 2004. *Elementary statistics: a step by step approach*, McGraw-Hill.

BOON, S. & SHARP, M. 2003. The role of hydrologically-driven ice fracture in drainage system evolution on an Arctic glacier. *Geophysical Research Letters,* 30**,** 4.

BOX, J. E., BROMWICH, D. H., VEENHUIS, B. A., BAI, L.-S., STROEVE, J. C., ROGERS, J. C., STEFFEN, K., HARAN, T. & WANG, S.-H. 2006. Greenland ice sheet surface mass balance variability (1988-2004) from calibrated polar MM5 output. *Journal of Climate,* 19**,** 2783-2800.

BOX, J. E. & SKI, K. 2007. Remote sounding of Greenland supraglacial melt lakes: implications for subglacial hydraulics. *Journal of Glaciology,* 53**,** 257-265.

References

BOX, J. E., YANG, L., BROMWICH, D. H. & BAI, L. S. 2009. Greenland Ice Sheet Surface Air Temperature Variability: 1840-2007. *Journal of Climate,* 22**,** 4029-4049.

BRAITHWAITE, R. J. 1984. Calculation of degree-days for glacier-climate research. *Zeitschrift fur Gletscherkunde und Glazialgeologie,* 20**,** 1-8.

BRAITHWAITE, R. J. & OLESEN, O. B. 1984. Ice Ablation in West Greenland in relation to air temperature and global radiation. *Z. Gletscherk. Glazialgeol.,* 20**,** 155-168.

BRAITHWAITE, R. J. & OLESEN, O. B. 1989. Detection of climate signal by inter-stake correlations of annual ablation data qamanarssup sermia, west greenland. *Journal of Glaciology,* 35**,** 253-259.

BRUN, E., DAVID, P., SUDUL, M. & BRUNOT, G. 1992. A numerical-model to simulate snow-cover stratigraphy for operational avalanche forecasting. *Journal of Glaciology,* 38**,** 13-22.

CATANIA, G. A., NEUMANN, T. A. & PRICE, S. F. 2008. Characterizing englacial drainage in the ablation zone of the Greenland ice sheet. *Journal of Glaciology,* 54**,** 567-578.

CHEN, C. C., MCCARL, B. & CHANG, C. C. 2012. Climate change, sea level rise and rice: global market implications. *Climatic Change,* 110**,** 543-560.

CHOW, V. T., DAVID R. MAIDMENT, LARRY W. MAYS 1988. *Applied Hydrology,* Singapore, McGraw-Hill Book Company.

CHURCH, J. A., GREGORY, J. M., HUYBRECHTS, P., KUHN, M., LAMBECK, K., NHUAN, M.T, QIN, D. & WOODWORTH, P. L. 2001. Changes in sea level. *In:* J. T. HOUGHTON, Y. D., D. J. GRIGGS, M. NOGUER, P. VAN DER LINDEN, X. DAI, K, MASKELL & C. I. JOHNSON (ed.) *Climate change 2001: the scientific basis. Contribution of Working Group 1 to the Third Assessment Report of the Intergovernmental Panel on Climate Change.* Cambridge, UK: Cambridge University Press.

CLASON, C., MAIR, D. W. F., BURGESS, D. O. & NIENOW, P. W. 2012. Modelling the delivery of supraglacial meltwater to the ice/bed interface: application to southwest Devon Ice Cap, Nunavut, Canada. *Journal of Glaciology,* 58**,** 361-374.

COLGAN, W., STEFFEN, K., MCLAMB, W. S., ABDALATI, W., RAJARAM, H., MOTYKA, R., PHILLIPS, T. & ANDERSON, R. 2011. An increase in crevasse extent, West Greenland: Hydrologic implications. *Geophysical Research Letters,* 38.

DAS, S. B., JOUGHIN, I., BEHN, M. D., HOWAT, I. M., KING, M. A., LIZARRALDE, D. & BHATIA, M. P. 2008. Fracture propagation to the base of the Greenland Ice Sheet during supraglacial lake drainage. *Science,* 320**,** 778-781.

DOYLE, S. H., HUBBARD, A. L., DOW, C. F., JONES, G. A., FITZPATRICK, A., GUSMEROLI, A., KULESSA, B., LINDBACK, K., PETTERSSON, R. & BOX, J. E. 2013.

Ice tectonic deformation during the rapid in situ drainage of a supraglacial lake on the Greenland Ice Sheet. *The Cryosphere,* 7**,** 129-140.

EBERT, E. E. & CURRY, J. A. 1993. An intermediate one-dimensional thermodynamic sea-ice model for investigating ice-atmosphere interactions. *Journal of Geophysical Research-Oceans,* 98**,** 10085-10109.

ECHELMEYER, K., CLARKE, T. S. & HARRISON, W. D. 1991. Surficial glaciology of jakobshavns isbrae, west greenland .1. Surface-morphology. *Journal of Glaciology,* 37**,** 368-382.

ETTEMA, J., VAN DEN BROEKE, M. R., VAN MEIJGAARD, E., VAN DE BERG, W. J., BOX, J. E. & STEFFEN, K. 2010. Climate of the Greenland ice sheet using a high-resolution climate model - Part 1: Evaluation. *Cryosphere,* 4**,** 511-527.

FAUSTO, R. S., AHLSTROM, A. P., VAN AS, D., BOGGILD, C. E. & JOHNSEN, S. J. 2009. A new present-day temperature parameterization for Greenland. *Journal of Glaciology,* 55**,** 95-105.

FETTERER, F. & UNTERSTEINER, N. 1998. Observations of melt ponds on Arctic sea ice. *Journal of Geophysical Research-Oceans,* 103**,** 24821-24835.

FETTWEIS, X. 2007. Reconstruction of the 1979-2006 Greenland ice sheet surface mass balance using the regional climate model MAR. *Cryosphere,* 1**,** 21-40.

FETTWEIS, X., FRANCO, B., TEDESCO, M., VAN ANGELEN, J. H., LENAERTS, J. T. M., VAN DEN BROEKE, M. R. & GALLÉE, H. 2013. Estimating the Greenland ice sheet surface mass balance contribution to future sea level rise using the regional atmospheric climate model MAR. *The Cryosphere,* 7**,** 469-489.

FETTWEIS, X., TEDESCO, M., VAN DEN BROEKE, M. & ETTEMA, J. 2011. Melting trends over the Greenland ice sheet (1958-2009) from spaceborne microwave data and regional climate models. *Cryosphere,* 5**,** 359-375.

FLOCCO, D. & FELTHAM, D. L. 2007. A continuum model of melt pond evolution on Arctic sea ice. *Journal of Geophysical Research-Oceans,* 112**,** 14.

FOUNTAIN, A. G. 1996. Effect of snow and firn hydrology on the physical and chemical characteristics of glacial runoff. *Hydrological Processes,* 10**,** 509-521.

FRANCO, B., FETTWEIS, X., LANG, C. & ERPICUM, M. 2012. Impact of spatial resolution on the modelling of the Greenland ice sheet surface mass balance between 1990-2010, using the regional climate model MAR. *Cryosphere,* 6**,** 695-711.

GEORGIOU, S., SHEPHERD, A., MCMILLAN, M. & NIENOW, P. 2009. Seasonal evolution of supraglacial lake volume from ASTER imagery. *Annals of Glaciology,* 50**,** 95-100.

References

GILLET-CHAULET, F., GAGLIARDINI, O., SEDDIK, H., NODET, M., DURAND, G., RITZ, C., ZWINGER, T., GREVE, R. & VAUGHAN, D. G. 2012. Greenland ice sheet contribution to sea-level rise from a new-generation ice-sheet model. *The Cryosphere,* 6**,** 1561-1576.

GREGORY, J. M., HUYBRECHTS, P. & RAPER, S. C. B. 2004. Climatology - Threatened loss of the Greenland ice-sheet. *Nature,* 428**,** 616-616.

GREUELL, W. & KONZELMANN, T. 1994. Numerical modeling of the energy-balance and the englacial temperature of the greenland ice-sheet - calculations for the eth-camp location (west greenland, 1155m asl). *Global and Planetary Change,* 9**,** 91-114.

GREUELL, W., REIJMER, C. H. & OERLEMANS, J. 2002. Narrowband-to-broadband albedo conversion for glacier ice and snow based on aircraft and near-surface measurements. *Remote Sensing of Environment,* 82**,** 48-63.

GREVE, R., SAITO, F. & ABE-OUCHI, A. 2011. Initial results of the SeaRISE numerical experiments with the models SICOPOLIS and IcIES for the Greenland ice sheet. *Annals of Glaciology,* 52**,** 23-30.

GUDMUNDSSON, G. H. 2003. Transmission of basal variability to a glacier surface. *Journal of Geophysical Research-Solid Earth,* 108**,** 19.

GULLEY, J. D., BENN, D. I., MULLER, D. & LUCKMAN, A. 2009. A cut-and-closure origin for englacial conduits in uncrevassed regions of polythermal glaciers. *Journal of Glaciology,* 55**,** 66-80.

HANNA, E., CAPPELEN, J., ALLAN, R., JONSSON, T., LE BLANCQ, F., LILLINGTON, T. & HICKEY, K. 2008a. New Insights into North European and North Atlantic Surface Pressure Variability, Storminess, and Related Climatic Change since 1830. *Journal of Climate,* 21**,** 6739-6766.

HANNA, E., CAPPELEN, J., FETTWEIS, X., HUYBRECHTS, P., LUCKMAN, A. & RIBERGAARD, M. H. 2009. Hydrologic response of the Greenland ice sheet: the role of oceanographic warming. *Hydrological Processes,* 23**,** 7-30.

HANNA, E., HUYBRECHTS, P., JANSSENS, I., CAPPELEN, J., STEFFEN, K. & STEPHENS, A. 2005. Runoff and mass balance of the Greenland ice sheet: 1958-2003. *Journal of Geophysical Research-Atmospheres,* 110.

HANNA, E., HUYBRECHTS, P. & MOTE, T. L. 2002. Surface mass balance of the Greenland ice sheet from climate-analysis data and accumulation/runoff models. *In:* WOLFF, E. W. (ed.) *Annals of Glaciology, Vol 35.* Cambridge: Int Glaciological Soc.

HANNA, E., HUYBRECHTS, P., STEFFEN, K., CAPPELEN, J., HUFF, R., SHUMAN, C., IRVINE-FYNN, T., WISE, S. & GRIFFITHS, M. 2008b. Increased runoff from melt

from the Greenland Ice Sheet: A response to global warming. *Journal of Climate,* 21**,** 331-341.

HANNA, E., JONES, J. M., CAPPELEN, J., MERNILD, S. H., WOOD, L., STEFFEN, K. & HUYBRECHTS, P. 2013. The influence of North Atlantic atmospheric and oceanic forcing effects on 1900-2010 Greenland summer climate and ice melt/runoff. *International Journal of Climatology,* 33**,** 862-880.

HANNA, E., MERNILD, S. H., CAPPELEN, J. & STEFFEN, K. 2012. Recent warming in Greenland in a long-term instrumental (1881-2012) climatic context: I. Evaluation of surface air temperature records. *Environmental Research Letters,* 7.

HOEN, E. W. & ZEBKER, H. A. 2000. Penetration depths inferred from interferometric volume decorrelation observed over the Greenland ice sheet. *Ieee Transactions on Geoscience and Remote Sensing,* 38**,** 2571-2583.

HOWAT I.M., A. N., T. SCAMBOS, T. HARAN, in prep. A high-resolution elevation model for the Greenland Ice Sheet from combined stereoscopic and photoclinometric data.

HOWAT, I. M., DE LA PEÑA, S., VAN ANGELEN, J. H., LENAERTS, J. T. M. & VAN DEN BROEKE, M. R. 2013. Brief Communication "Expansion of meltwater lakes on the Greenland Ice Sheet". *The Cryosphere,* 7**,** 201-204.

IRVINE-FYNN, T. D. L., HODSON, A. J., MOORMAN, B. J., VATNE, G. & HUBBARD, A. L. 2011. Polythermal glacier hydrology: a review. *Reviews of Geophysics,* 49.

JANSSON, P., HOCK, R. & SCHNEIDER, T. 2003. The concept of glacier storage: a review. *Journal of Hydrology,* 282**,** 116-129.

JAROSCH, A. H. & GUDMUNDSSON, M. T. 2012. A numerical model for meltwater channel evolution in glaciers. *Cryosphere,* 6**,** 493-503.

JOHANNESSEN, O. M., KHVOROSTOVSKY, K., MILES, M. W. & BOBYLEV, L. P. 2005. Recent ice-sheet growth in the interior of Greenland. *Science,* 310**,** 1013-1016.

JOHANSSON, A. M. & BROWN, I. A. 2013. Adaptive Classification of Supra-Glacial Lakes on the West Greenland Ice Sheet. *Selected Topics in Applied Earth Observations and Remote Sensing, IEEE Journal of,* PP**,** 1-10.

JOHANSSON, A. M., JANSSON, P. & BROWN, I. A. 2013. Spatial and temporal variations in lakes on the Greenland Ice Sheet. *Journal of Hydrology,* 476**,** 314-320.

JOUGHIN, I., ABDALATI, W. & FAHNESTOCK, M. 2004. Large fluctuations in speed on Greenland's Jakobshavn Isbrae glacier. *Nature,* 432**,** 608-610.

JOUGHIN, I., DAS, S. B., KING, M. A., SMITH, B. E., HOWAT, I. M. & MOON, T. 2008. Seasonal speedup along the western flank of the Greenland Ice Sheet. *Science,* 320**,** 781-783.

References

JOUGHIN, I., WINEBRENNER, D., FAHNESTOCK, M., KWOK, R. & KRABILL, W. 1996. Measurement of ice-sheet topography using satellite radar interferometry. *Journal of Glaciology,* 42**,** 10-22.

KNIGHTON, A. D. 1981. Channel form and flow characteristics of supraglacial streams, austre-okstindbreen, norway. *Arctic and Alpine Research,* 13**,** 295-306.

KOLTZOW, M. 2007. The effect of a new snow and sea ice albedo scheme on regional climate model simulations. *Journal of Geophysical Research-Atmospheres,* 112.

KRABILL, W., HANNA, E., HUYBRECHTS, P., ABDALATI, W., CAPPELEN, J., CSATHO, B., FREDERICK, E., MANIZADE, S., MARTIN, C., SONNTAG, J., SWIFT, R., THOMAS, R. & YUNGEL, J. 2004. Greenland Ice Sheet: Increased coastal thinning. *Geophysical Research Letters,* 31**,** 4.

KRAWCZYNSKI, M. J., BEHN, M. D., DAS, S. B. & JOUGHIN, I. 2009. Constraints on the lake volume required for hydro-fracture through ice sheets. *Geophysical Research Letters,* 36**,** 5.

KWOK, R. & FAHNESTOCK, M. A. 1996. Ice sheet motion and topography from radar interferometry. *Ieee Transactions on Geoscience and Remote Sensing,* 34**,** 189-200.

LABARBERA, C. H. & MACAYEAL, D. R. 2011. Traveling supraglacial lakes on George VI Ice Shelf, Antarctica. *Geophysical Research Letters,* 38.

LAMPKIN, D. J. 2011. Supraglacial lake spatial structure in western Greenland during the 2007 ablation season. *Journal of Geophysical Research: Earth Surface,* 116**,** n/a-n/a.

LAMPKIN, D. J. & VANDERBERG, J. 2011. A preliminary investigation of the influence of basal and surface topography on supraglacial lake distribution near Jakobshavn Isbrae, western Greenland. *Hydrological Processes,* 25**,** 3347-3355.

LAROUR, E., SEROUSSI, H., MORLIGHEM, M. & RIGNOT, E. 2012. Continental scale, high order, high spatial resolution, ice sheet modeling using the Ice Sheet System Model (ISSM). *Journal of Geophysical Research-Earth Surface,* 117.

LEESON, A. A., SHEPHERD, A., PALMER, S., SUNDAL, A. & FETTWEIS, X. 2012. Simulating the growth of supraglacial lakes at the western margin of the Greenland ice sheet. *Cryosphere,* 6**,** 1077-1086.

LEESON, A. A., SHEPHERD, A., SUNDAL, A. V., JOHANSSON, A. M., SELMES, N., BRIGGS, K., HOGG, A. E. & FETTWEIS, X. 2013. A comparison of supraglacial lake observations at the western margin of the Greenland ice sheet. *Journal of Glaciology*.

LEFEBRE, F., FETTWEIS, X., GALLEE, H., VAN YPERSELE, J. P., MARBAIX, P., GREUELL, W. & CALANCA, P. 2005. Evaluation of a high-resolution regional climate simulation over Greenland. *Climate Dynamics,* 25**,** 99-116.

References

LEFEBRE, F., GALLEE, H., VAN YPERSELE, J. P. & GREUELL, W. 2003. Modeling of snow and ice melt at ETH Camp (West Greenland): A study of surface albedo. *Journal of Geophysical Research-Atmospheres,* 108**,** 16.

LEMKE, P., J. REN, R.B. ALLEY, I. ALLISON, J. CARRASCO, G. FLATO, Y. FUJII, G. KASER, P. MOTE, R.H. THOMAS AND T. ZHANG 2007. Observations: Changes in Snow, Ice and Frozen Ground. *In:* SOLOMON, S., D. QIN, M. MANNING, Z. CHEN, M. MARQUIS, K.B. AVERYT, M. TIGNOR AND H.L. MILLER (EDS.) (ed.) *Climate Change 2007: The Physical Science Basis. Contribution of Working Group I to the Fourth Assessment Report of the Intergovernmental Panel on Climate Change.* Cambridge, United Kingdom and New York, NY, USA: Cambridge University Press.

LEWIS, S. M. & SMITH, L. C. 2009. Hydrologic drainage of the Greenland Ice Sheet. *Hydrological Processes,* 23**,** 2004-2011.

LIANG, Y.-L., COLGAN, W., LV, Q., STEFFEN, K., ABDALATI, W., STROEVE, J., GALLAHER, D. & BAYOU, N. 2012. A decadal investigation of supraglacial lakes in West Greenland using a fully automatic detection and tracking algorithm. *Remote Sensing of Environment,* 123**,** 127-138.

LIESTØL, O., REPP, K., AND WOLD, B. 1980. Supra-glacial lakes in Spitsbergen. *Norsk Geogr. Tidsskr.,* 34**,** 89-92.

LOTTER, G. K. 1932. *Considerations on hydraulic design of channels with different roughness of walls,* Leningrad, All-Union Scientific Research Institute of Hydraulic Engineering.

LUTHJE, M., FELTHAM, D. L., TAYLOR, P. D. & WORSTER, M. G. 2006a. Modeling the summertime evolution of sea-ice melt ponds. *Journal of Geophysical Research-Oceans,* 111**,** 1-17.

LUTHJE, M., PEDERSEN, L. T., REEH, N. & GREUELL, W. 2006b. Modelling the evolution of supraglacial lakes on the West Greenland ice-sheet margin. *Journal of Glaciology,* 52**,** 608-618.

LYAPUSTIN, A., TEDESCO, M., WANG, Y. J., AOKI, T., HORI, M. & KOKHANOVSKY, A. 2009. Retrieval of snow grain size over Greenland from MODIS. *Remote Sensing of Environment,* 113**,** 1976-1987.

MANNING, R. 1891. On the flow of water in open channels and pipes. *Transactions, Institution of Civil Engineers of Ireland,* 20**,** 161-207.

MASSOM, R. & LUBIN, D. 2006. *Polar Remote Sensing: Volum II: Ice Sheets,* Berlin, Springer.

MATHER, P., M. 2004. *Computer processing of remotely sensed images*, John Wiley & Sons Ltd.

References

MCMILLAN, M., NIENOW, P., SHEPHERD, A., BENHAM, T. & SOLE, A. 2007. Seasonal evolution of supra-glacial lakes on the Greenland Ice Sheet. *Earth and Planetary Science Letters,* 262**,** 484-492.

MEEHL, G. A., T.F. STOCKER, W.D. COLLINS, P. FRIEDLINGSTEIN, A.T. GAYE, J.M. GREGORY, A. KITOH, R. KNUTTI, J.M. MURPHY, A. NODA, S.C.B. RAPER, I.G. WATTERSON, A.J. WEAVER AND Z.-C. ZHAO, 2007. Global Climate Projections. *In:* SOLOMON, S., D. QIN, M. MANNING, Z. CHEN, M. MARQUIS, K.B. AVERYT, M. TIGNOR AND H.L. MILLER (ed.) *Climate Change 2007: The Physical Science Basis. Contribution of Working Group I to the Fourth Assessment Report of the Intergovernmental Panel on Climate Change.* Cambridge, United Kingdom and New York, NY, USA: Cambridge University Press.

MEYER, D., TACHIKAWA, T., KAKU, M., IWASAKI, A., GESCH, D., OIMOEN, M., ZHANG, Z., DANIELSON, J., KRIEGER, T., CURTIS, B., HAASE, J., ABRAMS, M., CRIPPEN, R. & CARABAJAL, C. 2011. ASTER Global Digital Elevation Model Version2 - Summary of Validation Results.

MOTE, T. L. 2007. Greenland surface melt trends 1973-2007: Evidence of a large increase in 2007. *Geophysical Research Letters,* 34.

NGHIEM, S. V., HALL, D. K., MOTE, T. L., TEDESCO, M., ALBERT, M. R., KEEGAN, K., SHUMAN, C. A., DIGIROLAMO, N. E. & NEUMANN, G. 2012. The extreme melt across the Greenland ice sheet in 2012. *Geophysical Research Letters,* 39.

NICHOLLS, R. J. 2002. Analysis of global impacts of sea-level rise: a case study of flooding. *Physics and Chemistry of the Earth,* 27**,** 1455-1466.

PALMER, S., SHEPHERD, A., NIENOW, P. & JOUGHIN, I. 2011. Seasonal speedup of the Greenland Ice Sheet linked to routing of surface water. *Earth and Planetary Science Letters,* 302**,** 423-428.

PARIZEK, B. R. & ALLEY, R. B. 2004. Implications of increased Greenland surface melt under global-warming scenarios: ice-sheet simulations. *Quaternary Science Reviews,* 23**,** 1013-1027.

PATERSON, W. S. B. 1994. *The Physics of Glaciers,* Oxford, Butterworth-Heineman.

PEDERSEN, C. A., ROECKNER, E., LUTHJE, M. & WINTHER, J. G. 2009. A new sea ice albedo scheme including melt ponds for ECHAM5 general circulation model. *Journal of Geophysical Research-Atmospheres,* 114.

PEROVICH, D. K., GRENFELL, T. C., LIGHT, B. & HOBBS, P. V. 2002. Seasonal evolution of the albedo of multiyear Arctic sea ice. *Journal of Geophysical Research-Oceans,* 107**,** 13.

PHILLIPS, T., LEYK, S., RAJARAM, H., COLGAN, W., ABDALATI, W., MCGRATH, D. & STEFFEN, K. 2011. Modeling moulin distribution on Sermeq Avannarleq glacier using ASTER and WorldView imagery and fuzzy set theory. *Remote Sensing of Environment,* 115**,** 2292-2301.

PHILLIPS, T., RAJARAM, H. & STEFFEN, K. 2010. Cryo-hydrologic warming: A potential mechanism for rapid thermal response of ice sheets. *Geophysical Research Letters,* 37.

PODRASKY, D., TRUFFER, M., FAHNESTOCK, M., AMUNDSON, J. M., CASSOTTO, R. & JOUGHIN, I. 2012. Outlet glacier response to forcing over hourly to interannual timescales, Jakobshavn Isbrae, Greenland. *Journal of Glaciology,* 58**,** 1212-1226.

RAE, J. G. L., AOALGEIRSDOTTIR, G., EDWARDS, T. L., FETTWEIS, X., GREGORY, J. M., HEWITT, H. T., LOWE, J. A., LUCAS-PICHER, P., MOTTRAM, R. H., PAYNE, A. J., RIDLEY, J. K., SHANNON, S. R., VAN DE BERG, W. J., VAN DE WAL, R. S. W. & VAN DEN BROEKE, M. R. 2012. Greenland ice sheet surface mass balance: evaluating simulations and making projections with regional climate models. *Cryosphere,* 6**,** 1275-1294.

RAMASAMY, R. & SURENDRAN, S. N. 2012. Global climate change and its potential impact on disease transmission by salinity-tolerant mosquito vectors in coastal zones. *Frontiers in physiology,* 3**,** 198.

RAMILLIEN, G., LOMBARD, A., CAZENAVE, A., IVINS, E. R., LLUBES, M., REMY, F. & BIANCALE, R. 2006. Interannual variations of the mass balance of the Antarctica and Greenland ice sheets from GRACE. *Global and Planetary Change,* 53**,** 198-208.

RAYMOND, C. F. & NOLAN, M. 2000. Drainage of a glacial lake through an ice spillway. *In:* NAKAWO, M., RAYMOND, C. F. & FOUNTAIN, A. (eds.) *Debris-Covered Glaciers.* Wallingford: Int Assoc Hydrological Sciences.

REEH, N. 1991. Parameterization of Melt Rate and Surface Temperature on the Greenland Ice Sheet. *Polarforschung,* 59**,** 113-128.

RIGNOT, E., ECHELMEYER, K. & KRABILL, W. 2001. Penetration depth of interferometric synthetic-aperture radar signals in snow and ice. *Geophysical Research Letters,* 28**,** 3501-3504.

RIGNOT, E. & KANAGARATNAM, P. 2006. Changes in the velocity structure of the Greenland ice sheet. *Science,* 311**,** 986-990.

RIGNOT, E. & THOMAS, R. H. 2002. Mass balance of polar ice sheets. *Science,* 297**,** 1502-1506.

RÖTHLISBERGER, H. 1972. Water pressure in intra- and subglacial channels. *Journal of Glaciology,* 11**,** 177-203.

References

RUSSELL, A. J. 1993. SUPRAGLACIAL LAKE DRAINAGE NEAR SONDRE-STROMFJORD, GREENLAND. *Journal of Glaciology,* 39**,** 431-433.

SCHOOF, C. 2010. Ice-sheet acceleration driven by melt supply variability. *Nature,* 468**,** 803-806.

SCOTT, F. & FELTHAM, D. L. 2010. A model of the three-dimensional evolution of Arctic melt ponds on first-year and multiyear sea ice. *Journal of Geophysical Research-Oceans,* 115.

SEDDIK, H., GREVE, R., ZWINGER, T., GILLET-CHAULET, F. & GAGLIARDINI, O. 2012. Simulations of the Greenland ice sheet 100 years into the future with the full Stokes model Elmer/Ice. *Journal of Glaciology,* 58**,** 427-440.

SELMES, N., MURRAY, T. & JAMES, T. D. 2011. Fast draining lakes on the Greenland Ice Sheet. *Geophysical Research Letters,* 38.

SELMES, N., MURRAY, T. & JAMES, T. D. 2013. Characterizing supraglacial lake drainage and freezing on the Greenland Ice Sheet. *The Cryosphere Discuss.,* 7**,** 475-505.

SHEPHERD, A., HUBBARD, A., NIENOW, P., KING, M., MCMILLAN, M. & JOUGHIN, I. 2009. Greenland ice sheet motion coupled with daily melting in late summer. *Geophysical Research Letters,* 36**,** 4.

SHEPHERD, A., IVINS, E. R., A, G., BARLETTA, V. R., BENTLEY, M. J., BETTADPUR, S., BRIGGS, K. H., BROMWICH, D. H., FORSBERG, R., GALIN, N., HORWATH, M., JACOBS, S., JOUGHIN, I., KING, M. A., LENAERTS, J. T. M., LI, J., LIGTENBERG, S. R. M., LUCKMAN, A., LUTHCKE, S. B., MCMILLAN, M., MEISTER, R., MILNE, G., MOUGINOT, J., MUIR, A., NICOLAS, J. P., PADEN, J., PAYNE, A. J., PRITCHARD, H., RIGNOT, E., ROTT, H., SØRENSEN, L. S., SCAMBOS, T. A., SCHEUCHL, B., SCHRAMA, E. J. O., SMITH, B., SUNDAL, A. V., VAN ANGELEN, J. H., VAN DE BERG, W. J., VAN DEN BROEKE, M. R., VAUGHAN, D. G., VELICOGNA, I., WAHR, J., WHITEHOUSE, P. L., WINGHAM, D. J., YI, D., YOUNG, D. & ZWALLY, H. J. 2012. A Reconciled Estimate of Ice-Sheet Mass Balance. *Science,* 338**,** 1183-1189.

SHIMIZU, H. 1969. Air permeability of deposited snow. *Low Temperature Science,* 22**,** 1-32.

SIMMONDS, I., BURKE, C. & KEAY, K. 2008. Arctic Climate Change as Manifest in Cyclone Behavior. *Journal of Climate,* 21**,** 5777-5796.

SKYLLINGSTAD, E. D., PAULSON, C. A. & PEROVICH, D. K. 2009. Simulation of melt pond evolution on level ice. *Journal of Geophysical Research-Oceans,* 114**,** 15.

SNEED, W. A. & HAMILTON, G. S. 2007a. Evolution of melt pond volume on the surface of the Greenland Ice Sheet. *Geophysical Research Letters,* 34**,** 4.

References

SNEED, W. A. & HAMILTON, G. S. 2007b. Evolution of melt pond volume on the surface of the Greenland Ice Sheet. *Geophysical Research Letters,* 34.

SOLE, A. J., D.W.F. MAIR, P.W. NIENOW, I.D. BARTHOLEMEW, M.A. KING, M.J. BURKE, I. JOUGHIN 2011. Seasonal speed-up of a Greenland marine-terminating outlet glacier forced by surface melt-induced changes in subglacial hydrology. *J. Geophys. Res,* in press.

STEPHENSON, D. B. 2000. Use of the "odds ratio" for diagnosing forecast skill. *Weather and Forecasting,* 15**,** 221-232.

SUNDAL, A. 2009. Determining supra-glacial lake area from MODIS satellite images. Edinburgh: University of Edinburgh.

SUNDAL, A. V., SHEPHERD, A., NIENOW, P., HANNA, E., PALMER, S. & HUYBRECHTS, P. 2009. Evolution of supra-glacial lakes across the Greenland Ice Sheet. *Remote Sensing of Environment,* 113**,** 2164-2171.

SUNDAL, A. V., SHEPHERD, A., NIENOW, P., HANNA, E., PALMER, S. & HUYBRECHTS, P. 2011. Melt-induced speed-up of Greenland ice sheet offset by efficient subglacial drainage. *Nature,* 469**,** 522-U83.

TAYLOR, P. D. & FELTHAM, D. L. 2004. A model of melt pond evolution on sea ice. *Journal of Geophysical Research-Oceans,* 109**,** 19.

TEDESCO, M. 2007. a new record in 2007 for melting in Greenland. *Eos, Transactions American Geophysical Union,* 88**,** 383-383.

TEDESCO, M. & FETTWEIS, X. 2012. 21st century projections of surface mass balance changes for major drainage systems of the Greenland ice sheet. *Environmental Research Letters,* 7.

TEDESCO, M., FETTWEIS, X., VAN DEN BROEKE, M. R., VAN DE WAL, R. S. W., SMEETS, C. J. P. P., VAN DE BERG, W. J., SERREZE, M. C. & BOX, J. E. 2011a. Record Summer Melt in Greenland in 2010. *Eos, Transactions American Geophysical Union,* 92**,** 126-126.

TEDESCO, M., LUTHJE, M., STEFFEN, K., STEINER, N., FETTWEIS, X., WILLIS, I., BAYOU, N. & BANWELL, A. 2012. Measurement and modeling of ablation of the bottom of supraglacial lakes in western Greenland. *Geophysical Research Letters,* 39.

TEDESCO, M., SERREZE, M. & FETTWEIS, X. 2008. Diagnosing the extreme surface melt event over southwestern Greenland in 2007. *Cryosphere,* 2**,** 159-166.

TEDESCO, M. & STEINER, N. 2011. In-situ multispectral and bathymetric measurements over a supraglacial lake in western Greenland using a remotely controlled watercraft. *Cryosphere,* 5**,** 445-452.

References

TEDESCO, M., WILLIS, I., ALEXANDER, P. & BANWELL, A. 2011b. Measurements of supraglacial lake drainage and surface streams over West Greenland and effects on ice dynamics, . *AGU Fall Meeting*. San Francisco, Calif.

THOMAS, R., FREDERICK, E., KRABILL, W., MANIZADE, S. & MARTIN, C. 2006. Progressive increase in ice loss from Greenland. *Geophysical Research Letters,* 33.

THOMSEN, H., THORNING, L., AND OLESEN, O. 1989. Applied glacier research for planning hydro-electric power, Ilulissat/Jakobshavn, West Greenland. *Ann. Glaciol,* 13**,** 257-261.

VAN DEN BROEKE, M., BAMBER, J., ETTEMA, J., RIGNOT, E., SCHRAMA, E., VAN DE BERG, W. J., VAN MEIJGAARD, E., VELICOGNA, I. & WOUTERS, B. 2009. Partitioning Recent Greenland Mass Loss. *Science,* 326**,** 984-986.

VAN DEN BROEKE, M., SMEETS, P., ETTEMA, J., VAN DER VEEN, C., VAN DE WAL, R. & OERLEMANS, J. 2008. Partitioning of melt energy and meltwater fluxes in the ablation zone of the west Greenland ice sheet. *Cryosphere,* 2**,** 179-189.

VAN DER VEEN, C. J. 2007. Fracture propagation as means of rapidly transferring surface meltwater to the base of glaciers. *Geophysical Research Letters,* 34**,** 5.

VAN MEIJGAARD, E., VAN ULFT, L. H., VAN DE BERG, W. J., BOSVELD, F. C., VAN DEN HURK, B. J. J. M., LENDERINK, G., AND SIEBESMA, A. P. 2008. The KNMI regional atmospheric climate model RACMO version 2.1, Tech. Rep.

VELICOGNA, I. & WAHR, J. 2006. Acceleration of Greenland ice mass loss in spring 2004. *Nature,* 443**,** 329-331.

VERNON, C. L., BAMBER, J. L., BOX, J. E., VAN DEN BROEKE, M. R., FETTWEIS, X., HANNA, E. & HUYBRECHTS, P. 2013. Surface mass balance model intercomparison for the Greenland ice sheet. *The Cryosphere,* 7**,** 599-614.

WALDER, J. S. 1986. HYDRAULICS OF SUBGLACIAL CAVITIES. *Journal of Glaciology,* 32**,** 439-445.

WILLMOTT, C. J., ACKLESON, S. G., DAVIS, R. E., FEDDEMA, J. J., KLINK, K. M., LEGATES, D. R., ODONNELL, J. & ROWE, C. M. 1985. Statistics for the evaluation and comparison of models. *Journal of Geophysical Research-Oceans,* 90**,** 8995-9005.

ZEBKER, H. A., WERNER, C. L., ROSEN, P. A. & HENSLEY, S. 1994. Accuracy of topographic maps derived from ers-1 interferometric radar. *Ieee Transactions on Geoscience and Remote Sensing,* 32**,** 823-836.

ZWALLY, H. J., ABDALATI, W., HERRING, T., LARSON, K., SABA, J. & STEFFEN, K. 2002. Surface melt-induced acceleration of Greenland ice-sheet flow. *Science,* 297**,** 218-222.